Final Report

Date of Report:	April 15, 2011
Contract Number:	DTPH56-05-T-0001
Prepared for:	United States Department of Transportation Pipeline and Hazardous Materials Safety Administration Office of Pipeline Safety
Project Title:	"Understanding Magnetic Flux Leakage (MFL) Signals from Mechanical Damage in Pipelines"
Prepared by:	Dr. Lynann Clapham Principal Investigator Applied Magnetics Group Queen's University Kingston, Ontario, Canada K7L 3N6 lynann@physics.queensu.ca Dr. Vijay Babbar Project Manager, Applied Magnetics Group Queen's University Kingston, Ontario, Canada K7L 3N6 babbar@physics.queensu.ca Mr. Ian Wood Director of Programs Electricore, Inc. 27943 Smyth Drive, Suite 105 Valencia, CA 91355 ian@electricore.org Mr. Mark Piazza Team Technical Coordinator Pipeline Research Council International, Inc. (PRCI) 3141 Fairview Park Drive, Suite 525 Falls Church, VA 22042 mpiazza@prci.org

Understanding Magnetic Flux Leakage (MFL) Signals from
Mechanical Damage in Pipelines – Phase III

Executive Summary

The pipeline industry has used commercially available inspection tools based on Magnetic Flux Leakage (MFL) principles for over three decades, and have developed and optimized them primarily for corrosion detection. MFL signals from mechanical damage are not sufficiently well characterized and understood to be used for reliable detection and characterization of pipeline dents and gouges. The objective of this project, co-funded by US Department of Transportation Pipeline and Hazardous Materials Safety Administration (US DOT PHMSA) and the Pipeline Research Council International (PRCI), is to understand the origin of MFL mechanical damage signals from dents and gouges, using experimental measurements as well as magnetic finite element analysis (FEA) models. Electricore, Inc. is the prime contractor and Queen's, University is the technical lead. Phases I and II of the project earlier examined MFL signals from dents, using both laboratory and field data for model verification. Phase III is concerned with understanding MFL signals from gouges, and gouges with associated denting.

MFL signals from gouges and gouge+dents are complex because three aspects may contribute to the signal –

1) Severe plastic deformation region may be created when a deformation tool contacts the pipe wall which may contribute additional MFL signal features.
2) Geometry effects will change the applied MFL field and includes any pipe wall perturbation associated with damage (i.e., metal loss, exfoliation, pipe wall bending, and gouge orientation with respect to the applied MFL field)
3) Residual stresses are elastic stresses that often surround mechanical damage which alter the magnetic permeability of the pipe wall and, thus, the MFL signal

Phase III examined all three of these possible contributing factors, using both experimental methods and magnetic modeling techniques -

Severe plastic deformation: The researchers at Queen's University examined effect of severe plastic deformation on MFL signals through MFL and magnetic Barkhausen Noise (MBN) measurements on steel plate samples that had been 'surface damaged'. They introduced damage through SiC 'scratching', surface grinding and backhoe damage. The MBN measurements on the damaged regions proved to be inconclusive because of problems coupling the MBN probe to the sample (i.e. liftoff). However, the MFL measurements indicated that MFL is very sensitive to surface deformation, when it is measured on the same surface as the damage. However, when the MFL measurement was made at the opposite side of the steel plate, no signal was observed. The conclusion was that, for internal MFL field tool measurements of gouges, it is unlikely that the thin layer of severe surface deformation contributes significantly to the signal.

Gouge geometry: Gouge geometry effects can only be studied using 'realistic' gouges – created in pressurized pipe sections using full scale gouging equipment. The team produced gouges of progressively increasing severity in pressurized 12 in. diameter , 9.2 mm wall thickness pipe at Stress Engineering Services (SES) in Houston. The technicians pressed a gouging tool into the pipe wall to specified depths, and the pipe pulled axially to create gouges approximately 5 cm long. The internal pipe pressures during gouging were either 50% or 100% MAOP. The extent of deformation ranged from 'residual stress-only' damage (no physical gouge created) to a gouge which extended 6 mm through the wall at its deepest point. Unfortunately, the team could not make a quantitative determination of the residual stresses in these samples, however, the MFL signal clearly exhibits both residual stress and geometry components. The general findings are as follows:

1) MFL measurements do not differ significantly when taken under or at zero pressure.
2) Damage introduced at higher internal pressures displays slightly smaller and less extensive MFL signals than those created at lower pressures which is consistent with the larger constraint in the high pressure pipe.
3) The gouges produced in the samples were created in 4 stages of progressively increasing severity. The least severe exhibited only residual stresses but no gouge geometry, while the most severe displayed a deep gouge, a large exfoliation and a significant dent. The MFL signals progressively changed as follows:
    - Inner wall MFL signals: in the least severe case only residual stresses were present yet these created a significant MFL signal, with the largest signal associated with the tool exit location. As the gouge geometry developed, a large peak at the tool exit end was associated both with these residual stresses and also the exfoliation. The tapered sidewalls of the gouge contributed smaller 'side peaks' to the MFL signal. Finally, the most severe gouges also exhibited large dents, and thus typical MFL "dent peaks" were superimposed on the gouge signals.
    - Outer wall MFL signals: The outer wall MFL signals follow a similar progression to the inner wall signals, with the exfoliation peak dominating. However at the outer wall there is also a MFL signal contribution from the thin layer of severe plastic deformation (created by direct tool contact) at the gouge base. The MFL signal from this severe deformation layer is not seen in the inner wall signal.

4) A pressure cycling verses MFL study was also conducted as part of the series of tests on the SES samples. One of the gouged samples (containing a gouge with a moderate dent) was subjected to a pressure cycling to 50% MAOP, with outer wall MFL measurements made after 1, 10, 100, 1,000 and 10,000 cycles. The Queen's team did not observe any variation in the MFL measurements with pressure cycling. This is contrary to anecdotal reports on isolated samples that pressure cycling produces an "MFL halo" around mechanical damage.

Residual stress measurement with neutron diffraction: Although a discussion of residual stresses necessarily formed part of the "geometry" study, this part of the study focused exclusively on residual stresses. Its contribution to the gouge MFL signal is difficult to determine because the

residual stresses around gouges are complex and, to date, have not been accurately modeled using stress modeling software. Thus, measurement of these stress distributions is necessary, and neutron diffraction is the only experimental method available. NIST performed the neutron diffraction measurements on two MD4-1 samples: BEA161 (primarily a gouge with little denting), and BEA178 (mild gouging, very large dent). Measurements were also conducted on coupon sample P22 that was created as part of an earlier study. Results are summarized as follows:

Samples BEA161 and P22 – primarily gouges with little denting:

- The local residual strain field is localized around the immediate gouge vicinity, except where there was some denting present.
- The axial and hoop stress variations thought the wall, and laterally were similar to one another.
- Through-wall residual stresses underneath and in the immediate gouge region the hoop and axial stresses were neutral or moderately tensile (50-100 MPa) at the outer wall, gradually becoming highly compressive (-600 MPa in some locations) at the inner wall surface.

Sample BEA178 – mild gouge with significant denting:

- This exhibits a very different residual stress pattern than P22 or BEA161 which the team attributes to the presence of the large associated dent. The complex denting process associated with this kind of gouge+dent dominates the residual stresses, making the residual stress distribution very complex. In addition, rather than having a residual stress field that is localized in the immediate gouge vicinity, the varying stress distribution extends to the edge of the dented region. Further studies are planned to quantify

Finally, since the residual stresses were measured for gouge BEA161 using neutron diffraction, and the researchers could readily determine the geometry, and they created a full magnetic model (including residual stresses + geometry) for this gouge. These were compared with MFL experimental measurements, and the modeling was successful in identifying most of the dominant aspects of the experimental signals. There were also some features of the MFL signal that appeared to be anomalous, and were likely a result of surface corrosion and pitting, or other background effects in the pipe wall.

The study concluded that the main feature associated with gouging is a localized peak at the tool exit location. The evidence suggests that this peak is a combination of both residual stresses and geometry effects (exfoliation and gouge end discontinuities). The rest of the MFL signal is fairly specific to the gouge-geometry and residual stress, and thus, will vary from gouge to gouge: For example, the MFL signal can be influenced by gouge sidewall geometry, the extent of residual stress at the gouge entry location, and, very importantly, the location and extent of denting. It is unlikely that MFL signal measured at the inner wall during a normal inspection scenario will be influenced by the thin severe deformation layer at the outer surface.

The study on MFL signals from dents and gouges will continue. The neutron diffraction study indicated that the residual stress patterns may be very different from one gouge to another.

Further neutron diffraction measurements need to be done to clarify the residual stress patterns associated with gouges, and this work (MD1-9, funded by PRCI in a 2-year study) will begin in June, 2011. Queen's will also conduct MFL measurements and continue modeling work on gouged samples that are part of the MD4-1 projects.

Table of Contents

LIST OF FIGURES

1.0 Introduction and Overall Project Objective

Pipeline inspection tools based on Magnetic Flux Leakage (MFL) principles represent the most cost-effective method for in-line detection and monitoring of pipeline corrosion defects[1]. These tools have been in commercial use for over three decades. Mechanical damage produces MFL signals, but as yet these signals are not sufficiently well characterized and understood to be used for reliable detection and characterization of pipeline dents and gouges. The objective of this project, co-funded by US Department of Transportation Pipeline and Hazardous Materials Safety Administration (US DOT PHMSA) and the Pipeline Research Council International (PRCI), is to develop magnetic finite element analysis (FEA) models that accurately predict the MFL signals produced by mechanical damage in pipelines. Information from the final models will be used to facilitate interpretation of MFL signals obtained from inspection tool data. Results of this study, including validated magnetic model results, along with corresponding experimental measurements, will be made available to inspection vendors, pipeline operators and other interested parties via a web-based dent+gouge MFL signal library.

MFL signals from dents include a geometry signal component in addition to a signal component due to residual stresses. If gouging is present, then there may also be an additional magnetic contribution from the thin layer of heavily worked material at the gouge base. The relative contribution of each of these components to the MFL signal depends on the size and shape of the dent/gouge in addition to other effects such as metal loss, wall thinning, corrosion, etc. The work included in this report represents the final stages of a project in which, magnetic Finite Element Analysis (FEA) is used to model MFL signals from mechanical damage 'defects' having various sizes, shapes, and configurations. These models can include geometry effects, residual stress contributions and also magnetic behavior changes due to severe deformation. The modeled results are then compared with experimental MFL signals from dents and gouges. These defects are introduced into pipeline sections under controlled conditions intended to replicate damage introduced in the field.

The Applied Magnetics Group (AMG) at Queen's University began working on mechanical damage in 2002. In 2002 and 2003, mechanical damage investigations formed a relatively small part (~30%) of a larger Gas Research Institute (GRI)-funded Queen's project involved with examining stress effects on MFL signals (GRI Contracts # 5093-260-2605 and 5093-260-8682[2]). At that early stage, the magnetic modeling software* was limited in its geometric modeling capabilities; i.e., the dent shape could not be accurately modeled. In 2004, a new version of the software was released which included an improved geometrical modeling capability. This capability, combined with our GRI-funded experience in modeling stress effects, enabled construction of more realistic magnetic MFL models to account for both the dent geometry and

* The Queen's group uses Infolytica MagNet magnetic modeling software, which is the only magnetic modeling software that allows for the incorporation of "stresses" into the magnetic model via local modifications of the magnetic permeability functions.

associated stress distribution. GRI funding in 2004 enabled further work on modeling and corresponding experimental efforts on simple circular dents in steel plate samples[3].

In 2005 co-funding for the continuation of this project was assumed by the DOT/PHMSA as well as PRCI, and the current contract began. Contract work during 2006 and 2007 focused on plain dents (Phase I and Phase II). In the first year (Phase I) magnetic models were produced for elongated plain dents – oriented both axially and circumferentially. Experimental verification was achieved using experimental MFL measurements on Queen's laboratory-produced elongated dents produced in plate samples. In Phase II, the work was extended to a modeling and experimental study of more realistic plain dents created using the Pipeline Aggression Rig (PAR) at the GdF Suez research facility in St. Denis, France.

Phase III is concerned with the complex problem of modeling MFL signals from gouges and gouges containing dents. In order to prepare representative MFL models, Phase III included a considerable amount of experimental work These experimental studies were needed to determine the how different physical features of the gouges/dents contribute to the MFL signal. The experimental results were, in turn, used to inform the magnetic modeling work. The subject matter is presented as four chronologically ordered summaries of Work Performed:

- *Section 5: Determination of the magnetic contribution of the highly deformed surface layer at the base of the gouge*: Many gouges contain a thin, highly deformed layer at their base, formed by direct contact with the gouging tool. Experimental work was required in order to determine the possible contribution of this layer to the MFL signal. The Magnetic Barkhausen Noise technique was employed to try to obtain information regarding the magnetic behavior of gouges, specifically the thin, highly deformed region. Backhoe-created gouges in plate were used as samples.

- *Section 6: Systematic Gouge Study with Stress Engineering Services*: The results obtained in Section 5 highlighted the need for a systematic study of gouges created using full scale gouging equipment. Gouges of progressively increasing severity were produced at Stress Engineering Services (SES) in Houston, Texas. Experimental MFL measurements were conducted at the outer and inner pipe wall of the gouges and gouges+dents. Modeling of gouge geometry was conducted as part of this study. Modeling the effects of residual stresses on the MFL signals was problematic because attempts to use stress modeling to predict residual stress patterns were unsuccessful, highlighting the need to measure the residual stress distribution using neutron diffraction.The work at SES also included an investigation of the effect of pressure cycling on MFL signals.

- *Section 7: Experimental studies on MD4-2 GdF Suez Gouge and Gouge+dent samples: neutron diffraction*, MFL modeling and experimental studies. Since structural modeling of residual stress patterns around gouges was unsuccessful, the neutron diffraction method was used to measure residual stress patterns around realistic gouges and dents+gouges. Two samples for neutron diffraction measurements were provided from the MD4-2 study – sample BEA161 (gouge), and sample BEA178 (gouge with dent). These two samples were in the form of full pipe rings. These residual stress

measurements were also complementary to the MD 4-2 study involving characterization of gouged and gouged+dented samples. In addition, another coupon sample containing a gouge also was examined using neutron diffraction.

- *Section 8: Modelling MFL signals from gouges:* The information gained from the earlier chapters is used to develop a magnetic model for the sample BEA161. The measured residual stress pattern was incorporated into the fully descriptive magnetic model, and modeled MFL results were compared to the measured MFL results from the same samples.

2.0 Work Plan

The entire program has been divided into three major phases which include:

- Phase I—Creation of the magnetic models for elongated plain
- Phase II—Modeling and experimental study of more realistic plain dents
- Phase III—Modeling and experimental study of MFL signals from gouges and gouges containing dents

Table 2-1 shows the major tasks for each of the Phases of the project.

Table 2- 1: Task Description

Phase	Task #	Task Description
I	1	Examine the Effects of Dent Ovality on MFL Signals
I	2	Investigate MFL Signals From Dents Containing Single Corrosion Pits
I	3	Modeling and Experimental MFL Testing of 'Field' Dents
I, II, III	4	Administration and Reporting
I, II, III	5	Pipeline Safety Research Peer Review
II	6	Study of MFL signals from plain dents in pipes
II	7	Study of MFL signals from gouged dents in pipes
II	8	Creation of web-based MFL dent signal database for Laboratory and Pipeline Dents
III	9	Characterizing magnetic response of gouged pipeline material
III	10	MFL signal from GDF Suez gouged pipeline samples
III	11	Experimental MFL measurements and MFL modeling of gouges in full-scale pipe sections
III	12	Neutron Diffraction measurements on GDF Suez gouged samples
I, II, III	13	Collaboration with DOT Project DTPH56-06-T-000016

Summary of all Previous Work: Phases I and II

The summary that follows outlines all of the work on MFL signals originating from mechanical damage that has been conducted by the Applied Magnetics Group (AMG); it begins in Section 2.1 with a description of the early findings of how stress affects MFL signals. Section 2.2 is a summary of the AMG work done in 2004 on mechanical damage MFL signals, funded by the Gas Research Institute (GRI). Section 2.3 summarizes the results of Phase I of the current DOT PHMSA/PRCI contract, and Section 2.4 summarizes the work completed in Phase II of the current DOT PHMSA/PRCI contract.

2.1 MFL and Stress Effects: Key Features

2.1.1 General description of samples and testing procedure

The MFL inspection technique involves applying a direct current (DC), axially-oriented magnetic field to the pipe wall using a set of large permanent magnets. The pipe wall is magnetized to near-saturation. Therefore, in regions of metal loss (such as a corrosion pit), some of the magnetic flux is forced (or 'leaks') into the surrounding air. A Hall probe or detector coil, mounted between the magnet pole pieces, detects the "leaking" flux as an MFL signal.

In corrosion detection, the size of the MFL signal correlates generally to the size of the corrosion region. However, a complicating factor in corrosion signal interpretation is the influence of stress. This is due to the fact that magnetism is strongly stress dependent, and there are many different 'sources' of stress in an operating pipeline including: applied (pressurization) stresses, residual stresses introduced during manufacturing and installation, in addition to stress concentrations around the defects themselves. In what is now recognized as a classic paper in the field[1], David Atherton (the founder of the Applied Magnetics Group at Queen's University) focused attention on the effects of stress on MFL corrosion signals, illustrating that stress may affect the magnitude of these signals by up to 50%. From 1998-2002, the AMG conducted an extensive GRI-funded study to characterize elastic and plastic deformation effects on MFL signals using both experimental and FEA techniques. This work provided an invaluable knowledge base in this field, which is summarized in GRI reports[2,3] and a number of technical papers[6-9].

The foundation of the present MFL mechanical damage study is the understanding of stress effects gained in this earlier GRI-funded study. The following selected results from this earlier work are of particular importance:

- Elastic tensile strain creates an increase, and compressive elastic strain a decrease, in the magnetic permeability* of a pipeline wall. Therefore, local pipe wall elastic strain such

* Magnetic permeability is the proportionality constant between applied field and induced flux density in a material. It is not constant, but is a function of applied field and the local stress level.

as that associated with dents can enhance or decrease MFL signals depending on their sign, magnitude and orientation with respect to the applied MFL field.

- Earlier work has shown that magnetic properties are highly dependent on elastic strain, but very much less sensitive to plastic strain up to about 20% total deformation[8]. Therefore, for a plain (ungouged) dent, only the elastic (residual) strain is expected to contribute to the MFL signal. It should be noted that gouges include much higher deformation levels, and the plastically deformed material associated with gouges may be expected to have an associated MFL signal. The effect of severe plastic deformation on MFL gouge signals is considered in Phase III of this project (section 6 of the this report).
- Because most of the effects on MFL signals arise from elastic (residual) strain, these effects can be largely removed in laboratory-sized samples by using standard 'stress relieving' heat treatments. Stress relieving heat treatments were used extensively in the early work to separate the individual geometry and strain-induced MFL signal components.
- Working closely with the Infolytica MagNet FEA software[9] company, magnetization functions were developed by the AMG and implemented within the magnetic modeling software to allow the magnetic permeability to be varied both locally and anisotropically (i.e., in the three orthogonal directions). This enables our group to conduct magnetic modeling of the multi-axial effects of stress on MFL signals.
- Extensive experimental testing of samples under stress and applied field conditions provided the critical magnetization function data needed for FEA modeling of stress effects on MFL signals.

2.2 Summary of 2004 GRI-Funded Study[3]: MFL Signals from Circular Dents (Modeled and Experimental)

In 2003, improvements in the Infolytica MagNet FEA modeling software [9] made it possible to more accurately represent dent geometries, and in 2004, the project team applied this capability to the modeling of MFL signals from plain circular dents (n.b., 'plain' implies no gouge is present). **Figure 2-1** shows the magnetic model used in the 2004 study.

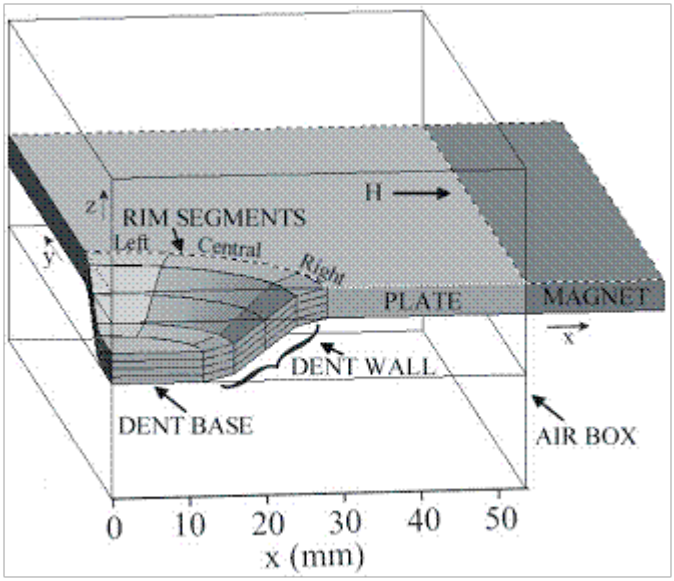

Figure 2-1: Magnetic FEA model used in the 2004 GRI-funded study of MFL signals from circular dents. Only a quarter-model is used because of symmetry considerations. The air box is the rectangular parallelepiped lying between the topmost horizontal surface and lowermost horizontal surface of the model.

As shown in **Figure 2-1**, the circular dent model is divided into 'dent rim' and 'dent base' regions, and these regions are further subdivided into blocks through the thickness of the wall. Different blocks can be assigned different anisotropic permeability functions, depending on the stress level in each block. The stress levels were determined using structural FEA modeling.

Additionally, it is worth noting that the result of the modeling process is a 3D magnetic vector field. The MFL signal itself is represented by either the radial, axial or circumferential component of this field in the region outside or inside the pipe wall. Experimentally, each of the MFL signal components can be measured separately through appropriate orientation of the detector (usually a Hall probe). Traditionally, pipeline inspection vendors have used the axial component of the MFL field (MFL_{axial}) in order to determine defect dimensions, however our experimental work typically involves obtaining all three signal components.

The overall FEA-model MFL_{radial} signal (radial component), incorporating both geometry and stress contributions, is shown in **Figure 2-2** (n.b., this is a quarter-model representing the upper right quadrant). **Figure 2-3** shows the experimental MFL_{radial} signal obtained from laboratory measurements on a 40-mm diameter circular dent of 7mm depth. The experimental (**Figure 2-3**) and modeling (**Figure 2-2**) results match very closely. Furthermore, since stress effects could readily be turned 'on' or 'off' in the magnetic FEA model, it was possible to identify the individual effects of stress and dent geometry. These modeling results enabled determination of the origin of each specific feature in the experimental result of **Figure 2-3**, specifically:

- The circular dent geometry gives rise to two central peaks of opposite polarity (labeled 'geometry peaks' in **Figure 2-3**).
- The stresses in the dent rim create a significant shoulder peak (labeled 'rim stress peak' in **Figure 2-3**). This appears to combine with the similar polarity outer geometry peak, creating what appears to be a "halo" effect.
- An additional stress peak is also associated with the dent base, but this peak is obscured by the main geometry peak (labeled "dent base stress peak' in **Figure 2-3**).

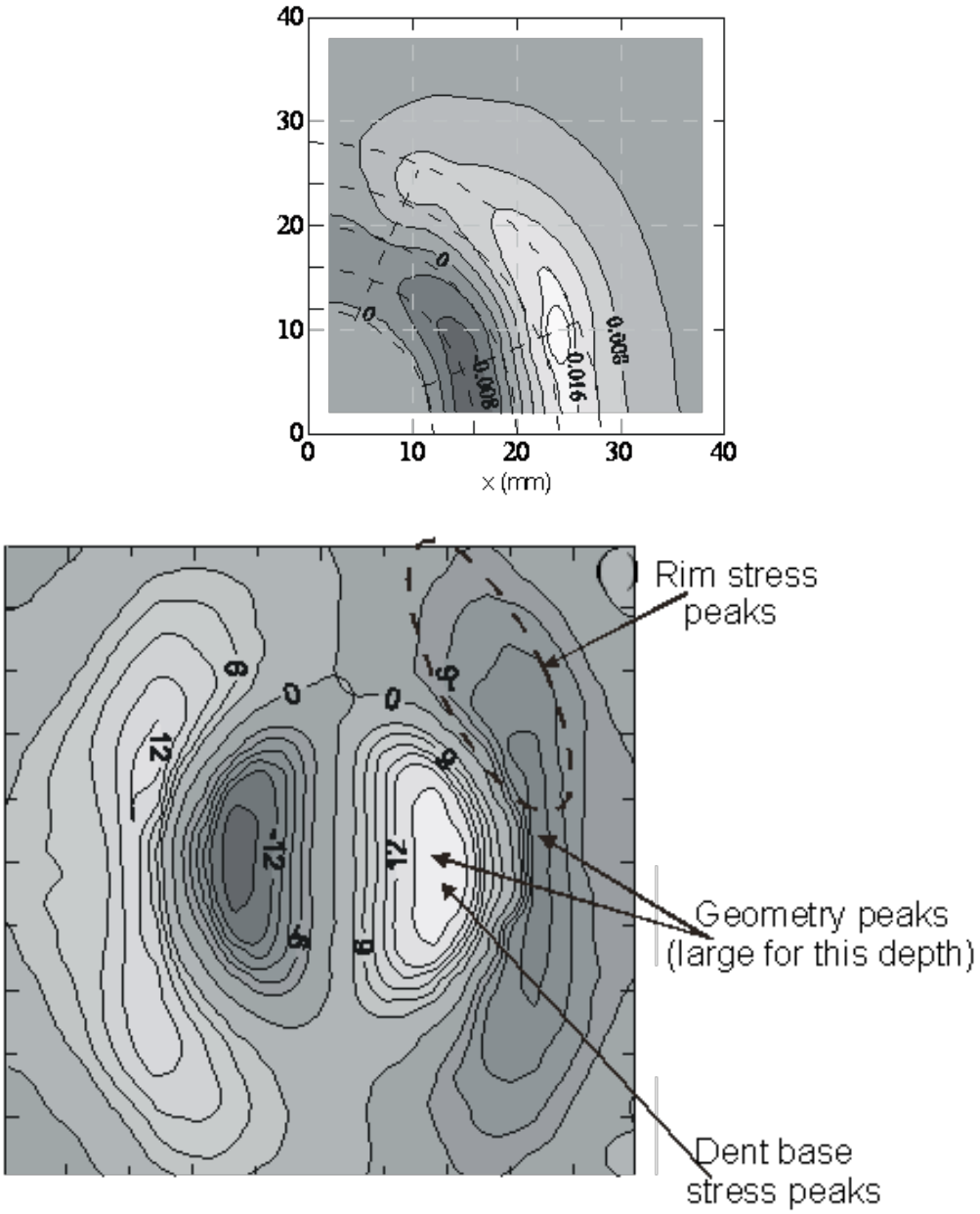

Figure 2-2: (Top) Quarter-model magnetic FEA result for the MFL signal (radial component) shown as a contour plot. This corresponds to the upper right-hand quadrant of the experimental signal shown in Figure 2.3. Both stress and geometry contributions to the MFL signal are included. (Bottom) The FEA modeled result shown in Figure 2.2 enabled the individual features of this MFL result to be associated with either geometry or stress as indicated in the diagram. (Note that the peak polarity is reversed compared with Figure 2.2 because the field is applied in the opposite direction.)

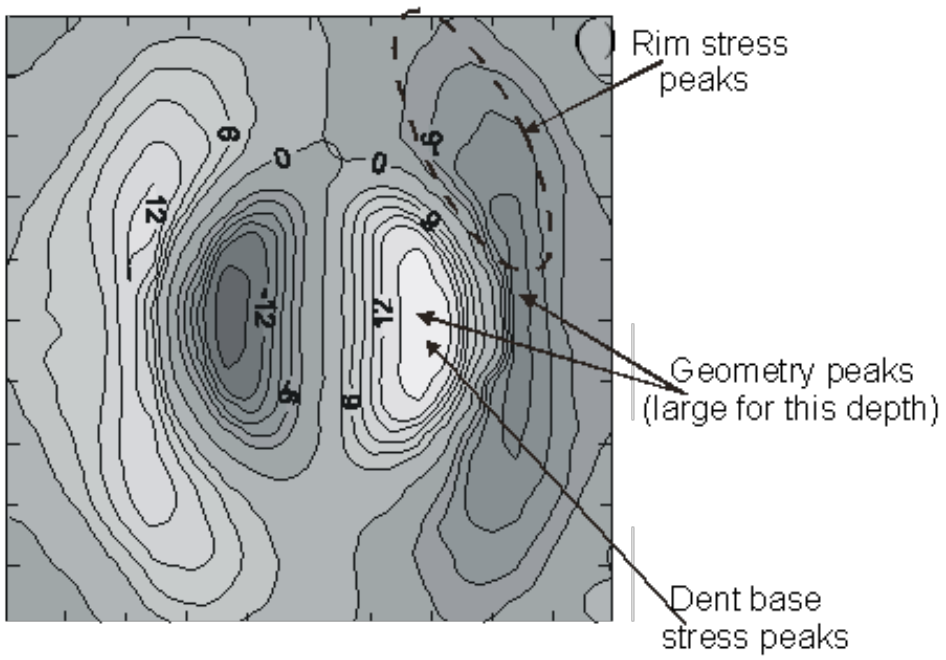

Figure 2-3: Experimental MFL radial component contour plot for a 40-mm diameter circular dent.

2.3 Summary of work in PHASE I of the current project

As noted in Section 2.2, work conducted prior to the current DOT PHMSA/PRCI contract involved preliminary experimental work and modeling studies of circular plain dents in plate samples with the dents created using a hydraulic press[2,3]. In Phase I of the current contract (which began 2005) this work extended to include 2:1 aspect ratio elongated dents, oriented in both the axial and circumferential directions. As with the earlier study of circular dents, the work involved a combination of modeling and experimental studies. On the modeling side, structural finite element analysis (FEA) modeling was used to evaluate the stress distribution around a dent. The elastic strain information from these structural FEA models was used to assign permeability functions within the magnetic models. As in the circular dent study, both MFL signal effects of dent geometry and local stress were examined.

Experimental work paralleled that of the modeling work. 2:1 aspect ratio dents of varying depths (3mm-8mm) were produced in 3mm thick steel plate samples (n.b., the dent depth was measured from the unperturbed topside of the plate, and these dents produce significant "bumps" extending below the bottom of the plate). Full contour plots of MFL signals from these dents were obtained in each of the radial, axial, and circumferential component directions. Selected dents were stress-relieved using standard annealing treatments, and then re-measured to examine the difference between the 'geometry+stress' and 'geometry-only' MFL signals. These experimental signals were compared to the modeling results in order to verify and further refine the models.

Table 2- 2 : The matrix of samples studied and MFL results obtained from this study

Location	2:1 Dent Orientation	Dent Depth (mm)	Metal Condition	Measurement Orientation	Number of Contour Plots Produced
Topside	Circumferential	3, 4, 5, 6, 7	Before annealing; After annealing	MFL_{radial} MFL_{axial} MFL_{circ}	30
Topside	Axial	3, 4, 5, 6, 7	Before annealing; After annealing	MFL_{radial} MFL_{axial} MFL_{circ}	30
Underside	Circumferential	3, 4, 5, 6, 7	Before annealing; After annealing	MFL_{radial} MFL_{axial} MFL_{circ}	30
Underside	Axial	3, 4, 5, 6, 7	Before annealing; After annealing	MFL_{radial} MFL_{axial} MFL_{circ}	30

The results of the Phase I study are briefly summarized in the sections that follow.

2.3.1 Axially-elongated 2:1 aspect ratio dents: modeling and experimental studies

A typical MFL_{radial} result for an axial 2:1 dent, in this case depth of 6 mm, is shown in **Figure 2-4**. The three color photos show the modeled result – the two at the top are the separate MFL signal contributions of geometry and stress, respectively, and the bottom left plot is the combined stress + geometry modeled result. The experimental result is on the bottom right, with good agreement shown.

Both geometry and stress have considerable and interesting effects on the axially elongated dent signals, as seen in **Figure 2-4**:

- The geometry signal displays a characteristic 'four peak' MFL_{radial} signature along the line of the dent in the applied field direction. The two outside peaks are associated with the outer dent rim 'corner', while the two inner peaks originate from the corner at the dent base. This result is similar to that seen in circular dents – however as the dent aspect ratio increases the peaks migrate further away from the dent center.

- The main stress contribution to the MFL_{radial} signal is associated with the dent rim 'sidewall' – i.e. the rim along the long side of the dent. This produces a significant vertical peak which tends to be positioned approximately over the central dent geometry peak.

- The combined effect of geometry+stress on MFL_{radial} signals is very interesting in this case, since the dent sidewall stress contribution lies over the inner dent geometry peak but is of opposite polarity. This has two effects:
    1. To diminish the size of the inner geometry peak; and
    2. To 'create' an apparent additional peak in the center dent sidewall rim region. This peak is actually a composite of geometry+stress effects. While this additional peak appears fairly slight in the 2:1 aspect ratio dent, studies on the 4:1 aspect ratio dent indicated that this produces a very evident 'additional peak' close to the center of the dent.

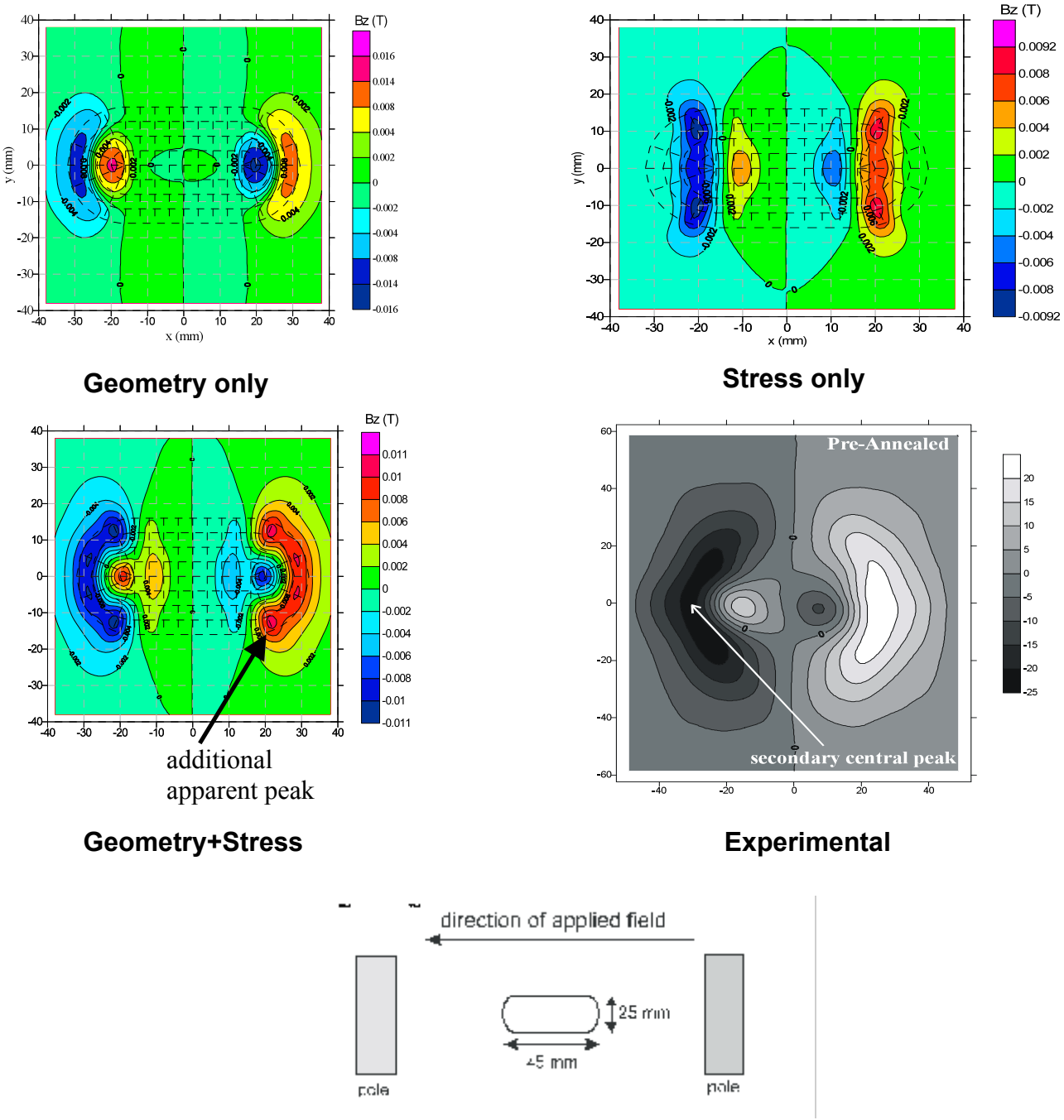

Figure 2-4: MFL_{radial} result for an axially elongated 2:1 dent, 6mm deep. The relative dent and applied field orientation are shown in the schematic at the bottom. The three color photos show the modeled result – the two at the top are the separate contributions of geometry and stress, respectively, and the bottom color plot is the combined modeled result. The experimental result is shown on the bottom right, with good agreement apparent.

2.3.2 Circumferentially-elongated 2:1 aspect ratio dents: modeling and experimental studies

Figure 2-5 shows a typical MFL_{radial} result for a circumferential 2:1 dent, in this case of depth 6mm. The three color photos show the modeled result – the two at the top are the separate contributions of geometry and stress, and the one at the bottom is the combined modeled result. The experimental result is shown on the bottom right, with good agreement shown.

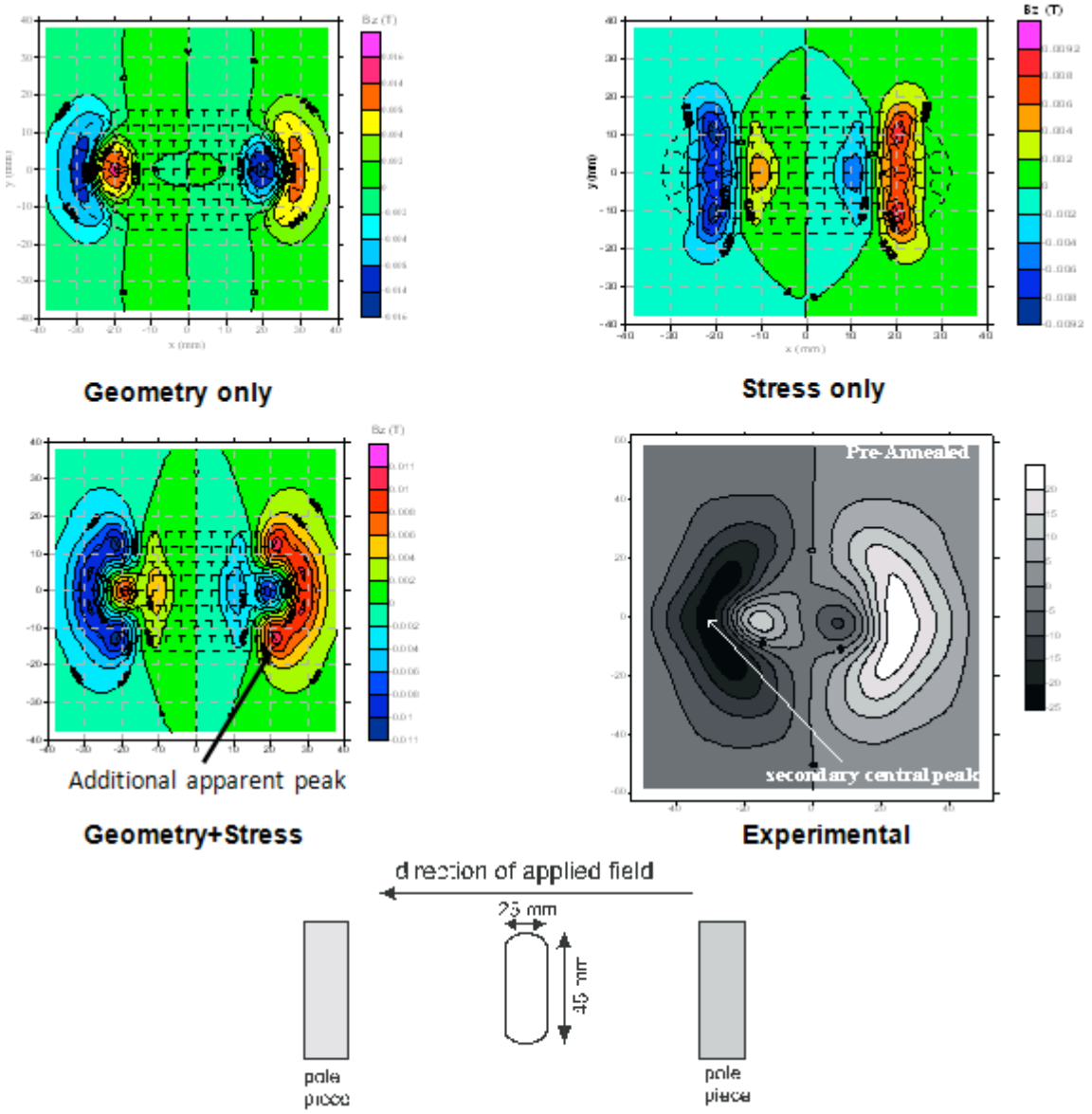

Figure 2-5: MFL_{radial} result for a circumferentially elongated 2:1 dent, 6mm deep. The relative dent and applied field orientation are shown in the schematic at the bottom. The three color photos show the modeled result – the two at the top are the separate contributions of geometry and stress, respectively, and the bottom color plot is the combined modeled result. The experimental result is shown on the bottom right, with good agreement apparent.

The experimental and modeled MFL_{radial} signal results for the circumferentially-oriented elongated dents are summarized below:

- The geometry signal consists of four peaks as in earlier circular and axial dent cases, however, due to the circumferential elongation of the dent, these central peaks are much closer together and also elongated in the circumferential direction.

- Sidewall dent rim stresses have little effect on the MFL signal for this dent orientation. The stress effects on the signal are mainly in the form of shoulder peaks at the extreme ends of the signal (in the circumferential direction).

- Combined stress + geometry signals are relatively simple to interpret in this case and reflect a straightforward superposition of the two effects on the signal.

2.3.3 Experimental comparison of MFL_{radial}, MFL_{axial} and MFL_{circ} dent signals

Experimental studies examined both topside and also underside MFL signals from a range of depths, both in the axial and circumferential orientation. The following points were noted:

- The MFL_{radial} signal component consistently displays the largest and most detailed signals. This is due to the fact that the sensor lies closer to the surface in this orientation than in the other two.

- The MFL_{radial} and MFL_{circ} signals contain distinct stress-related and also geometry-related features (peaks). For both these components the central peaks tend to be geometry related, with dent rim stresses reflected in shoulder peaks. The MFL_{axial} component appears to have no specific stress-related features and also appears similar to signals produced by corrosion pits.

- All MFL signal features diminish slightly with stress-relief annealing, however the magnitude of the shoulder peaks is considerably affected by annealing, reinforcing the conclusion that they tend to be related to residual stress.

A major conclusion from this aspect of the work is that for dent detection and sizing inspection tools should measure all three components of the MFL signal, rather than just the MFL_{axial} signal as is typical in most cases.

2.3.4 Circular dents containing corrosion pits: modeling and experimental studies

In addition to extensive studies of elongated 'plain' dents, the Phase I study also included circular dents containing centrally located corrosion pits. Through-wall pits of 2, 4 and 24 mm diameter were created in 40 mm diameter circular dents. Both modeling and experimental work indicated that the MFL signals for the combined pit+dent were a simple superposition of the two

signals. The pit was centered in the middle of the dent, so clear signals from pit and dent were seen when the dent was relatively small. In the 24 mm diameter pit there was considerable overlap with signals and interpretation became more difficult.

2.3.5 Web-based database – preliminary work

The ultimate goal of this project is to produce modeled and experimental MFL signal results from dents of known shapes and stresses. With a very large number of results, effective presentation becomes an issue. In Phase I, the project team presented a relatively simple proposed format for a web-based results spreadsheet which allows for easy access to both modeled and experimental results of this study. Further expansion and development of this database continued in Phase II and III.

2.4 Summary of work in PHASE II of the current project

As indicated above, Phase I of the current project involved modeling and laboratory measurements of MFL signals from circular and elongated plain dents produced in plate using a simple tool and die compression device. In Phase II of the current contract, MFL signals were measured from more realistic plain dents produced using the GdF Suez Pipeline Aggression Rig (PAR). MFL models were created from selected dents in these samples. The samples studied in Phase II were produced by GdF Suez as part of earlier investigations on plain dents. These investigations involve denting with the PAR and then pressurizing the pipe sections to failure. Coupons containing the dents were cut from the pipe wall and stored for later use. These dented coupon samples were measured using MFL in Phase II. An abbreviated summary of the work from Phase II is presented below. Reference 5 includes more details. The specific tasks that were part of Phase II are described below.

2.4.1 Upgrade of the existing MFL testing rig at Queen's to improve portability and for accommodation of Gaz de France samples

The Queen's team traveled to France in order to access the GdF Suez dented coupon samples. A number of modifications were made to the Queen's laboratory and MFL equipment in order to make it portable and to accommodate the range of sample geometries measured at GdF Suez. On the data acquisition side, these alterations included replacing the computer monitor, upgrading the software, refurbishing the XY scanner system, and building new carriage mounts for Hall probes for the radial, circumferential and axial component scans. The magnetic circuit was also rebuilt to accommodate the larger samples, and a number of pole piece end sections were produced to fit the different diameter dented pipe samples. The completed magnetic circuit was left in the GdF Suez research facility for future measurements.

2.4.2 Structural FEA modeling results from GdF Suez

In Phase II, GdF Suez provided the project team with some structural FEA modeling of dented pipeline samples. The structural models predicted elastic residual stresses associated with a dent in a pressurized pipe, immediately following the denting process. However, the dented coupons examined in Phase II were obtained from pipes that, after denting, had (in most cases) been subjected to grinding, pressurized to failure (and thereby depressurized) and then cut out of the larger pipe. As such, the "ideal" FEA-predicted local stresses from the GdF Suez modeling were unlikely to be representative of the actual stresses around the dents in these sample coupons. As a result, the subsequent MFL modeling work focused mainly on modeling MFL results generated from the dent geometry, rather than the dent stresses.

2.4.3 Improving and upgrading our magnetic FEA modeling techniques to accommodate larger and more realistic samples

Our earlier magnetic modeling work involved relatively small, symmetrical dents in flat plate samples. This modeling work is complex and time consuming, even for these relatively simple cases. However, 'real' pipeline dents, such as the ones produced at GdF Suez, are much more difficult to model since they are larger, generally asymmetrical, and located in curved pipe sections rather than flat plate. In Phase II, different methods were examined to determine the best way to produce magnetic FEA models that accurately reflect the features of the real dents. Three approaches were examined:

1. A direct 'manual' approach which involved measuring the main features of the dent and creating the model directly from these. This was very time consuming and ultimately unsuccessful.

2. A progressive asymmetry approach. This involved starting with a symmetric model having the same dimensions as the 'real' dent, and then progressively introducing asymmetry until the overall geometries match closely. This was successful and was the procedure ultimately adopted. A further conclusion from this study of asymmetry was that, although in general the MFL radial component appears to be the most distinctive for dent identification, this work indicates that the radial component is relatively insensitive to dent asymmetry. Rather, asymmetry was more clearly seen in the MFL axial component signals.

3. The laser scan import method for creating dent models in MagNet. While at GdF Suez the project team was able to obtain laser scan data for the 'topside' dent geometries for each of the dents measured. Ideally, one would like to be able to directly import those scans into the MagNet MFL modeling software, time was spent attempting to create software to do this. Ultimately, however, this approach was abandoned. Although the method is still 'promising' the resolution obtained was much lower than the progressive asymmetry approach and the model took too long to solve.

2.4.4 Results of modeling and experimental studies of GdF Suez dented samples

A total of six GdF Suez dented samples were measured using MFL, and these results compared with modeling results. Three of these samples were circular dents, one weld-free and the other two containing welds (one girth and one axial). Both of the circular dent samples with welds had been pressurized to failure. The other three samples contained axially-elongated dents. All three of these axially-elongated dents had been pressurized to failure, which in most cases caused the center region to partially re-round. As a result the elongated dents often end up with a geometry that resembles two adjacent circular dents.

In comparing the modeled and measured MFL results, the following points were noted:

1) The MFL modeling results for the GdF Suez circular and axially-elongated dents were similar in form to modeled MFL results obtained for smaller dents in the Phase I study of the previous year.
2) As noted earlier, MFL modeling in Phase II only included geometry effects - stress effects were not incorporated. This was due to the fact that the stress history of the GdF Suez samples was very complex, due to denting, grinding, pressurizing to failure, re-rounding and then coupon removal. Accurate stress FEA analysis accounting for all these steps was beyond the scope of this project.
3) For both the circular dents and also the axially-elongated dents, the geometry-induced MFL features predicted by the modeling are all consistent with those seen in the experimental results.
4) In addition to the large, significant geometry peaks predicted by the modeling, smaller peaks are seen often in the experimental MFL data. Although speculative, we attributed these to residual stresses around the dent (resulting from grinding, over pressurizing, and cracking).
5) The weld bead induced MFL signal is clearly evident as a ridge across the signal. In some of the dent samples this weld bead has been partially removed during the grinding process, resulting in an MFL signal with sporadic peaks, rather than a continuous ridge. It was interesting to note that, in pipes where the weld bead had been removed (so the weld was flush with the surface) there was little or no MFL weld indication. This suggests that MFL is relatively insensitive to the material and microstructural changes between the weld and parent material.
6) Significant MFL signals often resulted from the cracks which were created during pressurization to failure. However, it was not possible to determine if the large MFL signals were from the cracks themselves or the stresses associated with the cracks.
7) As mentioned above, many of the axially-elongated dents had geometries similar to two adjacent circular dents which is consistent with the MFL signals.

2.4.5 Preliminary results of modeling and experimental studies of a GdF Suez gouged sample

Although the main focus of the Phase II study was MFL signals from plain dents, one measurement was taken from an undented, gouged sample produced using the GdF Suez pipeline

aggression rig – sample P22. This preliminary measurement was conducted largely to determine whether gouges behave in a similar way to dents (whose signals have very significant geometry-induced MFL features). The gouge chosen for study was one which resembled a simple metal-loss defect – a surface depression in a pipe with no geometry change on the inside pipe wall. Despite the fact that the gouge appears visually similar to a metal-loss defect, modeling indicated that the MFL result is not consistent with a typical metal-loss signal. This indicates that further work needs to be done if MFL gouge signals are to be accurately characterized.

2.4.6 Web-based template library

The team has created a template library which is essentially an on-line appendix of MFL signals and also neutron diffraction data. The idea is that it could be readily accessed by vendors and operators. The results of the GdF Suez work were added to the template library.

3.0 Specific Objectives of Phase III

During Phases I and II of the DOT PHMSA/PRCI contract, the Queens University team focused exclusively on plain dents and obtained results from both modeling and experimental MFL studies of laboratory-produced dented plate samples, in addition to the more realistic dented coupon samples from GdF Suez.

Phase III was concerned with MFL signals from gouges, and also gouges+dents**.** Initially, the project team expected this work to take one year, however in this first year it became clear that modeling, and also experimental studies of MFL gouge signals were far more problematic than those involving dents. As a result, further work became necessary, and additional contract time was added, in order to more clearly understand the origin of the MFL signals from gouges and gouges+dents.

Thus the work plan for Phase III developed in an iterative manner as the study progressed, with each stage informing the next. The specific objectives of Phase III can be summarized as follows (in approximate chronological order):

Specific Objectives of Phase III

- To utilize the Magnetic Barkhausen Noise technique, in combination with MFL, to obtain information regarding the magnetic characteristics of the plastically deformed regions compared with those exhibiting residual stress. Gouged steel plate samples were prepared at Queen's, and useful results were obtained. However the gouge introduction method was problematic because the plastic deformation could not be produced independent of bending stresses. This highlighted the need for full sized pipe samples produced using realistic gouging techniques, such as are available at Stress Engineering Services and GdF Suez (the Pipeline Aggression Rig).
- To utilize the large-scale gouge introduction capabilities at Stress Engineering Services to conduct a systematic study of gouging, by creating gouges of progressively increasing severity. Ten different gouges of increasing severity were introduced into pressurized pipeline sections. Queen's AMG personnel conducted MFL measurements on the samples, from both the outside (pressurized and unpressurized) as well as the inside (unpressurized). One pipeline was pressure cycled with MFL measurements taken at periodic intervals. The experimental MFL measurements were compared with geometry-only MFL magnetic models. The stress distribution could not be included in the magnetic models since it is not known (it was not possible to accurately reflect the gouging process using structural models).
- To conduct neutron diffraction measurements on gouged and gouged+dented, GdF Suez PAR -produced pipe sections in order to determine the residual stress distribution. This information had two purposes – 1) to augment the gouge+dent database being compiled as part of MD 4-2; 2) to determine the residual stress distribution in order that it could be used in the magnetic modeling of these defects. MFL measurements were also conducted on these samples.
- To incorporate these results (modeled and measured) into the web-based MFL signal library database developed in the earlier phases of the study.

4.0 Work Plan for Phase III

Specific elements of the work plan for the project period starting January 1, 2008 and ending August 30, 2010 are outlined in task list (PHMSA payable milestones table) shown below.

Item #	Task #	Activity/ Deliverable	Quarter#
36	6.1	Renew MFL magnetic modeling software	VI
37	9.1	Upgrade MBN equipment for gouge magnetic characterization	VII
38	9.2	Produce test gouges in steel plate samples	VII
39	13.1	Structural modeling of stress patterns around dents in MD1-1 pull test samples	VII
40	13.3	Meetings of the Mechanical Damage working group	VII
41	5	Pipeline Safety Research Peer Review	VII
42	4	Eleventh Quarterly Status Report and Technical Committee Mtg.	VII
Mar-08		**Eleventh Payable Milestone**	**VII**
43	9.3	MBN probe characterization of the deformed material	VIII
44	9.4	Measurement of MFL signals from the test gouges	VIII
45	9.5	Determine magnetic response parameters	VIII
46	13.2	Magnetic modeling of MFL signals (geometry and stress components) from MD1-1 dents	VIII
47	13.3	Meetings of the Mechanical Damage working group	VIII
48	4	Twelfth Quarterly Status Report and Technical Committee Mtg.	VIII
Jun-08		**Twelfth Payable Milestone**	**VIII**
49	9.6	Develop gouge models and compare magnetic response to the experimental data obtained in Subtask 9.4	IX
50	13.3	Meetings of the Mechanical Damage working group	IX
51	4	Thirteenth Quarterly Status Report and Technical Committee Mtg.	IX
Sep-08		**Thirteenth Payable Milestone**	**IX**
52	8.3	Add results of tasks 9 and 10 to database	X
53	10.1	MFL Measurements on gouged pipeline sections at Gaz de France	X
54	10.2	Analyze and model Gaz de France results	X
55	13.3	Meetings of the Mechanical Damage working group	X
56	4	Fourteenth Quarterly Status Report and Technical Committee Mtg.	X
Dec-08		**Fourteenth Payable Milestone**	**X**
57	4	Fifteenth Quarterly Status Report and Technical Committee Mtg.	XI
Mar-09		**Fifteenth Payable Milestone**	**XI**
58	5	Pipeline Safety Research Peer Review	XII
59	6.1	Renew MFL magnetic modeling software	XII
60	11.1	Structural modeling of dents produced by SES gouging procedure	XII
61	11.3	SES to procure 5 pipeline sections of Grade X42 steel from same steel batch, weld end caps	XII
62	11.4	MFL magnet system components procured (magnets) or constructed (backing iron, shaped pole pieces) and sent to SES Houston facility. Necessary modifications made to MFL scanning system	XII
63	12.1	Prepare and submit proposal to CNBL for residual strain measurements on sample P22	XII
64	4	Sixteenth Quarterly Status Report and Technical Committee Mtg.	XII
Jun-09		**Sixteenth Payable Milestone**	**XII**
65	11.2	MFL modeling of SES gouges	XIII
66	11.5	SES to introduce gouges into each sample – two different pressures, 5 different depths	XIII

67	11.6	MFL measurements made at SES Houston by Queen's MFL team	XIII
68	12.3	Prepare and submit proposal to CNBL for residual strain measurements on sample BEA159	XIII
69	4	Seventeenth Quarterly Status Report and Technical Committee Mtg.	XIII
Sep-09		**Seventeenth Payable Milestone**	**XIII**
70	11.2	MFL modeling of SES gouges	XIV
71	11.7	Analysis of MFL signals from experimental and modeled SES gouges	XIV
72	11.8	Pressure Cycling of one of the SES gouged test sections	XIV
73	11.9	MFL testing of SES gouged+cycling samples and analysis of results	XIV
74	12.5	Prepare and submit proposal to CNBL for residual strain measurements on sample BEA161	XIV
75	4	Eighteenth Quarterly Status Report and Technical Committee Mtg.	XIV
Dec-09		**Eighteenth Payable Milestone**	**XIV**
76	11.7	Analysis of MFL signals from experimental and modeled SES gouges	XV
77	12.6	Conduct residual strain measurements on P22 and analyze data	XV
78	4	Participation in PRCI Peer Review Meeting	XV
79	4	Nineteenth Quarterly Status Report and Technical Committee Mtg.	XV
Mar-10		**Nineteenth Payable Milestone**	**XV**
80	12.6	Conduct residual strain measurements on BEA159 and analyze data	XV
81	4	Twentieth Quarterly Status Report and Technical Committee Mtg.	XV
Jun-10		**Twentieth Payable Milestone**	**XV**
82	12.6	Conduct residual strain measurements on BEA161 and analyze data	XV
83	4	Twenty First Quarterly Status Report and Technical Committee Mtg.	XV
Sep-10		**Twenty First Payable Milestone**	**XV**
84	4	Final report/documentation and presentation on Tasks 8 through 13	

5.0 Results: Determination of the magnetic contribution of the highly deformed surface layer at the base of the gouge

5.1 The origin of MFL signals from gouges

The investigation covered by this phase of the project focuses on understanding the origin of MFL gouge signals. In some cases, these gouges may have little or no associated dent; in many other cases denting is also present. MFL signals from gouges tend to be complex, since magnetic behavior is a function of material properties, stresses and component geometry. Specifically for gouges, the possible contributing factors to MFL signals are as follows:

1) The geometry of the gouge, including exfoliation, metal removal, edges and corners
2) Residual stresses created by the gouging process
3) The severe plastic deformation layer at the base of the gouge resulting from direct tool contact

In addition, if there is denting associated with the gouge then the following may also contribute:

4) The dent geometry
5) The residual stresses associated with the dent

The contribution of the severe plastic deformation layer (#3 above) is considered in this section (beginning in Section 5.3). Geometrical effects (#1 above), dents (#4 above) and stress effects (#2, 3, and 5) are discussed in Section 6, where the results of a study of gouges of progressive severity are reported. Section 7 reports on a residual stress study (#2 above) where, for selected gouges, residual stress patterns were measured using neutron diffraction. Finally, in section 8, a summary of the results is used to model GdF Suez gouge BEA161 and compare these modeled signals with experimental results.

5.2 Previous studies of MFL signals from gouges

Although various "single sample" MFL measurements have been made on experimental and field samples to date, no systematic study had been conducted to study the origin of MFL signals from gouges. Limited work from earlier studies[5.10,11] suggests that gouging may produce a characteristic "axial dipole" signal such as those seen in **Figure 5-1**. The top diagram in **Figure 5-1** is a MFL (axial) result from a study by Battelle[11], where the dipole was assumed to be associated with a "plowing" and a "gouging" effect. The middle MFL (axial) signal result is from the dual field tool study by Rosen[10]. Lastly, the result at the bottom of **Figure 5-1** was obtained from a gouge sample from GdF Suez as part of Phase II of the current contract. The plowing/gouging feature can be identified in each of these plots.

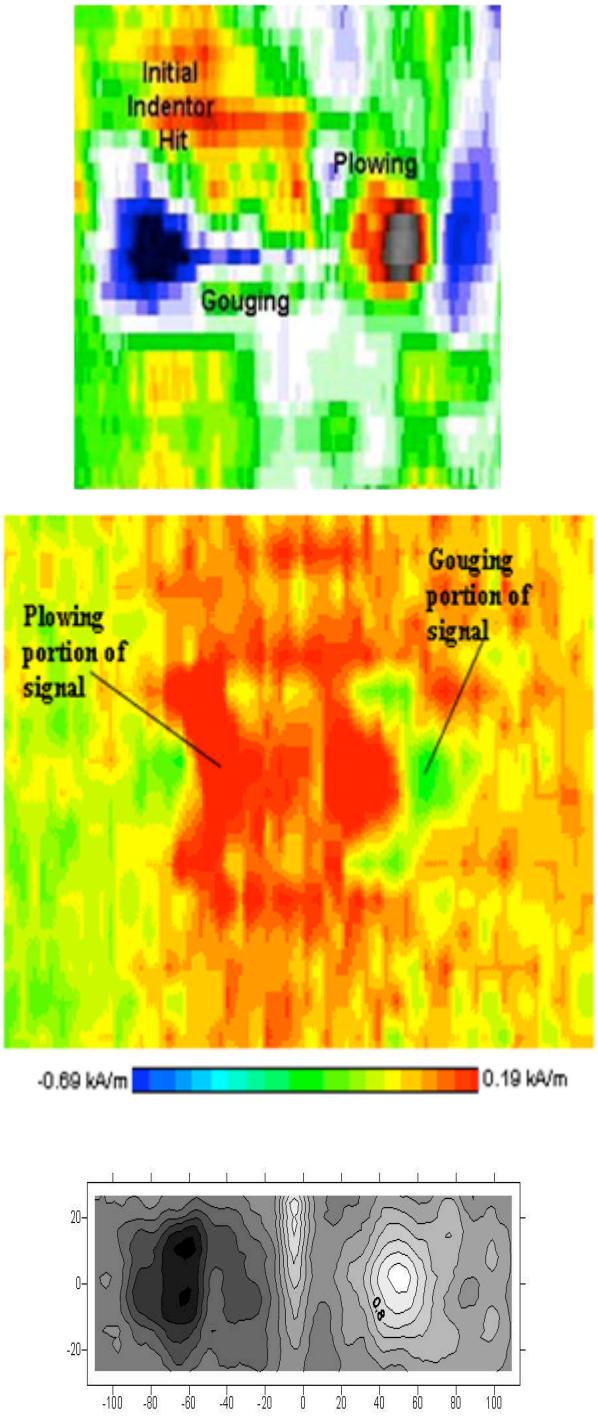

Figure 5- 1: MFL(axial) signals obtained from earlier work. In general these results suggest that a "dipole" signals is characteristic of the MFL(axial) signal for gouges – with one end of the dipole associated with the "plowing" end of the gouges and the other with the "gouging" end. Top: from Battelle (ref 11) Middle: from Rosen (ref 10) Bottom: from measurements as part of Phase II of the current contract – sample from GdF Suez.

5.3 Studies of the magnetic signals originating from severe, thin plastic deformation layers on steel plate

By its nature, gouging involves a scraping mechanism along the outer pipe surface. The tool pressure plus movement produces severe damage at the immediate contact point, and material from the tool may even be transferred to the pipe wall. These changes will undoubtedly affect the magnetic properties of this contact region and thus are likely to influence the MFL signal. However, this severe plastic deformation region is known to be very thin – typically less than 100μm[12]. Furthermore, as the gouge is nearly always located at the pipe outer surface, the MFL signal associated with this severe deformation layer may not extend to the interior pipe wall where it can be detected during an MFL inspection. [n.b., this severe plastic deformation region should not be confused with the residual stresses produced during the gouging process. Residual stresses are longer range stresses associated typically with the pipe wall bending inwards during contact, and then springing back afterward. These residual stresses can be measured using neutron diffraction and will be discussed in Section 7.]

This portion of the contract work was devoted to understanding the contribution of a thin, severely plastic deformed surface region to the MFL signal. In earlier studies involving the Applied Magnetics Group, the Magnetic Barkhausen Noise (MBN) technique has been used successfully to characterize the magnetic properties of pipe walls and explain MFL behavior. In what follows we describe MBN and MFL studies on thin regions of surface plastic deformation in plate samples, then draw conclusions as to the contribution of this layer to an the inner wall MFL signal.

5.3.1 Experimental technique

5.3.1.1 The Magnetic Barkhausen Noise Technique

The MBN technique has been used often by the AMG to characterize pipe wall magnetic behavior and thus assist in interpreting MFL signals. The method involves applying an oscillating magnetic field to a sample. As the sample is magnetized in one direction and then the other, magnetic domains move within the sample. The moving domain walls are pinned and then released, which gives rise to a high-frequency magnetic "noise" pulse which can be detected by a search coil located at the sample surface. The MBN probe is small (2-3 cm across) and the detector measures magnetic behavior on the scale of millimeters. Thus MBN can be used to measure the relative magnetic behavior of local regions on a sample surface.

A typical MBN probe is schematically illustrated in **Figure 5-2** (top) along with the MBN signal it generates (bottom). A ferromagnetic C-core is wound with an excitation coil, which is used to create an alternating magnetic field in the C-core and sample, with the feedback system used to ensure a consistent flux in the sample. The discontinuous changes in the sample during magnetization generate a signal in the small sensor coil placed between the poles of the magnet. This signal is amplified, filtered and input into a digital oscilloscope for analysis. The MBN signal envelope at the bottom of **Figure 5-2** is obtained over one full magnetization cycle.

The parameter used by the AMG to characterize this signal is the "MBN energy" defined as the time integral of the square of the voltage over the MBN envelope.

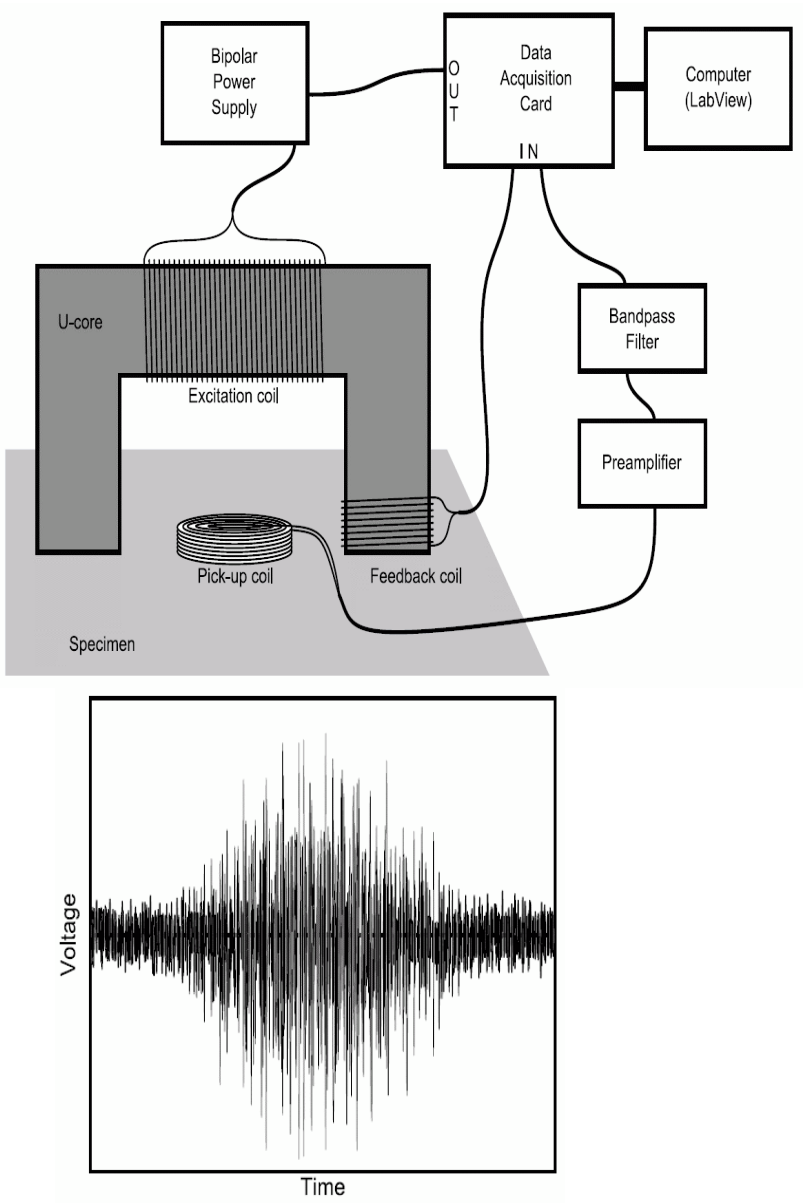

Figure 5- 2: (top) schematic diagram of Magnetic Barkhausen noise equipment, and (bottom) a typical Barkhausen noise envelope obtained over one full magnetization cycle.

The MBN signal is sensitive to many material parameters, but in general reflects the magnetic permeability of the immediate surface in a specific direction. A lower permeability region may produce MFL signals under certain conditions so the MBN result can be used to inform MFL interpretation.

5.3.1.2 Samples and Experimental techniques

The goal of these experiments was to obtain MBN and MFL measurements from samples that contained only a region of localized, plastic deformation, but nothing else that would contribute a "magnetic" signal. Mild steel plate of 5 mm thickness was used as the sample material, however producing surface deformation proved to be somewhat problematic, since it is difficult to produce severe localized deformation without also creating a geometry effect or bending the plate (which produces residual stresses). However the results still proved to be interesting and useful. The samples that were considered include:

- **SiC scratched samples:** These flat plate samples were scratched uni-directionally with varying grades of SiC sandpaper in a localized region, and then measured with MBN and MFL techniques.

- **Backhoe gouged samples:** These flat plate samples were subjected to gouging with a backhoe. The backhoe tooth was placed on the sample and dragged backwards. A number of such gouges were produced, and MBN and MFL measurements were conducted on all. Two examples were selected for discussion below. Note that the backhoe pressure also created some bending in the samples. While this did not influence the flat plate results significantly, it did emphasize the need, when studying gouges, for large-scale equipment (such as that available at GdF Suez or Stress Engineering Services) to produce gouges having characteristics like those seen in the field.

- **Grinding wheel gouges**: A number of attempts were made to produce grinding wheel surface deformation without simultaneously introducing a geometry (metal-loss-type) defect. Unfortunately this was not successful, with all MFL results exhibiting metal-loss signal patterns. Thus these results are not discussed here.

5.3.2 Results of plastic deformation studies: SiC scratching

The flat plate samples were scratched in a local (~3 cmx3 cm) region using different grades of SiC paper: 400, 220, 180 and 80 grit. The results of the 80 grit scratched region are presented below since they represent the most significant scratches and thus the largest effect.

MBN and MFL field perpendicular to scratches: **Figure 5-3** shows the MBN results, and **Figure 5-4** shows the MFL results, respectively, for the 80 grit SiC scratches. In this situation it is important to note that the MBN field and the MFL field are applied perpendicular to the scratches. In **Figure 5-3,** the photo shows the scratched region which has scratches running vertically. The MBN probe traverses with the magnetic field aligned along the axial direction (perpendicular to the scratch direction-note the glyph at the bottom of the graph showing the pole piece orientation). The dashed arrow in the photograph indicates the direction of MBN probe travel – from the unscratched into the scratched region. The MBN signal clearly diminishes as the probe moves into the scratched region. This would normally suggest that a decreased permeability exists in the scratched region, at 90^{o} to the scratches. However care must

be taken with this interpretation since it is also possible that the MBN signal drops because the scratches reduce the magnetic coupling into the sample in this region.

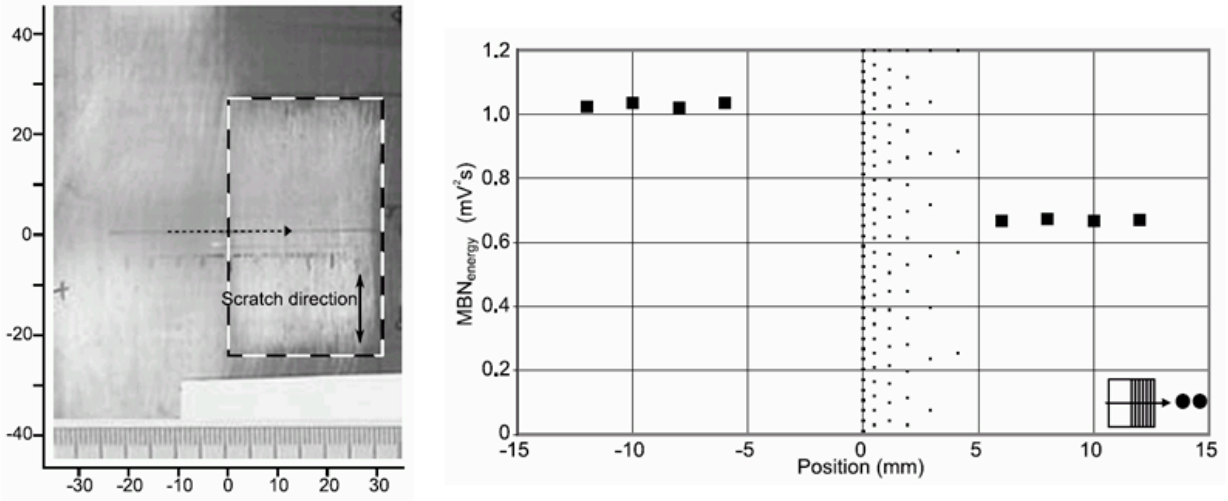

Figure 5- 3: Photo of the 80 grit SiC scratched region (left) and the result of the MBN probe scan across this region (right). Glyph at lower right hand side indicates scan direction and direction of probe field compared to scratch direction (perpendicular).

Figure 5-4 shows the MFL (axial) and MFL (radial) signals taken at the top surface over this scratched region (again, with the MFL applied field perpendicular to the scratches). Features A, B (in the MFL(radial) signal as well as C (in the MFL(axial) signal are readily identifiable peaks that appear to be associated with the scratched region, thus the scratches appear to have created an MFL signal in this case.

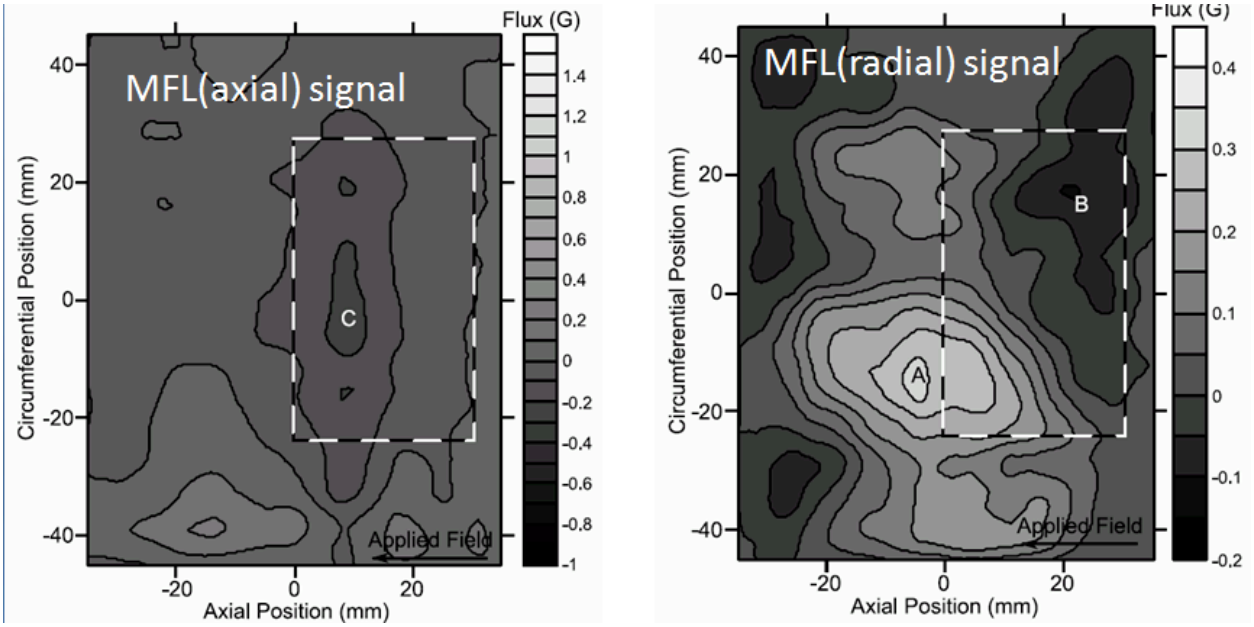

Figure 5- 4: MFL (axial) and MFL (radial) component signals taken from the top surface. The MFL and MBN field are both applied opposite to the direction of the scratches.

Finally it is important to note that MFL measurements were also taken at the opposite side of the wall (i.e. on the inside surface). This MFL scan yielded no features, nor any variation in the MBN signal.

MBN and MFL field parallel to scratches: **Figure 5-5** and **5-6** show a similar series of diagrams to that of **Figures 5-3** and **5-4**, however in this case the MBN and MFL applied field directions are parallel to the scratches (note the difference in the glyph at the bottom right of **Figure 5-5**). The MBN result, as in **Figure 5-3**, indicates that the MBN signal is once again lower in the scratch region, even in this orientation. Since it is unlikely that the permeability in this region is lower in both parallel and perpendicular directions, this result suggests that the MBN signal is diminished because of a reduced detector coupling in this region.

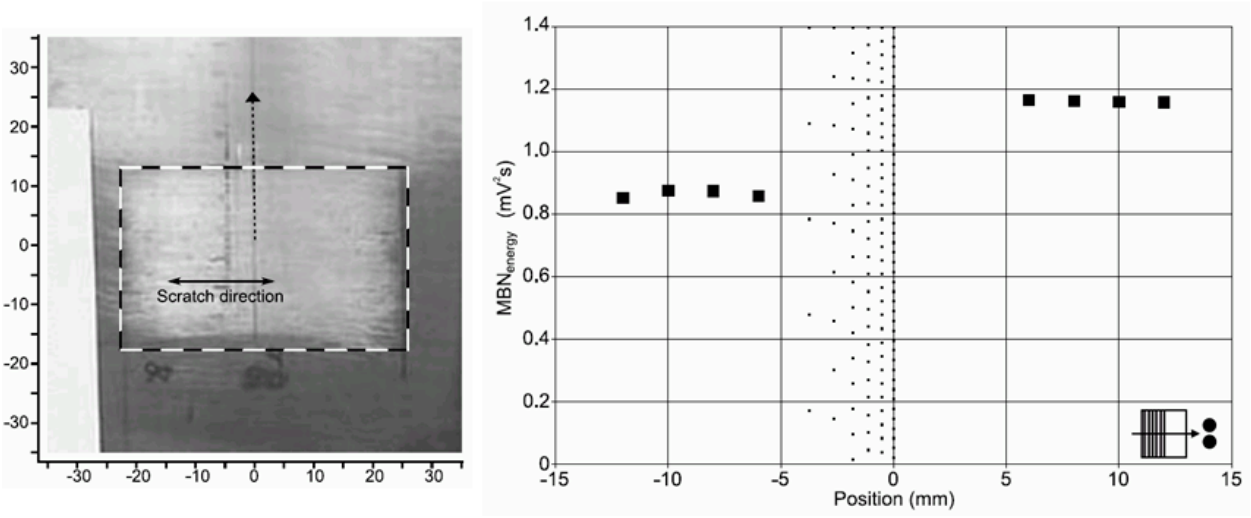

Figure 5- 5: Photo of the 80 grit SiC scratched region (left) and the result of the MBN probe scan across this region (right). Glyph at lower right hand side indicates the direction of the probe field compared to scratch direction (parallel). Note that the direction of the scan of the MBN probe is perpendicular to the scratches, even though the MBN applied field is parallel to the scratches.

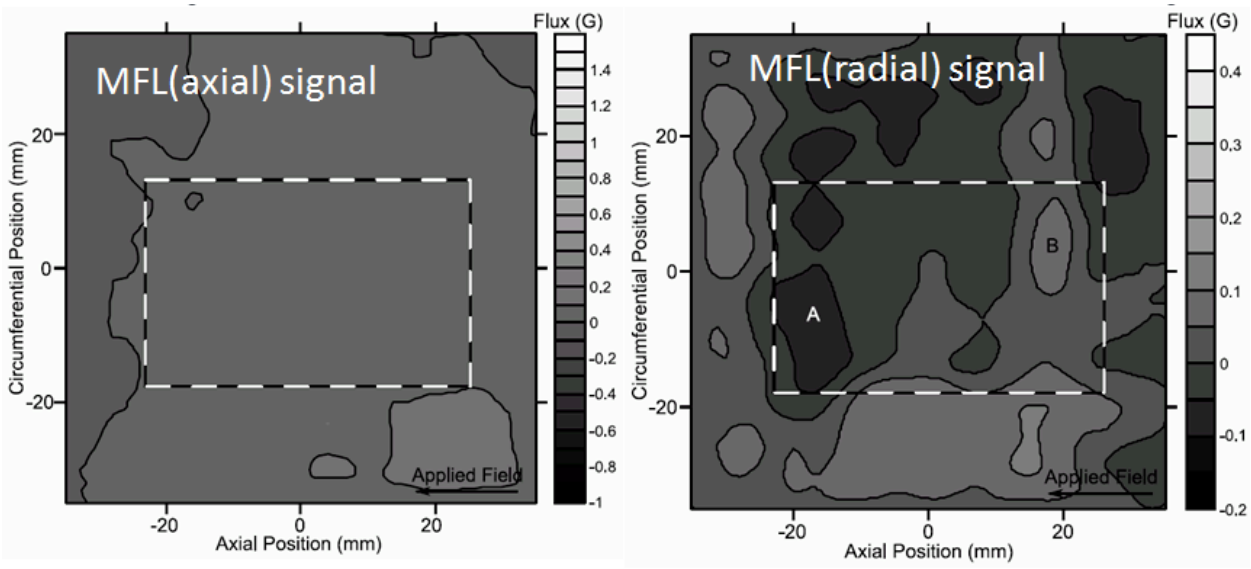

Figure 5- 6: MFL (axial) and MFL (radial) component signals taken from the top surface. The MFL and MBN field are both applied in the same direction as the scratches.

Figure 5-6 shows the MFL (axial) and MFL (circumferential) results for the case where the MFL applied field lies parallel to the scratches. Comparing this result with **Figure 5-4** (perpendicular to scratches) indicates a significant difference – for the parallel case there is essentially no signal, compared to a small but noticeable signal for the perpendicular case (**Figure 5-4**). Once again no MFL signal was detectable on the inside surface of the plate.

Thus we conclude that, although the information available from the MBN study is limited, under some conditions MFL is able to detect even these very minor surface scratches when the MFL technique is applied on the same side as the damage. However no MFL signal for this damage can be detected at the inner wall.

5.3.3 Results of plastic deformation studies: Backhoe-damaged flat plate samples

Backhoe damage – MFL perpendicular to the scratch direction. The second study involved examining backhoe damage from these flat plate samples. As mentioned above, a backhoe was used to create scratching at the surface of the flat plate. The backhoe produced significant visible scratches (examples of which are seen in **Figure 5-7** and **5-9**) however there was no gouging apparent and the scratch depth was estimated to be only about 0.2mm.

Figure 5-7 includes a photo of a selected region of backhoe damage, with two adjacent scratches. In this case the MBN result, as in the previous scratched samples, indicates a drop in signal in the damage region. Again, this is likely a result of a coupling effect, rather than a true permeability change (note that in this case the only measurement available was with the MBN field parallel to the scratches).

Of more interest are the MFL axial and radial signals for these scratches, shown in **Figure 5-8**. There is a clear indication for the MFL (radial) signal; however the MFL (axial) signal is much smaller and harder to distinguish. Again, no indication of MFL signal could was observed when a measurement was made on the inner surface of the flat plate.

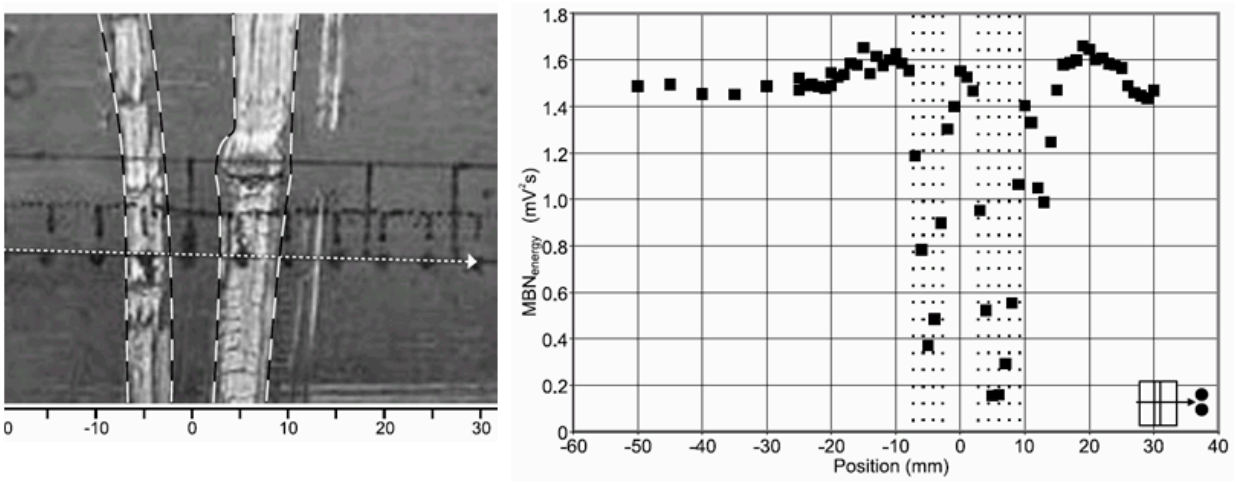

Figure 5- 7: Photo (left) of one of the backhoe – damaged regions, showing the path of the MBN probe. The MBN result is shown on the right. Note that in this case AND in the following one (Figure 6.9) the MBN probe is aligned parallel to the backhoe scratches (see glyph bottom right) – even though the MFL result (below) is obtained with the MFL field perpendicular to the scratches.

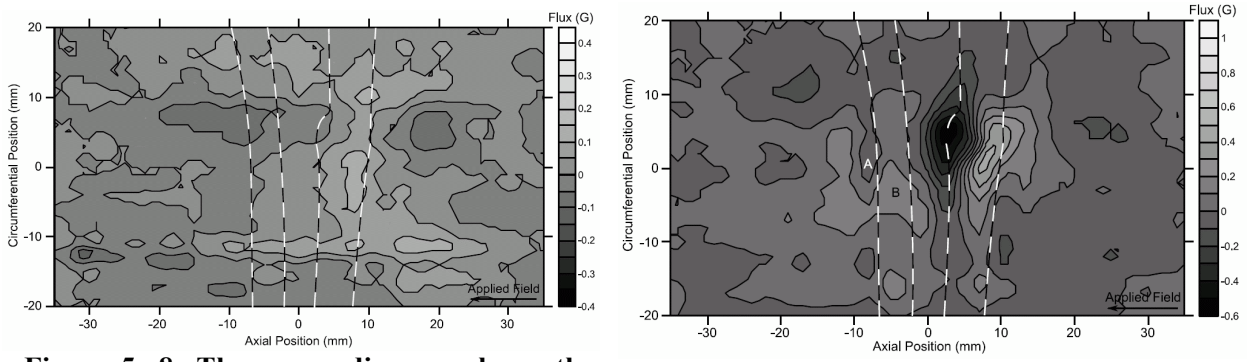

Figure 5- 8: The upper diagram shows the MFL(axial) and the lower diagram the MFL(radial) component signals measured at the tup surface of the plate. The MFL field here has been applied perpendicular to the scratch direction.

<u>Backhoe damage – MBN and MFL parallel to the scratch direction.</u> **Figure 5-9** shows another typical backhoe scratch from the present study. The white arrow indicates the direction in which the MBN scan was performed (with the MBN applied field again in the same direction as the scratches). The MBN result shown on the left, as with the other results, indicates a drop in signal as the probe passes the scratched region.

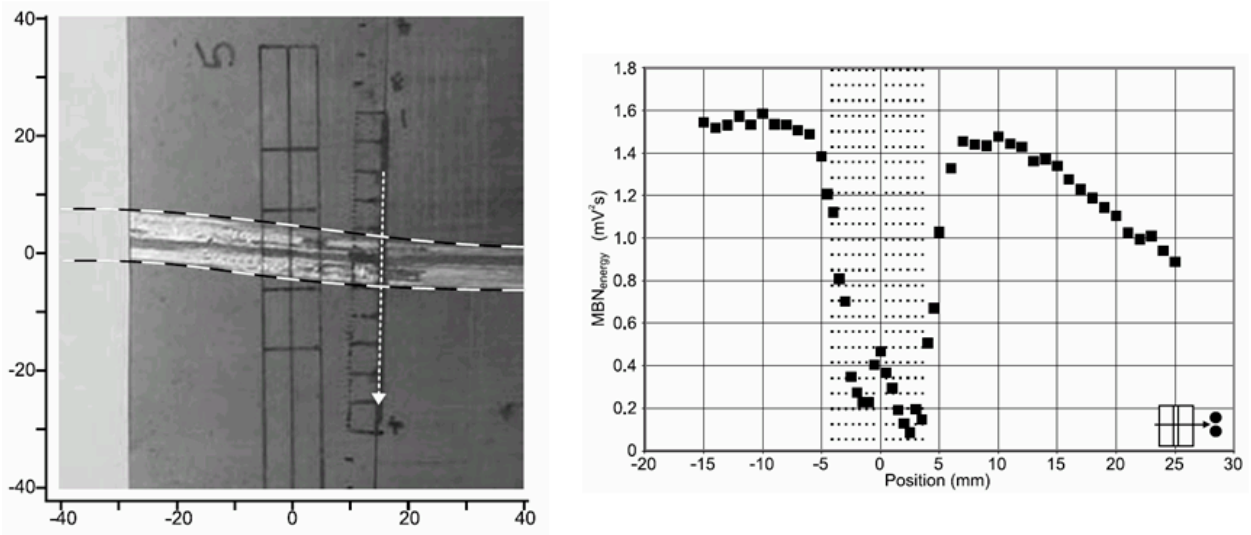

Figure 5- 9: Photo (left) of another of the backhoe – damaged regions, showing the path of the MBN probe. The MBN result is shown on the right. Note that in this case the MBN probe is aligned parallel to the backhoe scratches (see glyph bottom right).

Figure 5-10 shows the MFL signal from these backhoe scratches; in this case with the MFL applied field parallel to the scratch direction. Once again, an MFL signal is clearly seen in the MFL (radial) case, and for this scratch there is also a significant MFL (axial) signal (peaks are labeled with letters). As in the other scratched samples, no MFL indication of these scratches could be seen on the inner wall of the flat plate samples.

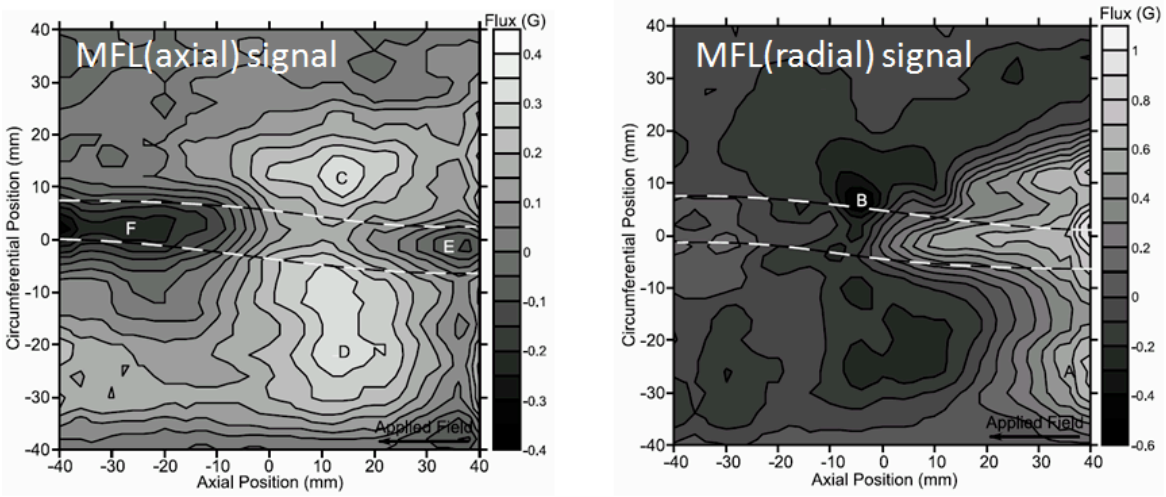

Figure 5- 10: MFL (axial) and MFL (radial) component signals taken from the top surface. The MFL field here has been applied parallel to the scratch direction.

5.3.4 Conclusion: Studies of the magnetic signals originating from severe, thin plastic deformation layers on steel plate

At the outset, this study was intended to use the MBN technique to characterize the magnetic parameters for the severely deformed material which typically exists at the base of a gouge. However most of the results indicate a consistent decrease in MBN signal (regardless of the MBN field direction), which is more likely a result of a liftoff issue rather than a change in magnetic permeability. Thus, the MBN results were inconclusive.

However, the MFL measurements on the scratched sample did prove to be informative. MFL was found to be very sensitive to surface deformation, as it was able to detect very minor damage (80 grit SiC scratches). Similarly, the backhoe-produced scratches were also readily detected using MFL. The conclusion from this study, therefore, is that the severe deformation at the base of a gouge is likely to contribute to the MFL signal provided the MFL measurement is done on the SAME surface as the gouge. Conversely, in the present study no MFL signals corresponding to the scratches were observed when the MFL probe was on the OPPOSITE (inner wall) surface. The flat plates used for this study were only 5mm thick – which is thinner than what is normally used for pipe wall (typically at least 9mm). The overall conclusion, therefore, is that during a typical MFL field inspection (normally done from the inside of the pipe) it is unlikely that a thin region of severe deformation at the base of a gouge will contribute to the observed MFL signal.

6.0 Results: MFL Measurements and Modeling of Gouged samples produced at Stress Engineering Services

6.1 Introduction

Work summarized in Section 5 indicated that, when studying gouges or gouges+dents it is necessary to produce these defects in a realistic manner that emulates a true 'field damage' experience. Thus the next stage in the contract work included enlisting the services of Stress Engineering Services (SES) in Houston Texas to produce realistic gouged samples. SES has an excellent track record of working with researchers and has the equipment necessary to produce gouges in full-sized, pressurized pipeline sections. The work conducted at the SES facilities was a systematic study of gouging, where gouges of progressively increasing severity were introduced into pressurized pipeline sections. For these experiments a number of parameters (tool shape and size, pipe material, etc) were held constant. In addition, one of the samples was used for a pressure cycling study, during which MFL measurements were made after specific cycling intervals.

Ten gouges were produced for this study. Gouges were introduced under internal pressures of either 50% or 100% maximum allowable operating pressure (MAOP). Subsequent outer wall MFL measurements of these gouges were conducted in Houston while the pipe was under pressure (50% MAOP). The pipes were subsequently cut and pipe sections containing the defects were sent to Queen's for additional "zero pressure" outer wall, as well as inner wall MFL measurements. Since MFL scans were conducted for two components (axial and radial) and under three different conditions (outer wall pressurized, outer wall unpressurized and inner wall unpressurized), there were approximately 50 scans done overall. Furthermore, in order to make effective comparisons between the results, it is necessary to examine the plots at different scales. Thus all 50 scans are presented at three different MFL signal scales: -1 to +1 Gauss, -3 to +3 Gauss, and -5 to +5 Gauss. This yields a total of 150 separate MFL scan results. Since it is not possible to include all of these in the body of the report, these scans at these different ranges are included in three separate sections in Appendix A. Individual plots will be extracted and reproduced for the discussion below.

6.2 Gouging Apparatus, Samples and Experimental Parameters

Figure 6-1 shows equipment available at SES for introducing mechanical damage into a pressurised pipe section. **Figure 6-2** includes example photographs of the example gouges, taken from different angles. **Table 6-1** summarizes the gouge introduction parameters and the resulting gouge features.

The pipe samples were X42 grade steel, 12 in. diameter, with 9.2 mm wall thickness. Pipe sections were cut 5m long and caps were welded on the ends to allow the pipes to be

pressurized. As shown in **Figure 6-1**, the end-capped, pressurized pipe section was secured onto a moving platform, and connected at one end to a hydraulic cylinder via chains. The gouging tool (shown in **Figure 6-1** inset upper right) is hydraulically lowered into the pipe wall to a pre-determined displacement below the original pipe wall position (indicated in the "Gouging depth during gouging" column in **Table 6-1**), then the pipe is pulled to the left, creating a gouge. The inset photographs at the lower right of **Figure 6-1** shows the tool in the pipe wall during the gouging process, for a tool displacement of 6.4 mm (250 mils).

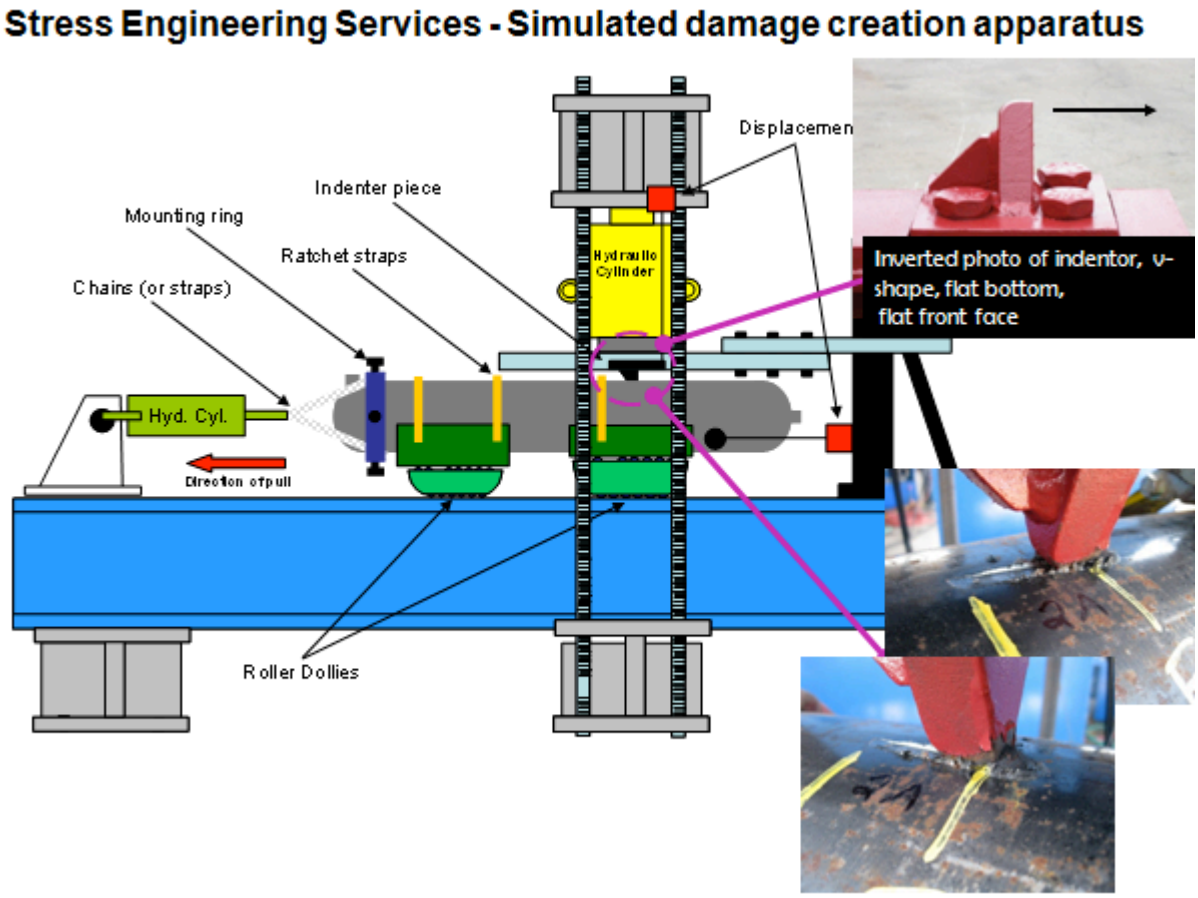

Figure 6- 1: The simulated damage creation apparatus at SES in Houston. Sample:s are 12 in diameter, 5 m long pipeline sections, end capped, and pressurized pressurized. The tool (shown inverted, upper left) is pressed into the pipe surface by the hydraulic cylinder (yellow) and then a pulled with chains towards the left hand side of the diagram as shown. The insert photographs at the lower right show the tool in the process of gouging for gouge 2A.

All gouges were introduced while the pipe sections were internally pressurized. As seen in **Table 6-1**, two pressures were used during gouge introduction, corresponding to 50% and 100% MAOP. In addition, one of the gouged pipe sections (pipe 3) was used for a pressure cycling study. Two gouges were introduced into each pipe: initially the pipe was pressurized to 100% MAOP and one gouge was introduced (these are termed the "A" gouges – gouge 1A, 2A, 3A, 4A, 5A). After this the pipe was rotated 180^{o}, the pressure lowered to 50% MAOP, and a

second gouge introduced (thus the two gouges are opposite one another in the pipe section). This lower pressure gouge series is identified as the "B" gouges (1B, 2B, 3B, 4B, 5B).

Table 6-1: Parameters for gouges introduced using the SES simulated damage apparatus

Pipe #	Gouge #	Internal Pressure (psi) 100% MAOP 50% MAOP	Fatigue Cycles	Gouge Depth during gouging mm (mils)	Residual gouge depth (deepest point) Measured relative to the original wall position (mm)	
1	1A	1780	No	2.5 (100)	0	barely a scratch
	1B	890	No	2.5 (100)	0	
2	2A	1780	No	6.4 (250)	1.5	
	2B	890	No	6.4 (250)	2	
3	3A	1780	Yes	6.4 (250)	-	pressure cycled
	3B	890	Yes	6.4 (250)	-	
4	4A	1780	No	9.5 (375)	3.5	
	4B	890	No	9.5 (375)	5	
5	5A	1780	No	12.7 (500)	8	
	5B	890	No	12.7 (500)	6	

The visible mechanical damage resulting from the gouging process varied considerably. The shallowest gouges in Pipe 1 (gouges 1A and 1B), were not gouges at all; the gouging process left only what appeared to be a scratch on the sample. Pipes 2 through 5 had gouges that resembled that seen in **Figure 6-2**, with varying depths. In terms of associated denting, Pipes 1 through 3 displayed little or no denting with the gouge damage, however the deepest gouges in Pipes 4 and 5 had some associated denting, with the most significant denting apparent at the tool entry location. No pipes failed during or after the gouging process.

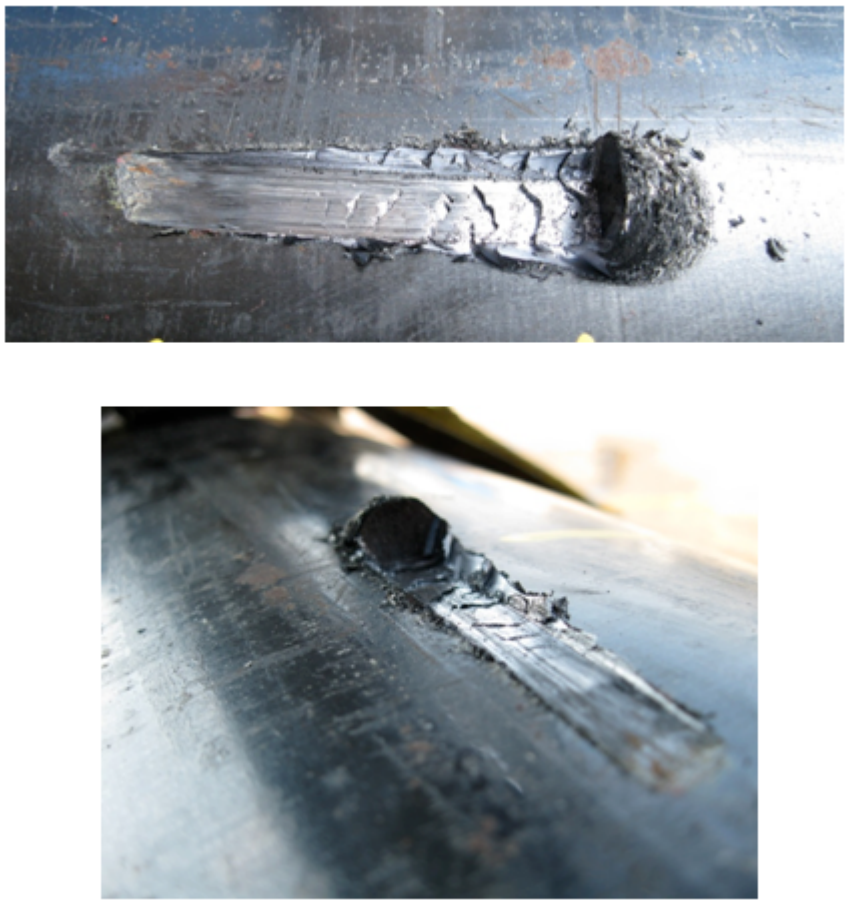

Figure 6- 2: Two examples of typical gouge geometries produced using the SES gouging apparatus, shown at different angles. The length of the gouge is approximately 5cm. Note that the gouging process did not produce this gouge geometry in the Pipe 1 samples – in fact the samples appeared barely scratched.

For the outer wall measurements, the MFL probe had to negotiate significant geometrical obstacles as it passed over many of the gouges during the scans. In order to avoid the probe getting hung up on these geometry features, (such as the large region of exfoliated material, or in the hole left by the gouge) modeling clay was used to provide a smooth path for the detector to traverse the defect. A typical example of defect covered in the modeling clay is shown in **Figure 6-3**. The clay was only necessary on the outer wall, since the inner wall retained a smooth contour.

Figure 6- 3: Photograph of the gouge defect 5B, which has been covered with clay to allow a smooth path for the MFL detector probe.

MFL measurements were made initially in Houston on the pressurized pipe section, at the outer wall surface, with the internal pipe pressure at a level corresponding to 50% MAOP. (Note that the designation "50% MAOP" and "100% MAOP" in Table 6.1 refer to the internal pipe pressure during the *gouging process***,** not during MFL measurements. All MFL measurements in Houston were done at 50% MAOP). The pipe wall was magnetized (to magnetic saturation ~ 1.8T) using a stationary permanent magnet housing mounted on the outer pipe wall. MFL measurements were made by XY scanning a Hall probe over the region of interest. Hall probes were mounted such that measurements were obtained for both the radial and axial MFL signal components. As mentioned in earlier sections, axial MFL signals are the ones most commonly used for field measurements, however radial MFL signals are also very useful; the radially-oriented probe has less liftoff than the axial probe (due to the intrinsic nature of the probe geometry) and thus the radial signal is stronger and displays some of the more subtle features not seen with the axial probe.

The MFL background result was subtracted from the MFL gouge signal measurements - both in the "x" and "y" directions. The background signal results from the detector measuring a signal in close proximity to the magnet pole pieces, as the pole pieces create a sloping background signal from the positive to the negative end. The slope of the background signal is roughly linear, thus it can be approximated as such and subtracted from the 'raw' MFL signal. For example, the "x" direction subtraction is done by drawing a line between the MFL signal values at the extreme x positions along a given scan line. The values corresponding to the line are considered to be "background" and are subtracted from the MFL signal. The same procedure is carried out for the "y" direction. Occasionally, near the extreme ends of the scans the linear approximation breaks down and large peaks of opposite polarity are seen (these will be noted

when they appear). Finally, standard software smoothing routines were used to smooth the data before presentation.

After completion of all of the outer wall MFL measurements done with the pipe at 50% MAOP, pipe rings were cut in order to be able to make MFL measurements at the inner pipe wall. The pipe ring samples (cut to lengths approximately 60cm long with the gouges centered along the length) were shipped to the Queen's research labs where MFL measurements were done (at zero internal pressure) on the inner wall. MFL measurements were also repeated at the outer wall under this zero pressure condition in order to compare the "pressurized vs. zero pressure" cases. Note that the designation "50% MAOP" and "100% MAOP" refer to the internal pipe pressure during the *gouging process***,** not during MFL measurements. All MFL measurements were either done at 50% MAOP or at zero pressure.

Finally, it should be noted that some of the measurements done in the Queen's AMG lab were conducted at slightly higher flux density than those in Houston. The inner wall MFL signals for gouges are smaller than those measured at the outer wall, since the gouge geometry is localized at the outside of the pipe, thus the signal is diminished and broadened as it passes through the pipe wall. As such, the decision was made to strengthen the magnetic field in some cases in order to be able to see more clearly some of the specific features of the inner wall MFL signals. The figure captions for the plots in Appendix A, indicate the MFL signals obtained using the higher field.

In this study, however, we are primarily interested in the *features* (peaks) that are present in the signals, rather than the absolute magnitude of the signals. So care should be taken when attempting to compare the absolute signal magnitude between MFL scans.

In the following, Sections 6.3 to 6.6 consider the results from Pipes 1, 2, 4, and 5. Pipe 3 was pressure cycled, and the pressure cycling results will be considered separately at the end of Section 6.7.

6.3 Comparison of outer wall MFL signal results: The difference between MFL measurements done "at pressure" vs. MFL measurements done on unpressurized samples

Table 6.1 indicates that the gouges designated "A" were introduced at 100% MAOP, and those designated "B" were introduced at 50%MAOP. After gouge introduction the pressure was reduced to zero. Outer wall MFL measurements in Houston were done after re-pressurizing the pipes to 50% MAOP. Later, however, after the pipes were cut and sent to Queen's, measurements were necessarily done at zero internal pressure. This section compares the outer wall MFL measurements of the same region at 50% MAOP compared to the same measurement done at zero internal pressure.

In the results compilation in Appendix A, the outer wall pressurized (50% MAOP) scan results are shown at the top of each page, the outer wall zero pressure results are shown in the center, and the inner wall zero pressure scan results are at the bottom. Thus, it is possible to determine whether or not the same features (peaks, etc) are present for the outer wall scans, with and without pressure.

When examining the MFL results for pressurized vs. unpressurized, one might expect to see fewer isolated "features" for the pressurized pipe, since the internal pressure makes the overall wall stress higher and more consistent. Thus, fewer "stress anomalies" should be present. What we observe is that there are differences between the pressurized and unpressurized outer wall results, however the main features are similar and there is no consistent trend observed between the two cases. **Figures 6-4** and **6-5** show a comparison of outer wall MFL(axial) results for the pressurized (top) vs. unpressurized (bottom). In **Figure 6-4** the unpressured sample (bottom) appears to yield a more detailed MFL result, however the opposite is seen in **Figure 6-5**. The differences in features between pressurized and unpressured sample scans are more likely caused by the fact that at the outer wall the detector housing must travel over the large geometrical features of the gouge, which may shift the detector somewhat sideways or turn it slightly. This is likely to have a more significant effect on the fine details of the scan than the pressurization condition does. However the main point is that the same peaks and basic features are generally present in both the pressurized and unpressurized cases.

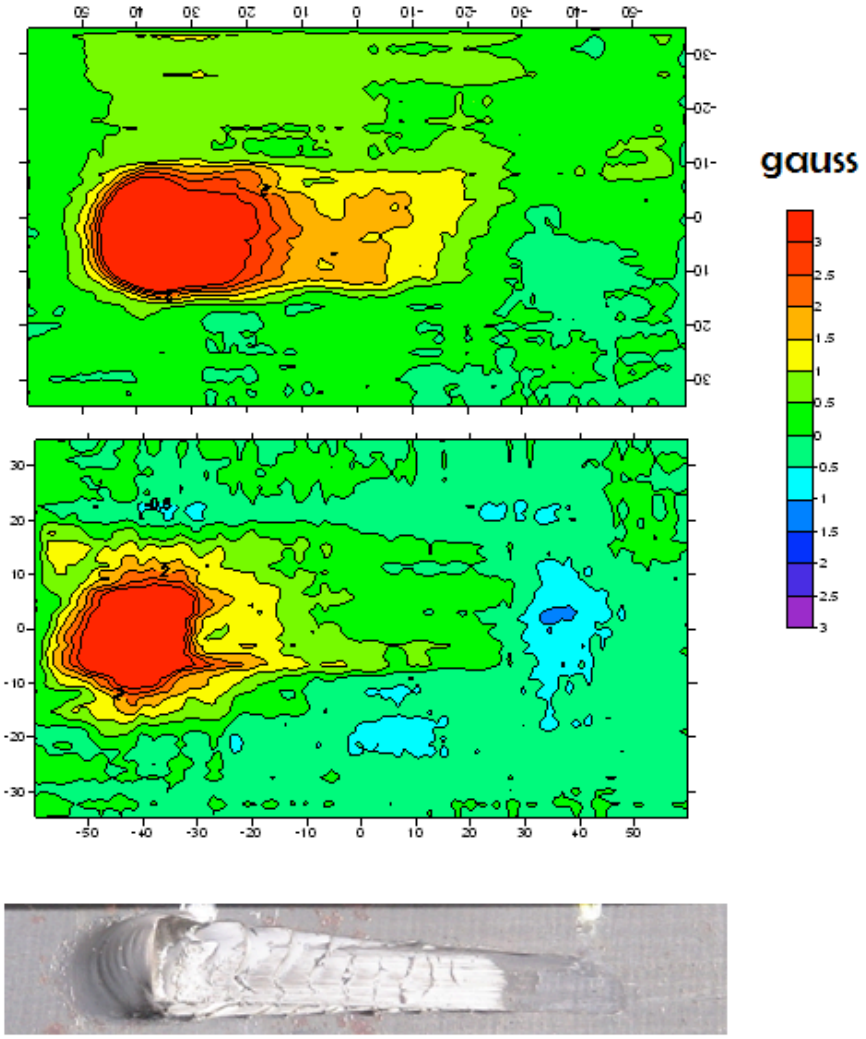

Figure 6- 4: Comparison of outer wall, MFL (axial) scans for gouge 2B with residual depth 2mm (top: pressurized, bottom: unpressurised). In this case the unpressurized scan yields more detail regarding the features – since a second peak is observed at the tool entry end.

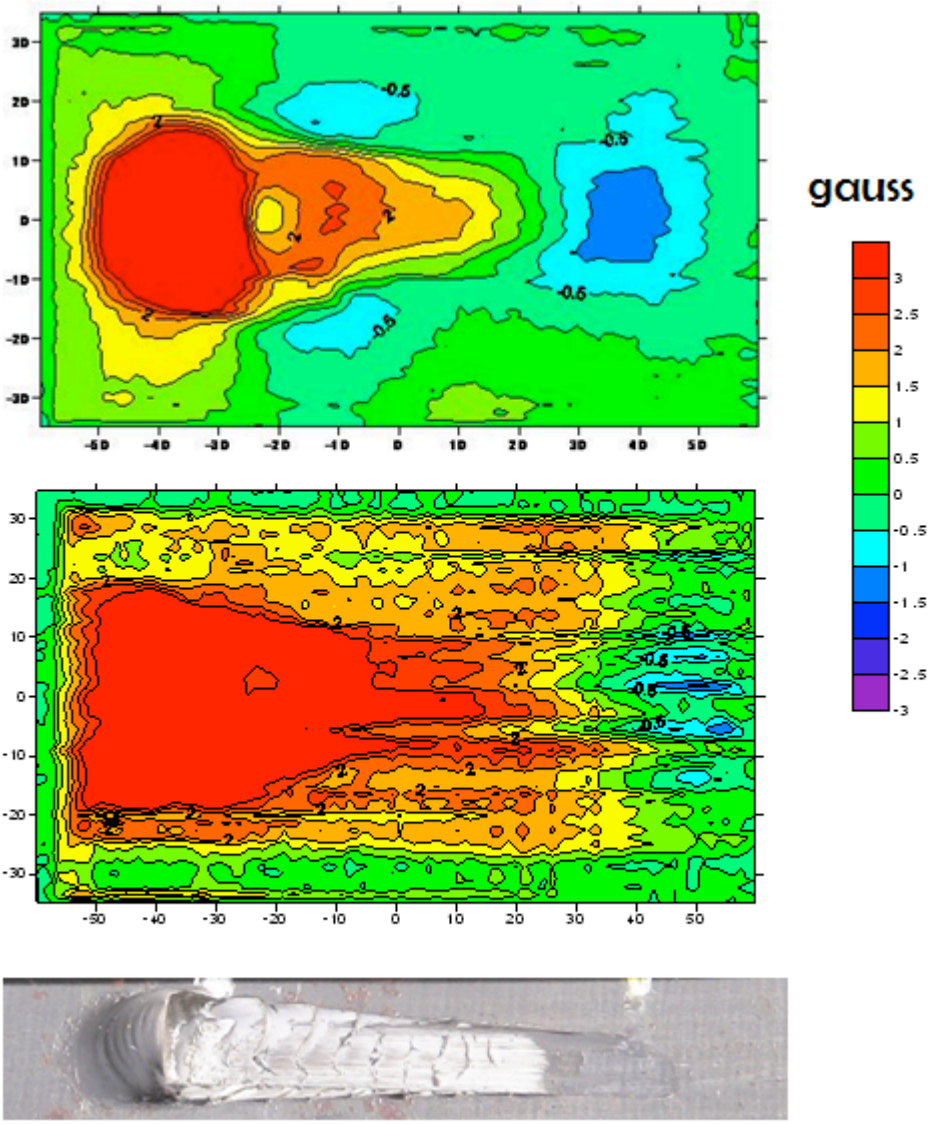

Figure 6- 5: Comparison of outer wall, MFL (axial) scans for gouge 5B with a residual depth of 6 mm (top: pressurized, bottom: unpressurised). Here the pressurized sample result at the top displays well defined peaks, although the two main peaks are seen in both cases.

6.4 Comparison of MFL signal results: The effect of internal pressure during gouging on MFL signals.

During the gouging process, the extent of damage depends on the pipeline pressure. In general, higher pressures produce a larger constraint (i.e. the pipe wall is "stiffer"), thus damage tends to be less pronounced and more localized. It is expected that the MFL signals will be smaller for the gouges produced under higher pressure compared to those produced at lower pressures. In general, this was true for the present study. An example of this is seen in the MFL signals obtained from Pipe 1. **Figure 6-6** shows MFL (radial) signal results for Pipe 1 damage produced at 50% MAOP (upper diagrams) and 100% MAOP (lower diagrams). The plots on the

left were measured from the outer surface (pressurized) and the ones on the right are from inner surface measurements (unpressurized). In both cases, and in most other gouge results of this study, the MFL signal is less pronounced when the pressure is highest. The remainder of this discussion will focus mainly on the "B" series gouges where the damage was introduced under 50% MAOP (the lower pressure).

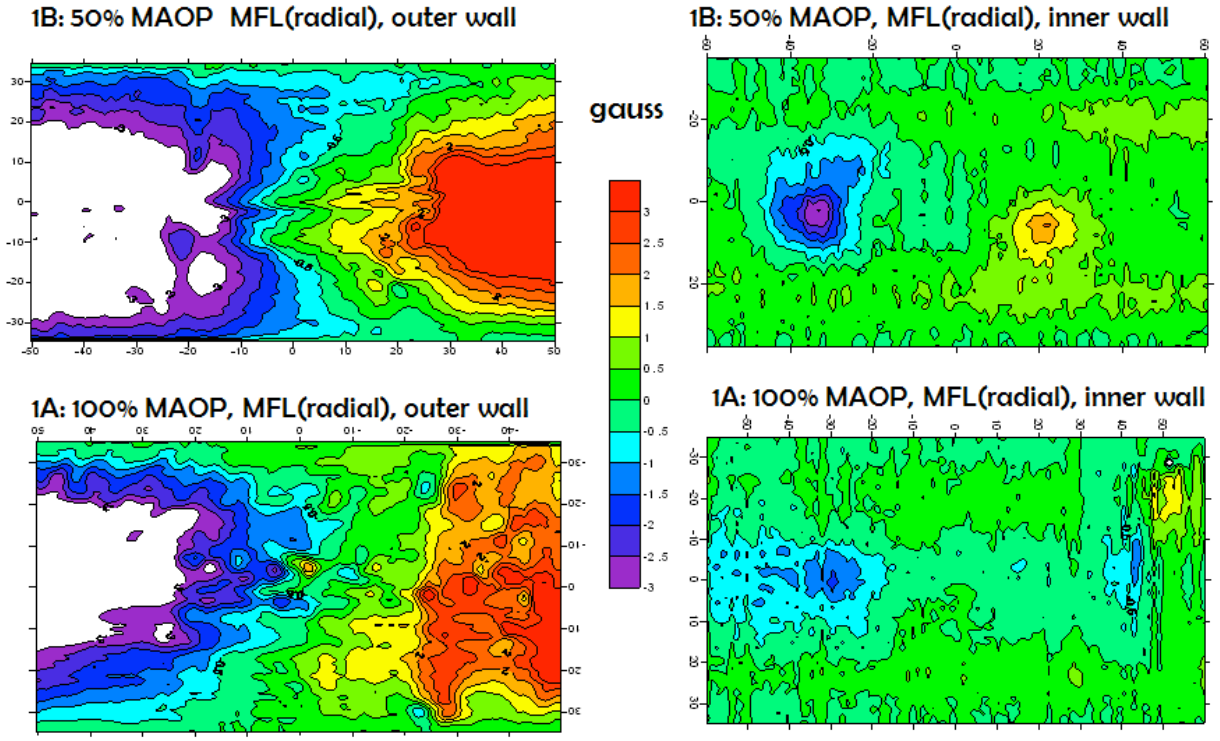

Figure 6- 6: Pipe 1 defects - no visible gouging. Plots of MFL (radial) signal show the effects of gouging under lower internal pressure (gouge 1B – 50% MAOP) compared with higher internal pressure (gouge 1A – 100% MAOP). Both outer wall MFL signals (left) and inner wall MFL signals (right) indicate that the damage is more severe (i.e. the MFL signal is larger) when the pressure during gouging is 50% MAOP. Note that the white areas in the plots indicate where the signal is off scale.

6.5 Comparison of MFL signal results: Comparing MFL outer wall signals with inner wall signals for the Pipe 1 sample (damage without gouge)

The Pipe 1 sample in the present study is particularly interesting, because there was no gouge created during the 'gouging' process. During Pipe 1 gouging, the tool was depressed into the surface to a depth of 2.5mm. The pipe wall was pushed inwards by the tool but rebounded after the tool moved along and was then removed. Ultimately only a very slight scrape was apparent (at the tool exit point of the gouge). From an MFL perspective this is very interesting because this defect is likely to have a 'gouge-type" strain pattern without the associated gouge geometry.

Figure 6-7 shows the MFL signals for defect 1B. The upper diagrams in **Figure 6-7** show MFL (radial) signals; the lower diagrams show MFL (axial) signals. Note the different scales between MFL radial and axial signals; the MFL (axial) signals are always smaller because the probe is further from the surface.

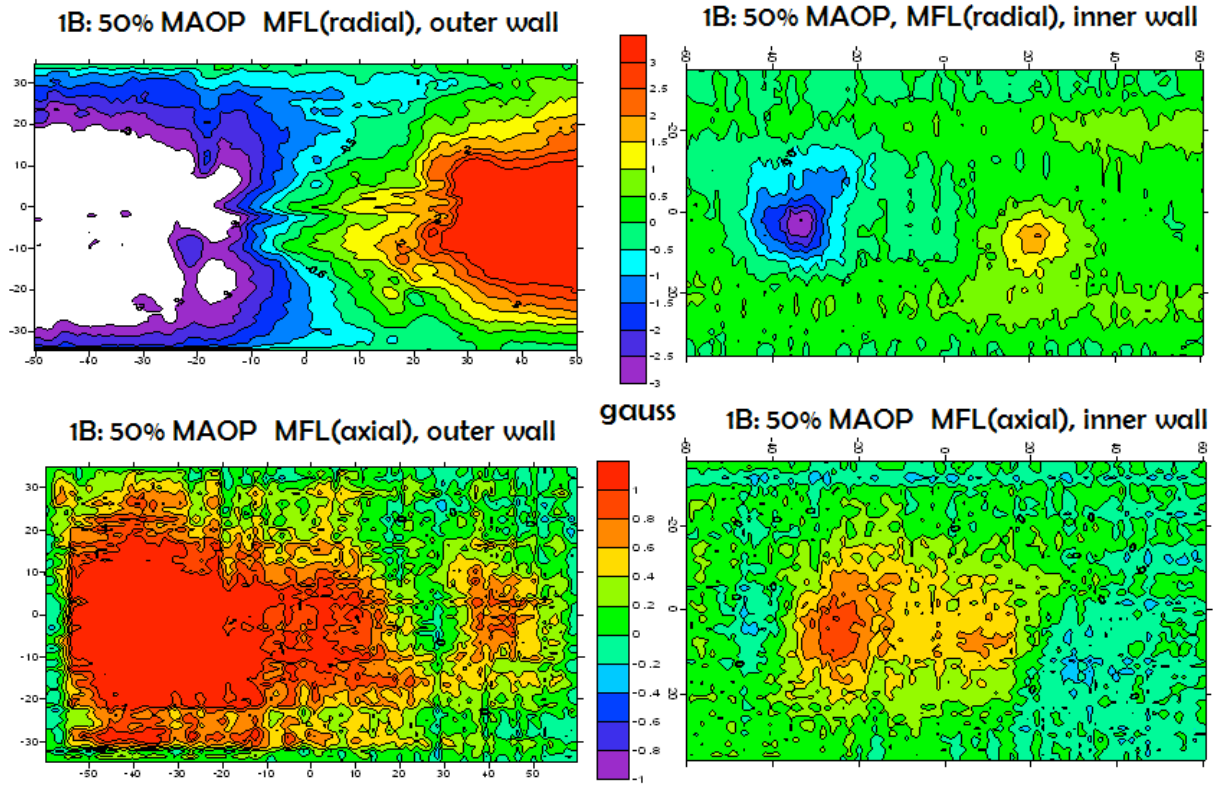

Figure 6- 7: Pipe 1 defects, no visible gouging. Comparison of outer wall MFL signals (left) versus inner wall MFL signals (right) for MFL radial component (top plots) and also MFL axial component (bottom plots). Note that the MFL axial component signals are smaller (since the probe is necessarily further from the surface) so the bottom plots are on a smaller scale. The white areas in the plots indicate where the signal is off scale.

The outer wall MFL signals (on the left) indicate that, although there is no gouge geometry present, the stresses are sufficiently large to create a very significant outer wall MFL (radial) signal (top) and a smaller, yet clearly observable MFL (axial) signal (bottom).

Conversely, the inner wall signals, although visible, are much less significant (right hand side of **Figure 6-7**). This result can be considered in light of the findings of the previous chapter which showed that a local severely plastically deformed surface layer may strongly contribute to the outer wall signal but not to the inner wall signal. In Pipe 1 samples, there is likely to be some very localized severe surface plastic deformation present. However, because of the pipe wall bending and rebounding, considerable residual stresses will also be present, and these will extend through the pipe wall to the inner surface. The signal seen on the inner wall (right) for both the radial and axial cases is most likely associated with the residual stress, rather than the severe plastic deformation at the top surface.

6.6 Comparison of MFL signal results: Progressive changes in MFL signals with increasing gouge severity

In this section the changes in the MFL axial and radial signals as the gouges increase in severity from pipe 1 to pipe5 are considered. Both the inner wall signals and the outer wall signals are examined. Only the MFL signals from the gouges created at 50% MAOP (i.e. the "B" series of samples) are highlighted; the signals from the gouges created at 100% MAOP (the A series) are similar but less pronounced. They can be found in Appendix A for the interested reader.) The MFL signals will be considered in the following order:

- Inner wall MFL signals: MFL(axial) and MFL(radial)
- Outer wall MFL signals: MFL(axial) and MFL(radial)

The inner wall MFL signals are considered first because these are the ones for which geometrical modeling results are available. (The outer wall results are problematic because of the discontinuous detector path as it negotiates the hills and valleys of the gouge).

Section 6.6.1 below includes a physical description of the gouges themselves as they progressively increase in severity. In Section 6.6.2 modeling results for the relevant defect geometries are presented, to assist in interpreting the signals from the gouges. Section 6.6.3 describes and considers the development of the MFL signals at the inner wall of the pipe, and finally Section 6.6.4 considers the same for the pipe outer wall signals.

6.6.1 Physical description of the "B" series gouges as they increase in severity

Figure 6-8 shows two of the gouge defects from which the MFL signals originate; Gouge 2B, a relatively shallow gouge, and Gouge 5B, which was the most severe gouge produced. Prior to discussing MFL signal results, it is useful to reiterate the visible changes in the gouges themselves as their severity increases:

- 1B: No visible gouge. A small mark is present on the outer surface for the last cm of the tool travel; a very slight scrape can be felt there.
- 2B (**Figure 6-8**): The next 3 gouges (2B, 4B, and 5B) have essentially the same shape, but increase in severity. The form of these gouges is seen in **Figure 6-8**. Gouge 2B (shown at the left in **Figure 6-8**) has no visible indication on the inner pipe wall (i.e. no inner wall bump). At the side edges of the gouge there is some exfoliated material.
- 4B: This gouge is deeper than Gouge 2B and has a larger exfoliation mound at the tool exit end. A small dent is visible; in particular there is a bump on the inner surface, in the vicinity of the tool entry end. Side edge exfoliation is more severe than in 2B.
- 5B: This is the deepest gouge with the largest exfoliation mound at the tool exit end (shown in the two left diagrams of **Figure 6-8**). The dent (bump) for this gouge is very pronounced on the inner surface, again associated more with the tool entry end of the gouge than the tool exit end. This denting at the tool entry

end can be seen on the 5B photograph in **Figure 6-8** (where the tool enters). Note that there is little denting apparent at the tool exit end in 5B. Side edge exfoliation is significant and as seen in the lower 5B photograph, the side edges are not vertical but tapered significantly.

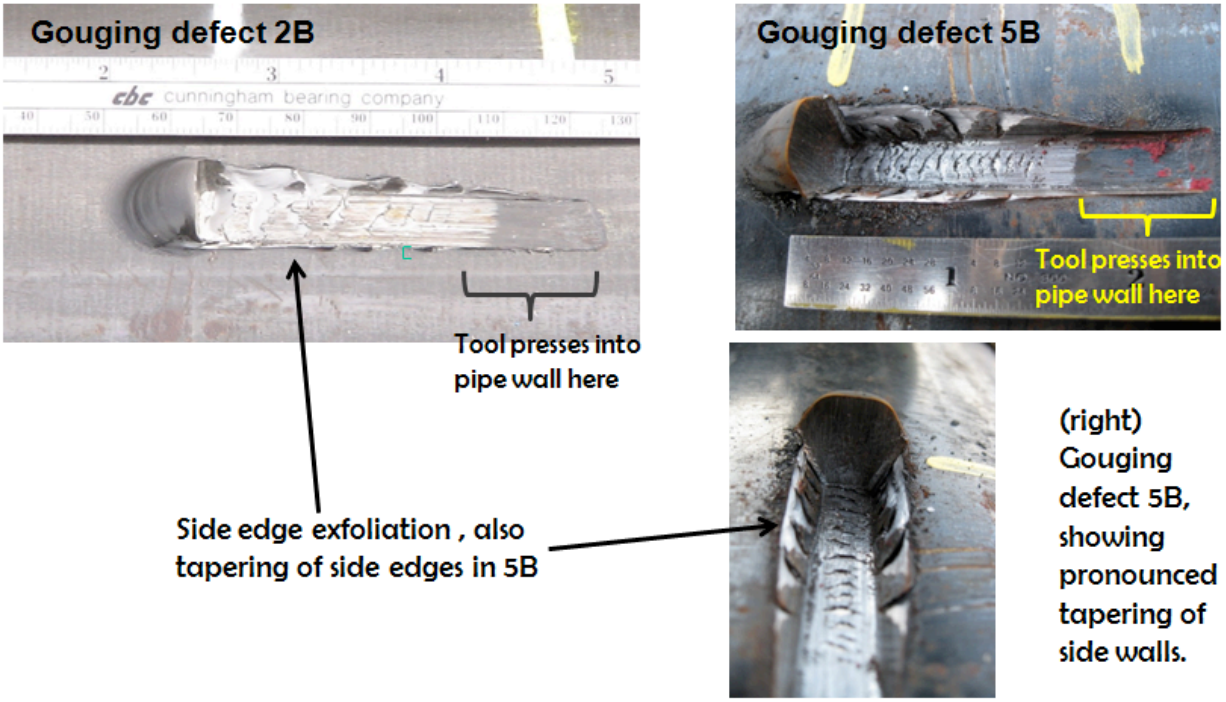

Figure 6- 8: Photographs of gouging defects 2B and 5B produced at SES as part of the current study. The tool is pressed into the pipe wall at the right hand side of the gouge, then the pipe is pulled to the right. The tool scrapes the surface and progressively deepens the gouge as it proceeds. The exfoliated metal accumulates ahead of the tool (which has a flat front face as seen in Figure 6.1). Exfoliated metal also piles up at the sides of the gouges, particularly in the deeper gouges like 5B.

6.6.2 Geometry models of the gouge and associated dent geometries

Figure 6-9 shows the geometry-only magnetic model created for the gouges produced at SES. The red regions at the end of the half model are the magnets themselves. Note that the model is similar to that seen experimentally in the 2B gouge; there is no associated dent, and the gouge sidewalls are essentially vertical. No stresses are included in this model because they could not be obtained using stress modeling (too complex) and the project team had not attempted neutron diffraction measurements at this point (these are being conducted in a later phase in 2011).

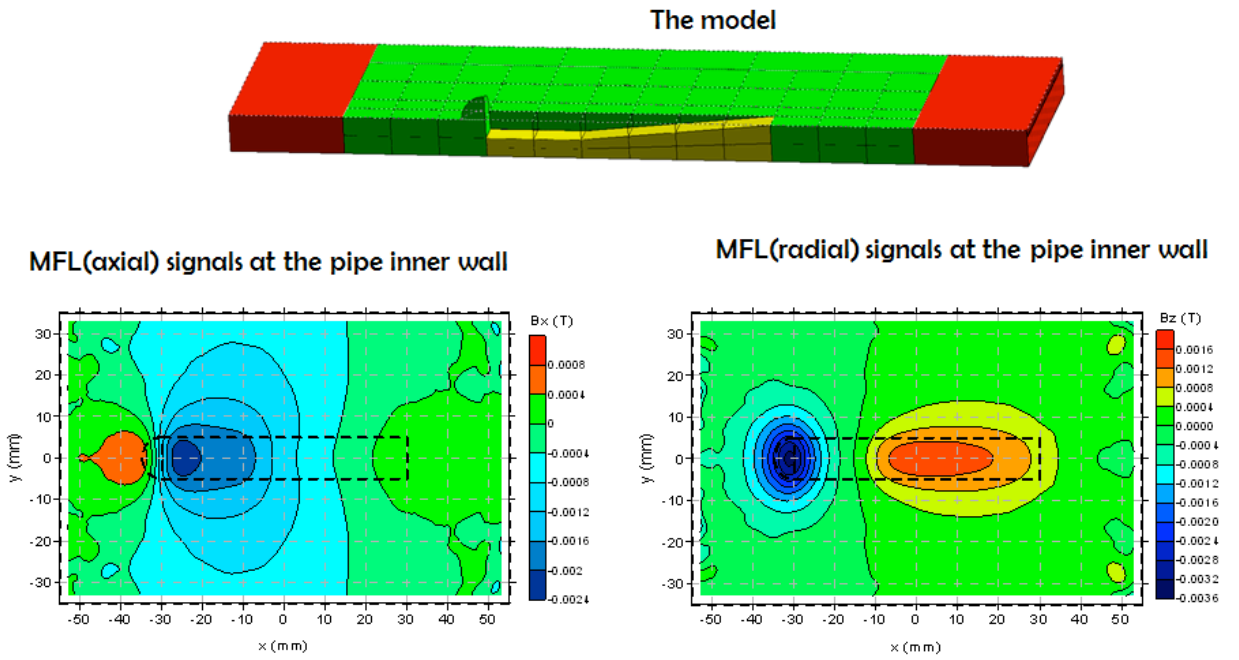

Figure 6- 9: Geometry-only magnetic model for the gouges observed in the present study. The top diagram shows the model itself – a half-model can be used because of the symmetry. The red regions at the end are the magnets. Note that the model does not include a dent – typical MFL signals from dent geometries are shown in Figure 6.10. No stresses are included in the model since stresses are difficult to predict for gouges. Also the model results below are shown for the inner wall. The measured outer wall results were done on top of the clay overlay and this detector trajectory was not modeled at this time.

The MFL modeling results for the inner wall signals are shown at the bottom of **Figure 6-9**; the MFL(axial) on the left and the MFL(radial) on the right. The outer wall modeled signals were not plotted, since the experimental signals were obtained using an altered detector path (due to the clay placed on top so that the detector could negotiate the geometry).

As mentioned above, gouges 4B and 5B also contain considerable dents which are most apparent on the inner pipe wall. The dents are not included in the models of **Figure 6-9**, however typical MFL signals for circular dents are shown in **Figure 6-10**; MFL (axial) signals on the left and MFL(radial) signals on the right. Earlier work has shown that MFL signals are additive, so these dent results (**Figure 6-10**) will be considered with the gouge results (**Figure 6-9**) in interpreting the experimental results below.

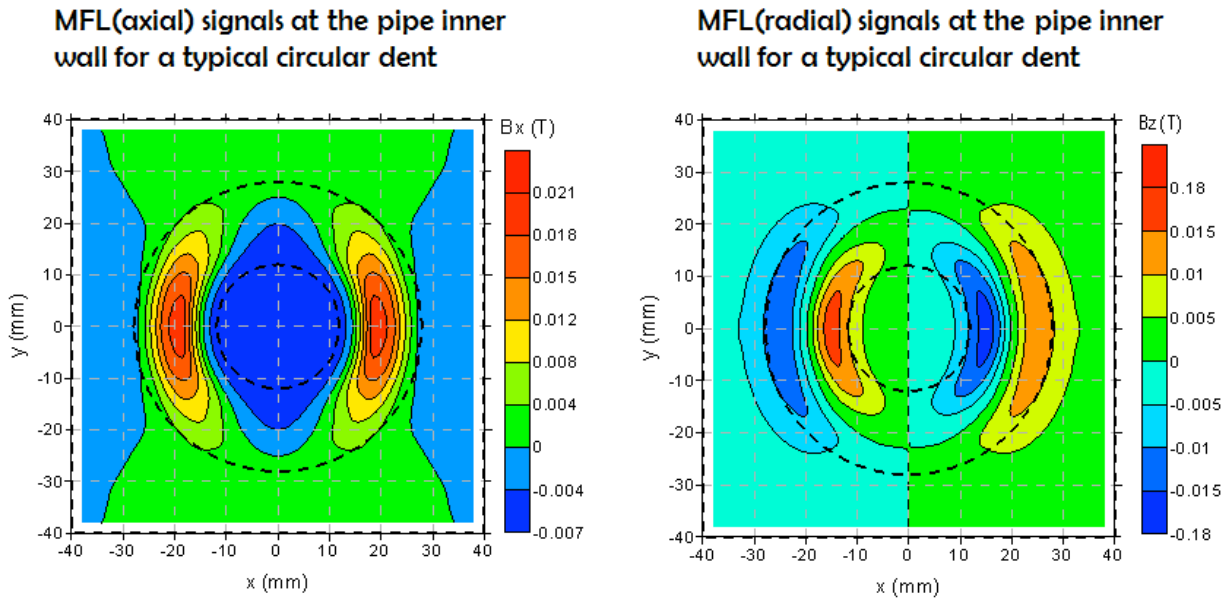

Figure 6- 10: Geometry-only magnetic model results for typical circular dents, taken from earlier work. Of the gouges created in the present study, gouges 4B and 5B exhibited noticeable dents. These dents were manifest as inner wall "bumps" associated with the tool entry end of the gouge.

6.6.3 MFL signal development as gouge severity increases: Inner wall MFL signals

Figures 6-11 and **6-12** show the MFL signals at the inner wall as gouge severity increases from 1B to 5B. **Figure 6-11** shows the MFL (axial) component signals, and **Figure 6-12** shows the MFL (radial) component signals. Note that the two figures are at different scales for the magnetic flux; the MFL (axial) is at a +1G to -1G range while the MFL (radial) signal is much larger and is best viewed at a +3G to -3G range.

The MFL (axial) signal will be considered first, then the results for the MFL (radial) signal. The progression of each will be discussed using the modeling results of **Figure 6-9** and **6-10** as a guide.

MFL (axial) inner wall results are shown in **Figure 6-11-**

- Sample 1B – Recall that this defect displays no gouge and as discussed earlier this positive peak is likely from residual stresses extending through the pipe wall.
- Gouge 2B – There is little or no dent associated with the gouge, therefore the experimental MFL (axial) signals seen in **Figure 6-11** resemble the modeled MFL(axial) signals seen on the left hand side in **Figure 6-9**. In the experimental plots of **Figure 6-11** the negative peak in the center of the plot is somewhat smaller than that predicted by modeling, and the positive (red) peak on the right is larger. This may result from residual stresses, since the result of 1B suggests that the residual stresses will produce a positive MFL axial peak at this surface (and, in fact, a larger positive peak might be expected for 2B since the deformation is

larger). Thus residual stresses may enhance the positive peaks and diminish the negative ones.

- Gouge 4B: There is an associated dent with this gouge, although not as large as that for Gouge 5B. The superposition of the negative center inner wall dent signal (resembling **Figure 6-10** (left diagram)) and the negative gouge signal (**Figure 6-9** (left diagram)) reinforce one another to produce a very large negative peak. It is not clear why the positive peaks have essentially disappeared but it is likely that they coincide with negative peaks and are diminished.
- Gouge 5B: This gouge displays a considerable dent, and it clearly dominates the MFL signal, closely resembling the MFL (axial) dent signal in **Figure 6-10** (except with a bit more elongation). If one was unaware of the gouge, in fact, it might be concluded that this is a severe dent.

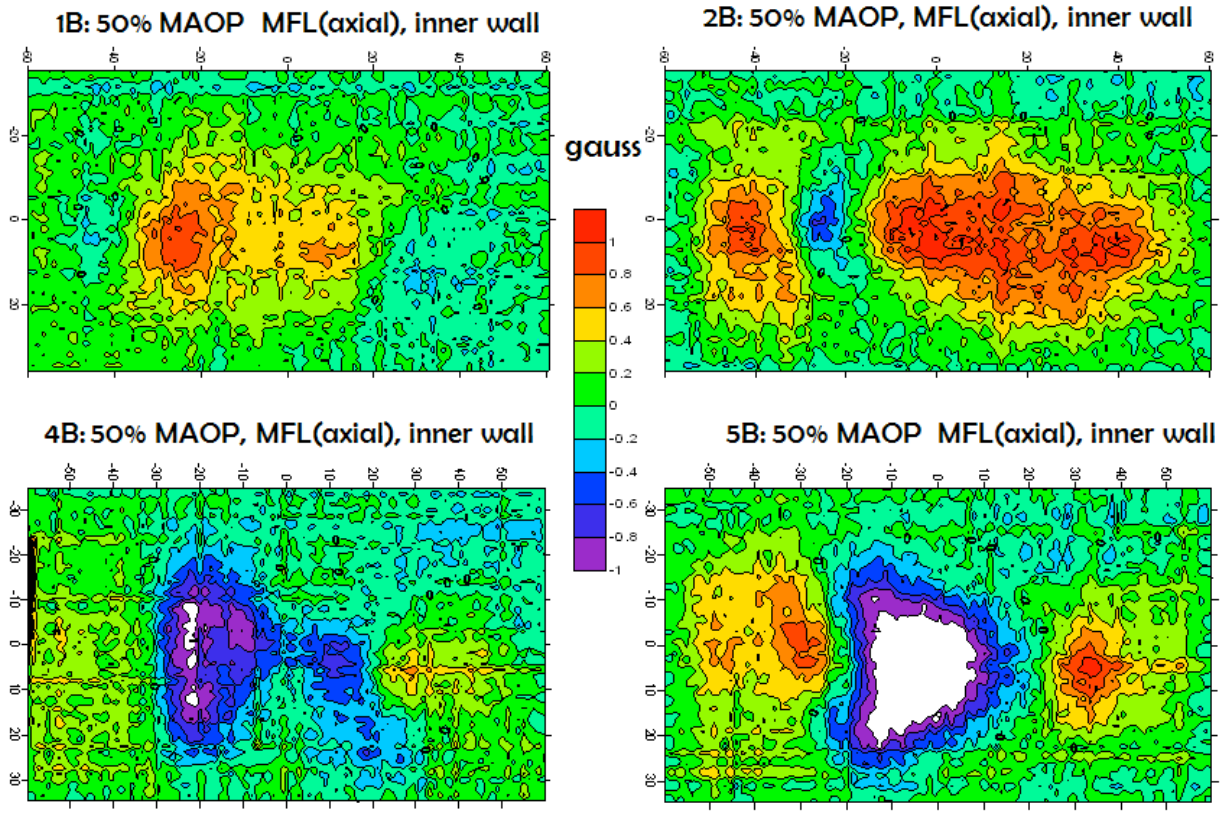

Figure 6- 11: Progressive changes in inner wall MFL (axial) signal as gouges increase in severity. Data shown is for the gouges produced at 50% MAOP. Note that the scale is from -1G to +1G. Note that the white areas in the plots indicate where the signal is off scale.

MFL (radial) inner wall result – **Figure 6-12**

As mentioned earlier, note that the scale on this figure is three times that of the MFL (axial) signal results. The radial probe is positioned closer to the pipe surface than the axial probe, so the MFL (radial) signal is larger; also the radial probe detects more subtle details than the axial probe does. A comparison is made between the experimental results of **Figure 6-12** and the MFL (radial) modeling results on the right side of **Figures 6-9** and **6-10**.

- Sample 1B: Again, there is no gouge associated with this defect, therefore the MFL signal results primarily from the residual strain in the pipe wall.
- Gouge 2B: Recall that this gouge contains no dent, therefore it can be compared directly with the modeled MFL (radial) signal in **Figure 6-9**. Upon comparing the two, it is clear that there are some differences. The strong negative peak associated with the large exfoliation peak is clear (it is also present in 4B and 5B). However the positive peak at the tool entry end (seen in **Figure 6-9**) is very weak. There is also a negative peak at the bottom right which may be residual stress-related but the most striking feature is the horseshoe-shaped positive region in the center of the plot. This may be a stress feature, but the 'side' features are almost certainly associated with the sidewalls of the gouge which are tapered, and also display some exfoliated material.
- Gouge 4B: This gouge also has an associated dent, although the dent signals (see model on the right hand side of **Figure 6-10**) are not as obvious as they appeared to be in the MFL (axial) signal. In this MFL (radial) signal the opposite polarity peaks associated with the gouge geometry are clearly seen, and again side peaks associated with the tapered sidewalls and exfoliation.
- Gouge 5B: This signal is a very complex combination of a gouge and a significant associated dent. The gouge peaks are obvious, and the tapered sidewall peaks are also present. However there is also a strong MFL (radial) dent signal (four peaks of alternating polarity; see **Figure 6-10**) superimposed on this, as well as dent and gouge residual stress peaks, making the overall signal very difficult to interpret.

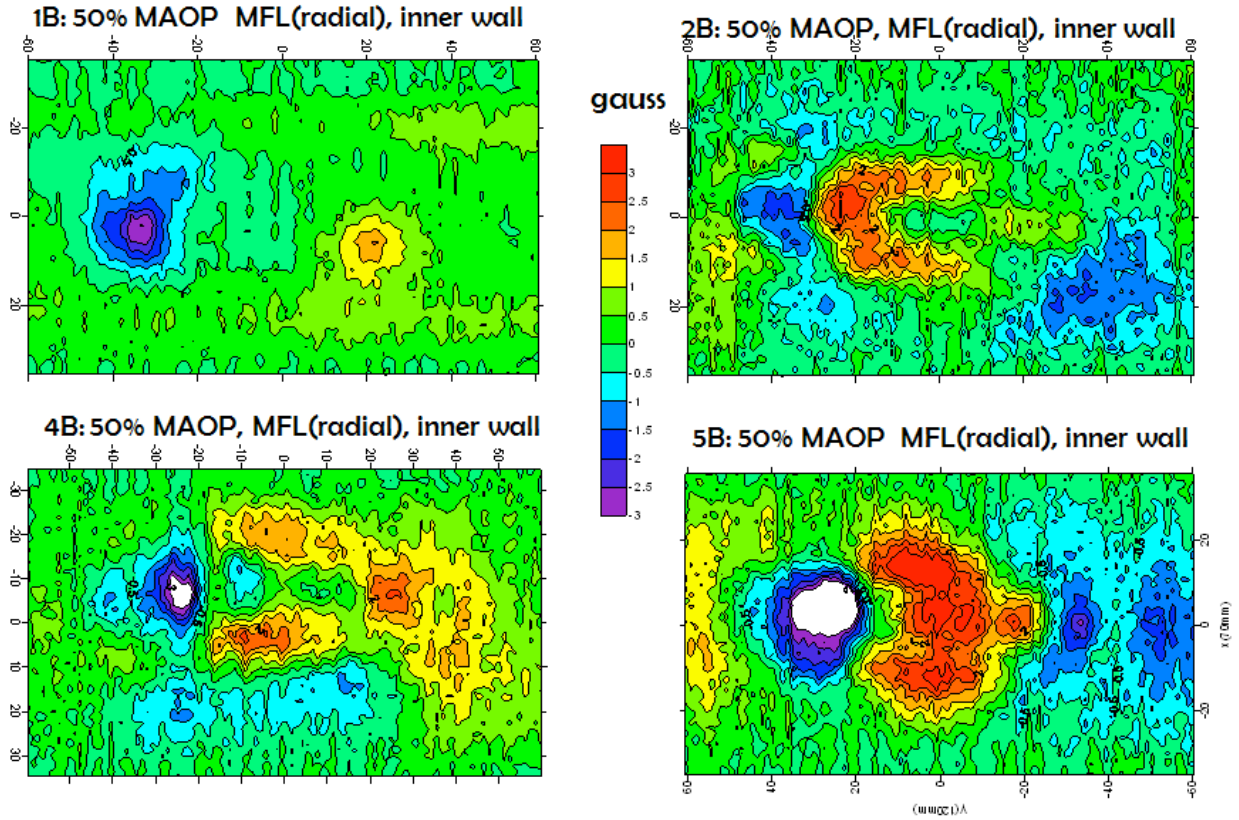

Figure 6- 12: Change in inner wall MFL(radial) signal as gouges get progressively deeper. Data shown is for the gouges produced at 50% MAOP. Note that the scale is from -3G to +3G. The white areas in the plots indicate where the signal is off scale.

6.6.4 MFL signal development as gouge severity increases: Outer wall MFL signals

Figures 6-13 and **6-14** show the MFL signals at the outer wall as gouge severity increases from 1B to 5B. **Figure 6-13** shows the outer wall MFL (axial) component signals, and **Figure 6-14** shows the MFL (radial) component signals. Note that the two figures are at different scales for the magnetic flux because the MFL (radial) always exhibits a larger signal and more detail because the detector lies closer to the surface. It is important to note that the presence of the clay layer over the top of the gouge was necessary but may mask many of the signal features. For example the taper down from the top of the exfoliation peak means that the detector travels above the base of the gouge by as much as 5 mm. Thus subtle signal effects are likely not seen, particularly in the MFL (axial) signal. In addition, the severe geometry at the outer surface causes the detector to occasionally stray off the intended path slightly, or tilt; this explains the "streaking" features down the center of the gouge in the MFL (radial) 2B, 4B and 5B signals. In the description that follows both the axial (**Figure 6-13**) and radial (**Figure 6-14**) signals will be considered together.

MFL Outer wall results: MFL (axial) and MFL (radial); **Figures 6-13** and **6-14**

- Sample 1B – No gouge but damage: Again this is the only sample in this series that does not have a geometry component, yet both the MFL (axial) and MFL (radial) peaks here are very significant. There is no clay on this sample (since there is no geometry), thus the detectors are measuring very close to the surface, and in particular the severely deformed layer is directly adjacent to the detector. Thus the peaks may be associated with this thin, severely deformed layer, or the residual stresses, but most likely both.
- Gouges 2B-5B: For these gouges,
  - The outer wall exfoliation peak is clearly the largest feature in the MFL signal, as expected. However the strong, positive and extensive MFL(radial) signal (**Figure 6-14**) surrounding this main peak suggest that residual stresses continue to contribute to the signal at this point.
  - The MFL (axial) signal is also significant at the outer wall; again the main feature is that associated with the exfoliation peak and this overwhelms the residual stress peak at the tool exit end.
  - As seen in the inner wall signal (see previous section) the signals from the sidewalls of the gouges, seen in the MFL (axial) **Figures 6-13** (4B) and (5B) and also MFL (radial) **Figure 6-14**, are likely a geometry effect resulting from the sidewall exfoliation and possibly taper.
  - There is a significant peak associated with the tool entry end for Gouges 4B and 5B in both MFL (axial) and MFL (radial). There could be a few possible contributions to this peak:
    - As seen in **Figure 6-8**, Gouge 5B (and also 4B, which is not shown) display an outer wall depression due to the initial tool pressure at this point. Thus there will be a metal-loss-type contribution to the signal.
    - Residual stresses below this point, these will be severe as a result of the depression
    - The depression creates a dent and a visible bump on the inner wall of the gouge, thus there will likely be a "dent signal" contribution.

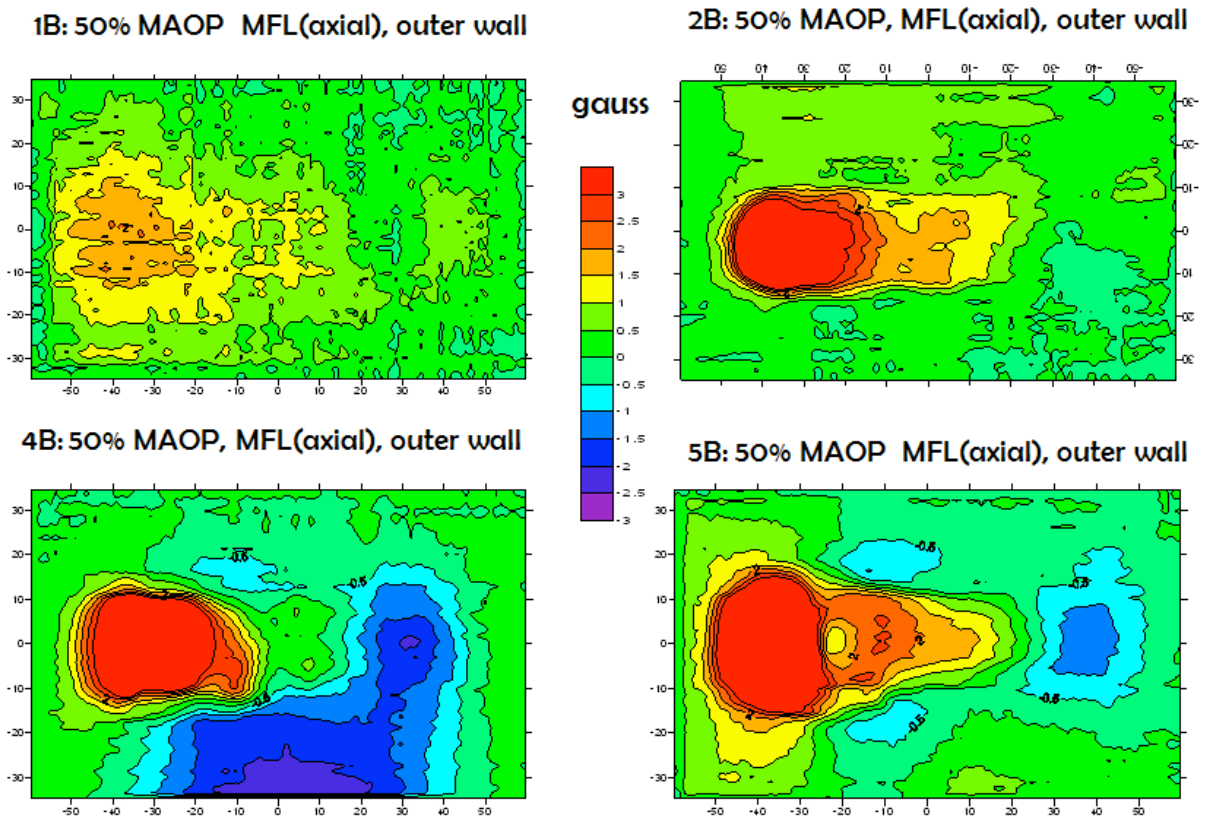

Figure 6- 13: Change in outer wall MFL(axial) signal as gouges get progressively deeper. Note that the scale used for these plots is from –3 G to +3 G. The large anomalous signal at the bottom edge of the 1B plot is likely associated with the detector rotating off horizontal as it negotiates the side of the clay sliding surface.

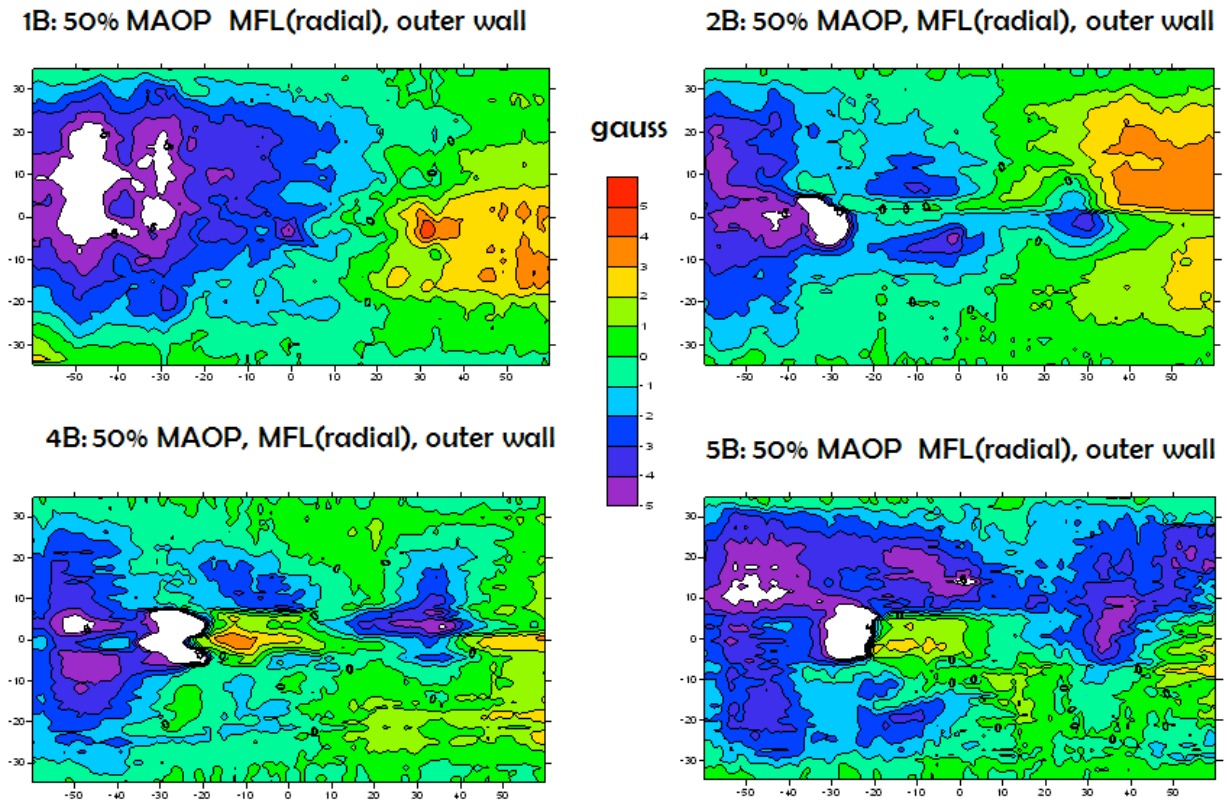

Figure 6- 14: Change in outer wall MFL (radial) signal as gouges get progressively deeper. Data shown is for the gouges produced at 50% MAOP. Note that the scale is from -5G to +5G. The white areas in the plots indicate where the signal is off scale.

6.6.5 Conclusion on the development of inner and outer wall MFL signals in gouges of increasing severity

The following are conclusions on the study of MFL signals for progressively severe gouges:

- For the defects considered in this study, MFL measurements made while the pipe is under pressure do not differ significantly from those made of the same defect under zero pressure.
- The defects created at higher internal pressures display, slightly smaller and less extensive signals than those created at lower pressures, due to the added constraint when the pipe is at high pressure.
- The Pipe 1 damage was very interesting because there was no geometry change in the pipe wall, yet the "defect" produced sizable MFL signals. Outer wall signals were likely a combination of a severe plastic deformation signal as well as a residual stress signal; inner wall signals were much smaller and likely only influenced by the residual stress pattern near the inner wall.
- Progression of MFL signals at the inner wall as gouge severity increased:

- 1B: Stress defect: Both MFL (axial) and MFL (radial) signals detected small residual stress signals when no gouge was present.
- 2B: Gouge with no dent: MFL (axial) signal is consistent with a combination of the gouge geometry signal as well as a residual stress contribution. However, in additions to the geometry features, the MFL(radial) signal (which is more sensitive) reflected a stress feature at the deepest gouge point as well as features associated with the exfoliation and possibly taper at the sidewalls of the gouge.
- 4B: Gouge with slight dent: MFL (axial) signal reflects a composite signal between a dent signal and a gouge signal. In the MFL (radial) signal the dent contribution appears less obvious, and again strong side peaks are seen which are associated with the tapered sidewall and exfoliation.
- 5B: Gouge with significant dent: MFL (axial) is dominated by a significant dent geometry signal. MFL (radial) signal is very complex – gouge peaks are obvious as are the tapered sidewall peaks, however the radial dent peaks and likely residual stress peaks (from both denting and gouging) make interpretation very difficult.

- Progression of MFL signals at the outer wall as gouge severity increased: Note that the signals in 2B, 4B and 5B are influenced by a clay masking layer that was added to facilitate detector movement, but created a significant detector liftoff above the gouge in many regions. Problems with detector movement as it negotiated the considerable geometry led to some 'streaking' of the MFL plots. The progression of the signals with increasing gouge severity are as follows:
  - 1B- Stress defect: Both MFL (axial) and MFL (radial) signals are significant; likely a combination of residual stress and the severe plastic deformation component.
  - 2B-5B: The MFL (axial) and MFL (radial) signals are dominated by the exfoliation peak. However, there are also contributions from the sidewall taper and exfoliation at the sides of both peaks. A significant signal also exists at the dent entry end, which could be related to stress, a 'metal loss' effect, or the dent bump.

6.7 The influence of pressure cycling on MFL signals

This study was of interest for two reasons:

- Pipelines are pressure cycled continuously throughout their lifetime. Residual stress re-distribution is known to occur as a result of this pressure cycling. Thus the potential exists for the stress redistribution to cause a change in the MFL signal with pressure cycling.

- Anecdotal evidence has suggested evidence of an MFL "halo" associated with pressure cycling[10]. This "pressure cycling halo" has been identified on inner wall MFL (axial) component signals during inspection tool runs. If such a halo exists then it should be readily observable in the present study, where MFL measurements will be made at well defined pressure cycling intervals up to a maximum of 10, 000 cycles.

Table 6-1 indicates that gouges were introduced into five different pipes for the current study. The gouges in Pipe 3 were exact replicas of those introduced into Pipe 2, however Pipe 3 was reserved for a study of how pressure cycling affects MFL signals. Gouges in Pipe 3 were introduced at 100% MAOP (Gouge 3A) and also 50% MAOP (Gouge 3B). As with the other samples, the pipe section was then reduced to zero pressure, and then re-pressurized to 50% MAOP for the initial set of outer wall MFL measurements made at SES in Houston. After the first measurement (which is considered to be done after one pressure cycle), this sample was pressure cycled up to 50% MAOP ten more times, after which further MFL measurements were conducted. This process was repeated after 100 cycles, and again after 1000 cycles. The pipe section continued to be pressure cycled at SES, up to 10,000 cycles (however no outer wall MFL measurements were obtained at this point). The pipe section was then cut (along with pipe sections 1,2,4 and 5) and pipe rings containing the gouged regions were sent to the Queen's AMG labs for additional "unpressurized" MFL testing at the outer and inner walls.

All of the Pipe 3 MFL signal results following pressure cycling are included in Appendix B. A few of the results (for Gouges 2B and 3B) will be reproduced in the discussion that follows in order to examine what additional MFL signal features, if any, are introduced as a result of pressure cycling. The results will be considered as follows:

- Outer wall results before pressure cycling* (2B and 3B) and after 1000 cycles (3B only):
  - (MFL(radial) results
  - MFL(axial) results
- Inner wall results before pressure cycling (2B only) and after 10,000 cycles (3B only):
  - (MFL(radial) results
  - MFL(axial) results

6.7.1 Pressure cycling and MFL signals – outer wall MFL signal results

Figure 6-15 shows MFL (radial) signal results measured at the outer surface. The top two figures show results for Gouges 2B (left) and 3B (right) immediately after gouge formation and after just one cycle. The reason for including both 2B and 3B here is to compare the two signals. These two gouges were made in identical pipes under identical conditions. A comparison of the MFL (radial) signals for these two gouges thus indicates

* note that his is actually after one cycle, since the pressure was reduced to zero, and then taken back up to 50%MAOP for the first MFL measurement

the degree of variation one may expect to see between two 'identical' gouges. The plot at the bottom of the page is the corresponding MFL (radial) signal for Gouge 3B after 1000 pressure cycles. Although there appears to have been some change in the size of the signal around the exfoliation peak, fundamentally there is little difference between the signals observed at one cycle compared to that after 1000 cycles.

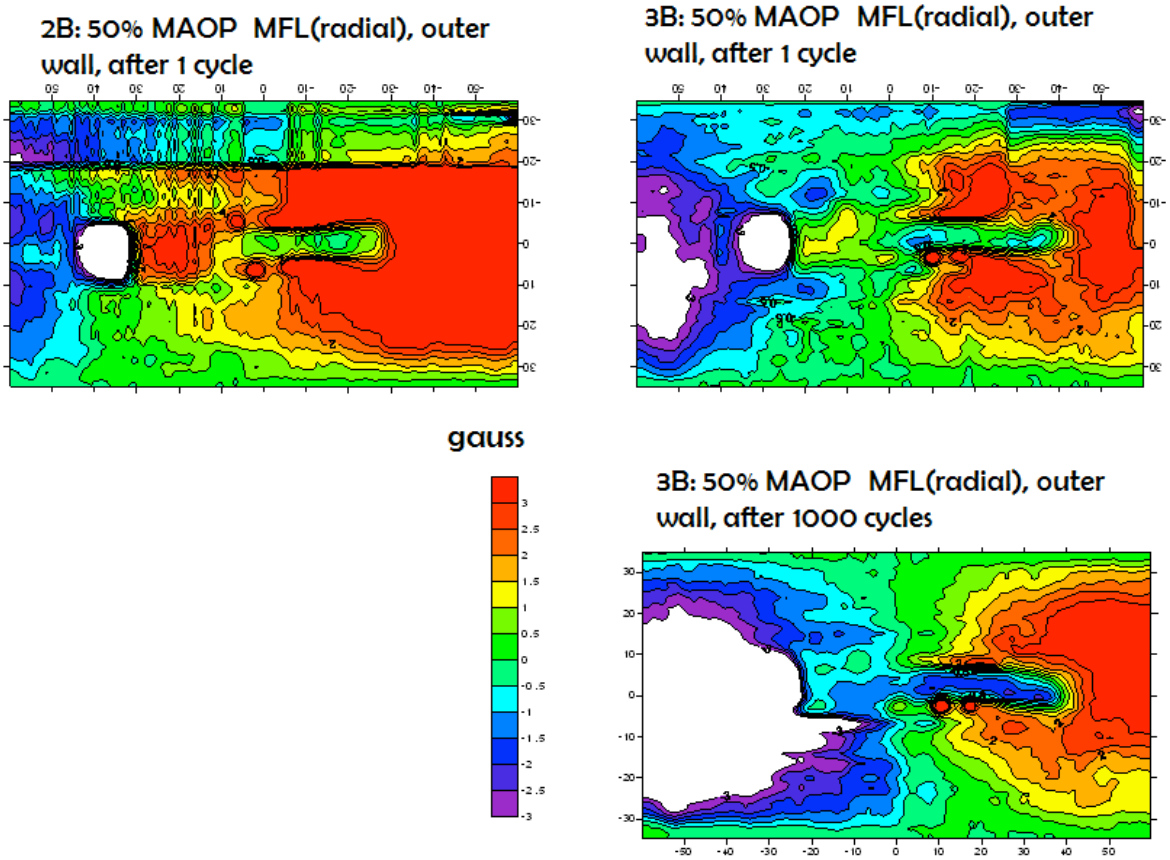

Figure 6- 15: MFL (radial) outer wall signals before (top) and after 1000 pressure cycles (bottom) to 50%MAOP. Results for Gouge 2B are on the left and Gouge 3B are on the right. Note that there is no 2B result after 1000 cycles because only pipe 3 was pressure cycled.

Figure 6-16 shows a similar set of signals as **Figure 6-15**, but for the MFL (axial) signals measured at the outer surface. Again there are some differences noted between the 2B and the 3B signal – most notably the extent of the exfoliation peak signal. After 1000 cycles there is noted the presence of some small negative peaks near the tool entry end and to one side of the defect (note that these small peaks were not observed after 10 cycles nor after 100 cycles – see Appendix B).

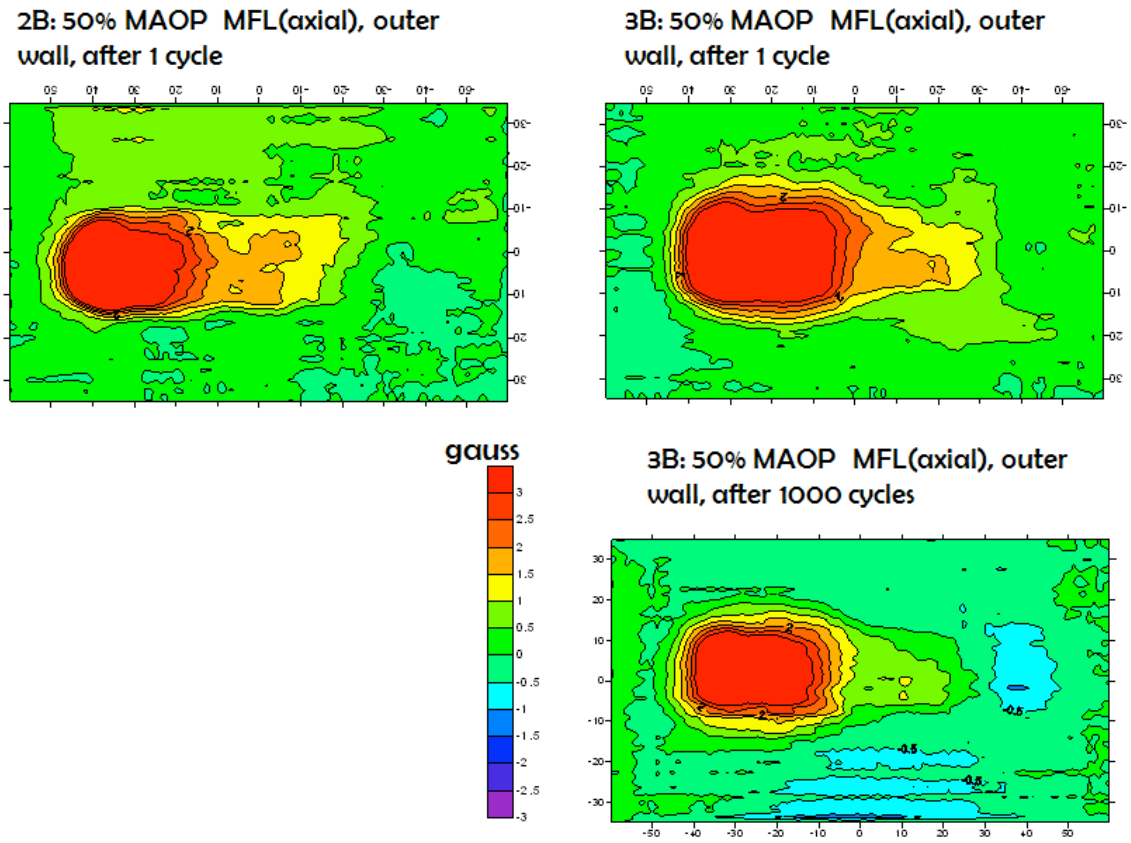

Figure 6- 16: MFL (axial) outer wall signals before (top) and after 1000 pressure cycles (bottom) to 50%MAOP. Results for Gouge 2B are on the left and Gouge 3B are on the right.

6.7.2 Pressure cycling and MFL signals – inner wall MFL signal results

The inner wall signals are more relevant than those measured at the outer wall, since they reflect what is accessible with an inspection tool. Unfortunately it was not possible to access the inner wall while the pipe section was under pressure, so no inner wall measurements for 3B were available until after 10000 cycles. However a comparison can be made with the results of 2B after one cycle. **Figure 6-17** shows a comparison of the MFL (radial) results for 2B after one cycle, with of 3B after 10000 cycles. These results indicate that essentially nothing has changed in the MFL signal, thus pressure cycling seems to have had no effect in this case.

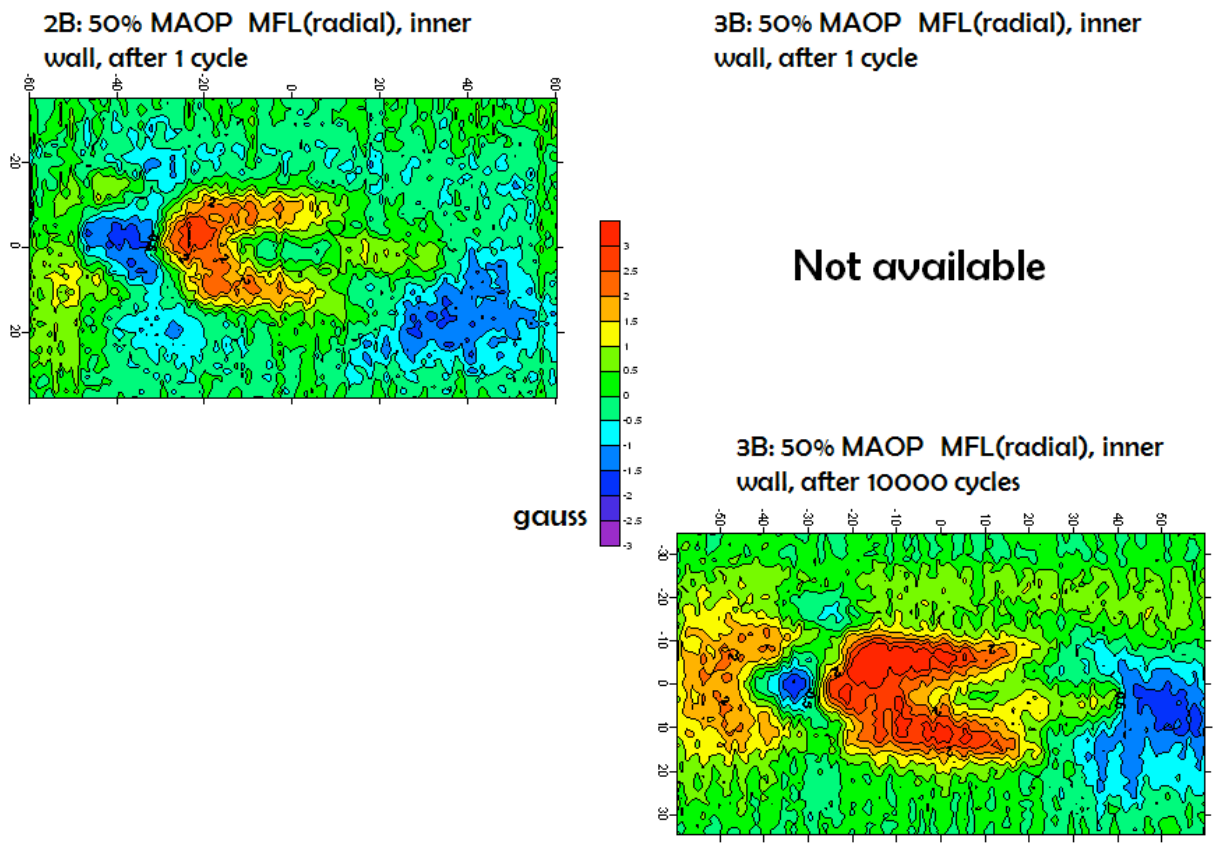

Figure 6- 17: MFL (radial) inner wall signals before (top) and after 10000 pressure cycles (bottom) to 50% MAOP. Results for Gouge 2B are on the left and Gouge 3B are on the right.

The MFL (axial) signal for the inner wall is presented in **Figure 6-18** for sample 2B after one cycle, compared to the 3B sample after 10000 cycles (note that the scale is smaller than previous diagrams because the MFL (axial) component signal is smaller). The results for the MFL (radial) signal in the previous figure show that the differences between the two signals are essentially insignificant, except for a slight difference in signal strength.

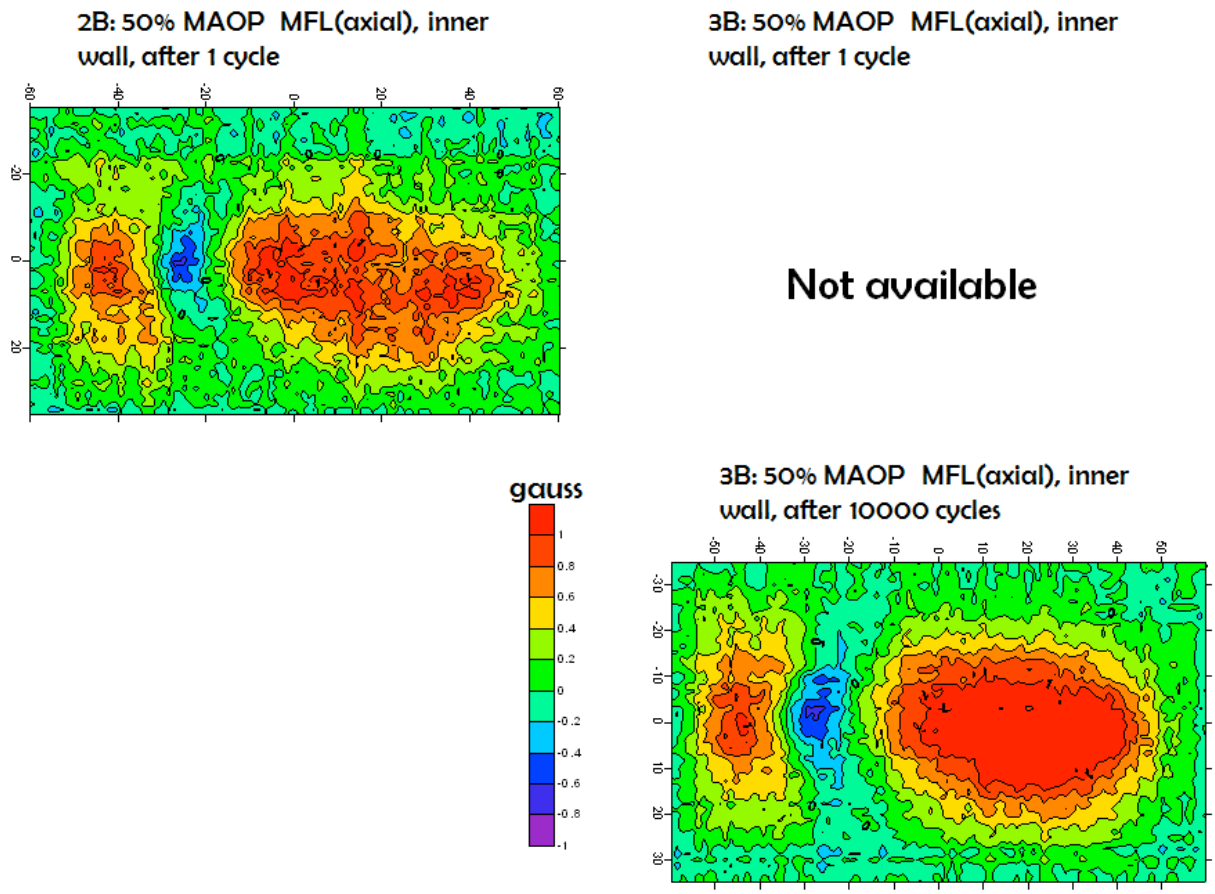

Figure 6- 18: MFL (axial) inner wall signals before (top) and after 10000 pressure cycles (bottom) to 50% MAOP. Results for Gouge 2B are on the left and Gouge 3B are on the right.

6.7.3 Conclusion – pressure cycling and MFL signals

The results seen in **Figure 6-15** through **6-18**, and also in Appendix B, clearly show while there may be slight differences in peak size and shape between samples and from measurement to measurement, pressure cycling has no significant influence on the MFL signals – either radial or axial, inner or outer wall. Furthermore, no evidence of a "pressure cycling halo" could be found in any of the results of this pressure cycling study.

7.0 Results: Neutron diffraction residual stress measurements for GdF Suez samples, and incorporation into MFL model

7.1 Introduction

As shown in the previous section, the structural modeling of residual stress patterns surrounding gouges is complicated, and thus limited success was achieved with such modeling in the case of gouges. However, knowledge of the residual strain distribution is critical to the MFL modeling, and also useful for understanding failure criteria. Since modeling was unsuccessful, direct measurement of these stresses became necessary. Neutron diffraction is the only effective, non-destructive residual stress measurement technique which can provide strain information at depth.

Three gouge or gouge+dent samples were supplied for neutron diffraction measurements. These samples were created using the Pipeline Aggression Rig (PAR) located in the GdF Suez research facilities in St. Denis, France. Ideally, the gouges for neutron diffraction measurement are part of a pipe ring sample, since cutting the ring into a coupon can significantly alter the residual stress distribution around the gouges. Of the three gouges studied, two (BEA161 and BEA178) were contained in pipe ring sections. These two gouged samples had been produced as part of the concurrent MD4-1 project study. The third gouge, P22, was a sample from an earlier study by GdF Suez, and was available in a coupon.

At the time when the neutron beam experiment was ready to begin, the P22 coupon sample was already at the Queen's labs in Canada, while the two pipe rings were being shipped from France. Although limited stress information could be obtained from the P22 coupon sample, it was decided to conduct initial neutron diffraction measurements on it to obtain information which would be useful in determining the optimum measurement locations for the BEA161 and BEA178 gouged pipe ring samples.

Additionally it is important to mention that these neutron diffraction experiments were initially scheduled to be performed at the National Research Council's Canadian Neutron Beam Centre (NRC-CNBC) which is the foremost facility in the world for residual stress measurements on engineering components (the technique was pioneered here). However, the CNBC facility had to go off-line for approximately one year. Fortunately, the team was able to obtain beam time at the National Institute of Standard and Technology (NIST) neutron beam facility near Washington, DC. Each measurement at the NIST facility took approximately three times longer (six weeks instead of two weeks) than it would have at the CNBC, in addition, the measurement locations had to be chosen in advance. Despite this, we were very grateful for the opportunity to use the NIST facility and for the dedication of Dr. Gneaupol-Herold, who conducted all of the measurements. The team was able to obtain very interesting results that provided useful information for both subsequent MFL modeling work as well as evaluations for fitness for service.

7.2 Gouged and gouged+dented samples

The three samples chosen for neutron diffraction measurements all contain gouges that were introduced into pressurized pipeline sections using the Pipeline Aggression Rig (PAR) facility located at the GdF Suez research laboratories in St. Denis, France (**Figure 7-1**). As mentioned previously, gouge coupon P22 was from an earlier study by GdF Suez. The other two gouges (BEA161 and BEA178) were produced as part of the MD4-1 study. Intact pipe rings containing the latter two gouges were cut and shipped to NIST for neutron diffraction measurements.

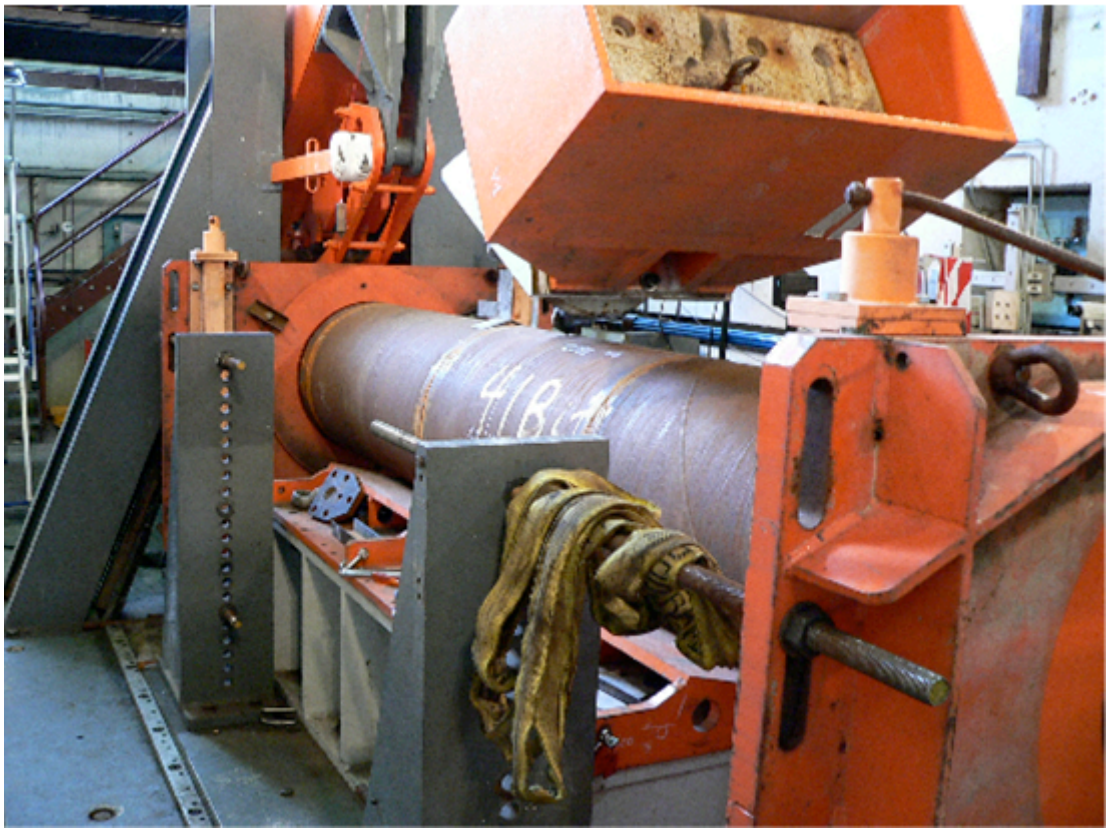

Figure 7-1: Photograph of the Pipeline Aggression Rig facility in GdF Suez St. Denis research facility. Shown is a pressurized pipe about to be gouged using the large simulated backhoe device (above).

The three samples are described below, and photographs of each are shown **Figure 7-2**.

- **P22:** This was a 17 cm long gouge located in a coupon sample approximately 25cm long x18cm wide. The gouge itself is approximately 1-2 mm deep at its deepest point. There is no dent apparent at the inner wall of the pipe.
- **BEA161:** This was a 13 cm long, wedge-shaped gouge, contained in a 60 cm ID, X52 pipe ring sample (Pipe 1) that was cut from a larger pipe section which was pressurized during gouge introduction. The pipe ring was 60cm long, with the cuts made such that the gouge was located near one end to facilitate neutron diffraction measurements. As

seen in **Figure 7-2**, the narrow end of the gouge corresponded to the tool entry location. There was a relatively small, localized dent near the exit (wide) end of the dent. This dent was observed at the inner surface of the pipe and extended along the final 4 cm of the gouge. It was located directly underneath the gouge at the inner wall and did not extend beyond the gouge perimeter. This was classified as a "medium gouge (26% depth through wall) with a shallow dent (1.1% OD)".

- **BEA178:** This was a massive, 30 cm long gouge with an associated large dent that extended well (10-15cm) beyond the perimeter of the gouge on all sides (**Figure 7-2**). As shown in **Figure 7-2**, the gouge was centered in a 60 cm ID, X52 pipe ring sample that was cut from a larger pipe section (of Pipe 1) , pressurized during gouge introduction. In MD4-1 this was classified as a "medium gouge (27% through wall) with a severe dent (5.7% of the pipe diameter).

Figure 7-2: The three gouges examined using neutron diffraction. Sample P22 (left) is a coupon sample containing a 17 cm gouge (tool entry at top end). Sample BEA161 (center) is a 13 cm long wedge-shaped gouged contained in a 60 cm long, 60cm diameter pipe ring of X52 steel (tool entry at top end) . Sample BEA178 (right) is also a pipe ring sample (X52 steel) containing a long gouge with a significant associated dent.

7.3 The neutron diffraction technique – a brief summary

In neutron diffraction, strain is determined by measuring the distances between lattice planes in the 'strained' material and comparing them to those in an 'unstrained' reference piece of the same material. Lattice plane spacing d_{hkl} (where *hkl* are the Miller indices) is determined using neutron diffraction by applying Bragg's law:

$$\lambda = 2\, d_{hkl} \sin\theta_{hkl} \qquad (7.1)$$

For example, for a known wavelength λ of the incident beam, a measurement of the angular position of the diffracted neutron beam $2\theta_{hkl}$, gives the lattice plane spacing. Once this lattice plane spacing is measured at a point of interest, the results are compared to "unstressed" d_{hkl} values to determine strain. More detail regarding the theory and applications for neutron diffraction can be found in references [13] and [14].

Figure 7-3 shows a schematic diagram of a typical neutron diffraction spectrometer, as well as an enlarged region near the measurement location. In the present experiment, Bragg diffraction from the 400 planes of a silicon monochromator was used to select neutrons of a desired wavelength from the Maxwellian distribution of neutron wavelengths that exit the reactor core. Slits of 1 mm width (at the incident beam exit) and 2 mm width (diffracted beam entry to detector) were used to define the size of the region of measurement, shown schematically in the lower right "enlarged" diagram of **Figure 7-3**. The intersection of the incident and diffracted beams is known as the *gauge volume* as indicated on the diagram.

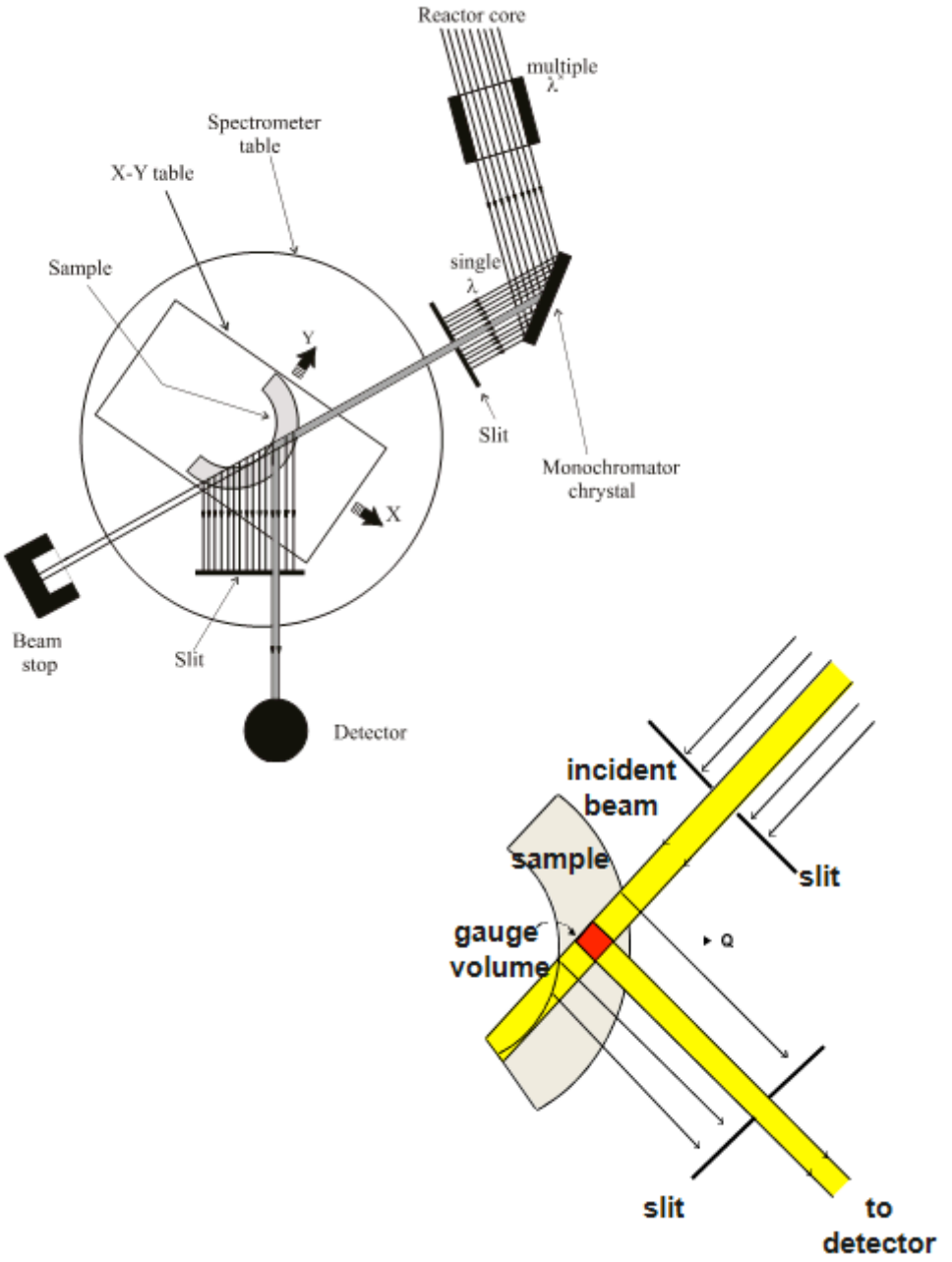

Figure 7-3: (top left) Plan view schematic diagram of a typical neutron diffraction spectrometer configured for strain measurements. (Bottom right), an enlargement of the region of intersection between the incident and diffracted beams. The red intersection region is the region of measurement, known as the gauge volume.

Because this technique is based on diffraction, the strain is measured in the sample direction parallel to the bisector of the incident and diffracted beams (this bisector is known as Q). For example, the configuration shown in **Figure 7-3** will measure the strain in the sample direction denoted 'X' (shown as Q in the lower diagram). To obtain the *stress* at a particular location in the sample, the strain must be measured in each of three mutually orthogonal

directions at that location. To accomplish this, the gauge volume remains at the same point in space, and the sample is re-positioned in three different orientations for three separate strain measurements. With the three measurements of strain at each position (in the radial (R), axial (A) and hoop (H) directions), the residual stress can be calculated through a generalized Hooke's Law. For example, axial stress (σ_A) is calculated by:

$$\sigma_A = \frac{E}{(1+\nu)}\left[\varepsilon_A + \frac{\nu}{(1-2\nu)}(\varepsilon_A + \varepsilon_H + \varepsilon_R)\right] \qquad (7.3)$$

where E is Young's modulus and ν is Poisson's ratio.

7.4 Results: Residual stresses in coupon sample P22

As indicated earlier, P22 is a coupon sample cut from a pipeline section. It contains a significant PAR-produced gouge – 17 cm long and 2 cm wide at its widest point. The gouge and its array of measurements points are shown in **Figure 7-4**. Measurements were made along the length of the gouge, as well as along lateral lines (shown extending vertically). Although this sample was useful for preliminary neutron diffraction measurements (since it was small and therefore easy to manipulate and measure) the removal of the coupon from the pipe section likely altered the 'background' stress pattern significantly. This leads to questioning of the validity of some of the results – most particularly the through-wall 'depth' scans. Despite this, many of the results are of use. In particular, on any given plane through the thickness, the relative measurements are still quite valid and provide very useful information. For example, many of the measurement points are made just below (depth of 0.7 mm) the top surface. These are very useful for examining the extent of the local stress field around the gouge, and the relative variation of stress along the length of the gouge at any chosen surface.

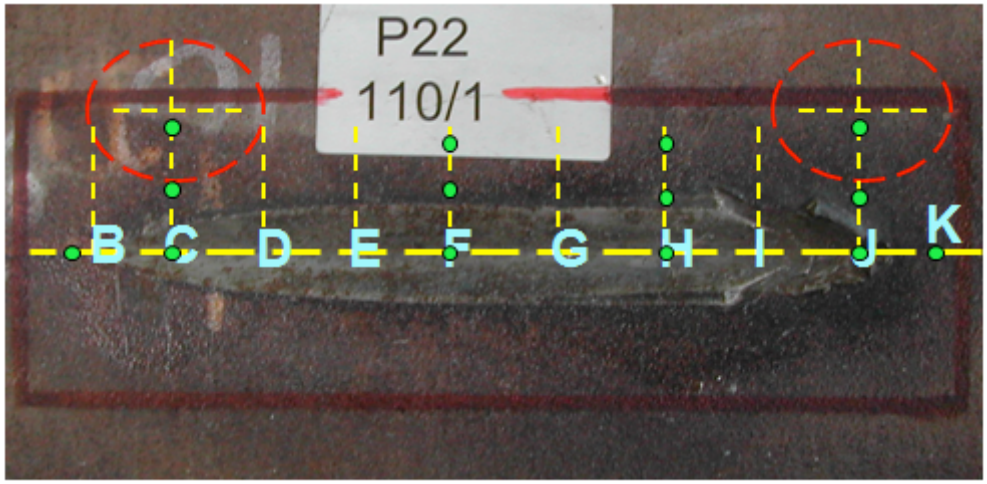

Figure 7-4: Gouge (shown horizontally oriented) in sample P22. Note that gouge in 17 cm long and 2 cm wide at its widest point in the center. Points B and K are outside the ends of the gouge. B is near the gouge entry point and K is near the exit point.

As mentioned earlier in Section 7.3, the volume of sample measured at each data point was defined by 1 mm wide slits at the incident beam and 2 mm slits for the diffracted beam. The height of the beam was 2 mm, thus the measurement volume (gauge volume) was 4 mm^3. The measurement location closest to the surface was centered 0.7mm below the outside surface.

7.4.1: P22: Residual Stress variation along the length of the gouge, immediately below (0.7mm) the surface

Figure 7-5 shows the variation in residual stress along the length of the gouge at a depth of 0.7 mm, starting at point B, with the final measurement point corresponding to point K (note there are many measurements points between that do not correspond directly with the labeled positions). Both hoop and axial residual stresses are shown. In general, results show that both hoop and axial residual stresses are primarily tensile, and relatively small (<100MPa). The only departure from this is an axial compressive region beyond the exit end of the gouge.

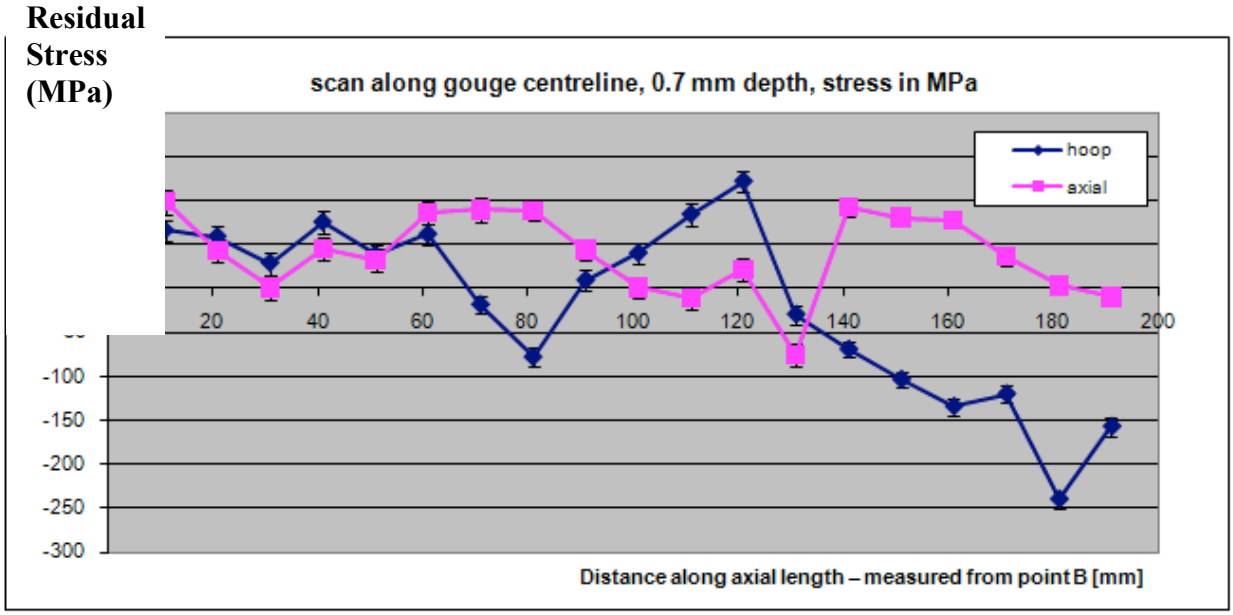

Figure 7-5: Hoop and axial scan at 0.7mm depth – down the center of the gouge. Reference points are shown along the bottom of the graph.

7.4.2 P22: Residual Stress variation lateral to the gouge, immediately below (0.7mm) the surface

The extent of local strain variation at the upper surface can be understood through examination of the lateral scans (shown as vertical dashed lines in **Figure 7-4**). **Figures 7-6** and **7-7** show the results from these lateral scans, with the origin being the centerline of the gouge. All of these measurements were again taken at a depth of 0.7 mm below the outer surface. Note

that there is no difference between **Figures 7-6** and **7-7**; the scans were simply split between two graphs to make the results more comprehensible.

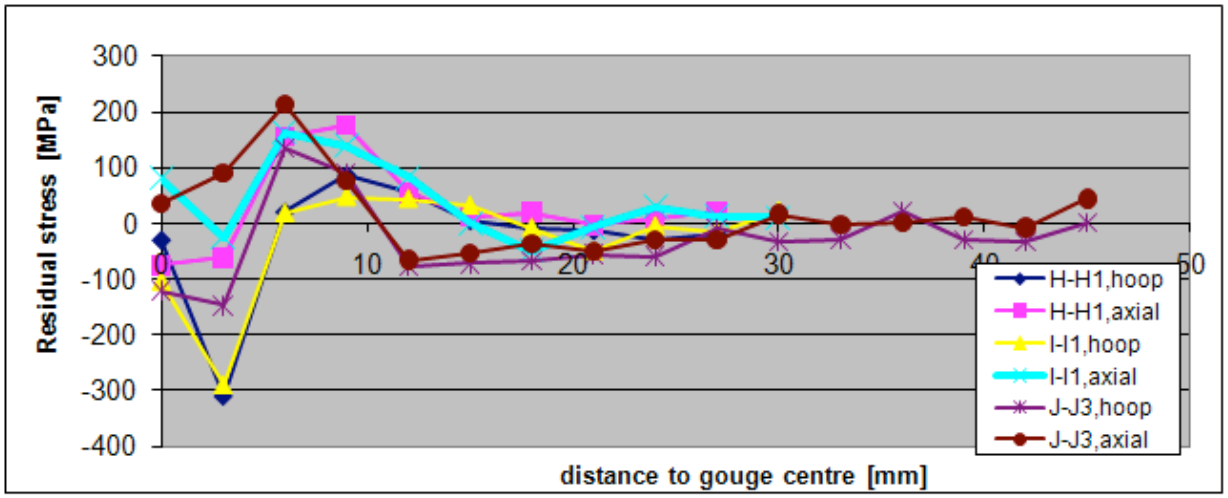

Figure 7-6: Lateral scans at selected locations starting at the gouge center. Hoop and axial results shown, indicating a similar pattern.

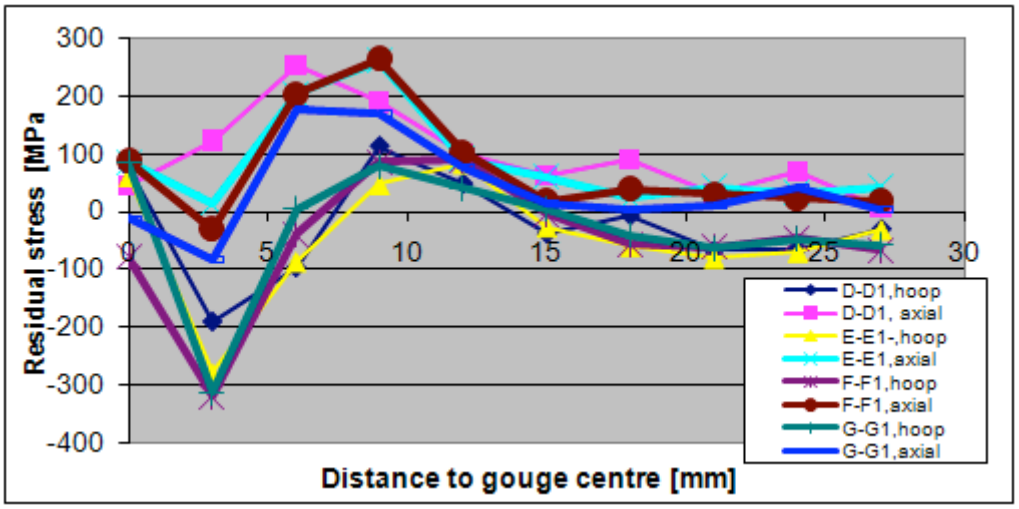

Figure 7-7: Same as Figure 7-3 but with the remainder of the points. Lateral scans at selected locations starting at the gouge center. Hoop and axial results shown, indicating a similar pattern.

The results show a marked consistency in the residual stress pattern at the upper surface. As indicated by **Figure 7-5**, the axial and hoop residual stresses along the midline position of the gouge are not high – between 100 and -100 MPa. Moving laterally, however, the material passes through a compressive region (as low as -300 MPa), and then at the side edge of the gouge it displays a tensile peak up to approximately 250 MPa in some cases. Within another 5 mm beyond the gouge edge the residual stress returns to its background level. This suggests that, at least at the surface, the residual stress effects resulting from a gouge are relatively short range.

7.4.3 P22: Residual Stress variation lateral to the gouge – 0.7mm below the surface, but outside the gouge region

Figure 7-8 shows the lateral scan axial and hoop results beginning at points B and K. B is approximately 1 cm beyond the entry end of the gouge, while K is about 1 cm past the exit end of the gouge. Neither of these scans shows any variation along the length of the measurement locus, which further suggests a very localized residual strain pattern and also relatively low values of strain at the top surface.

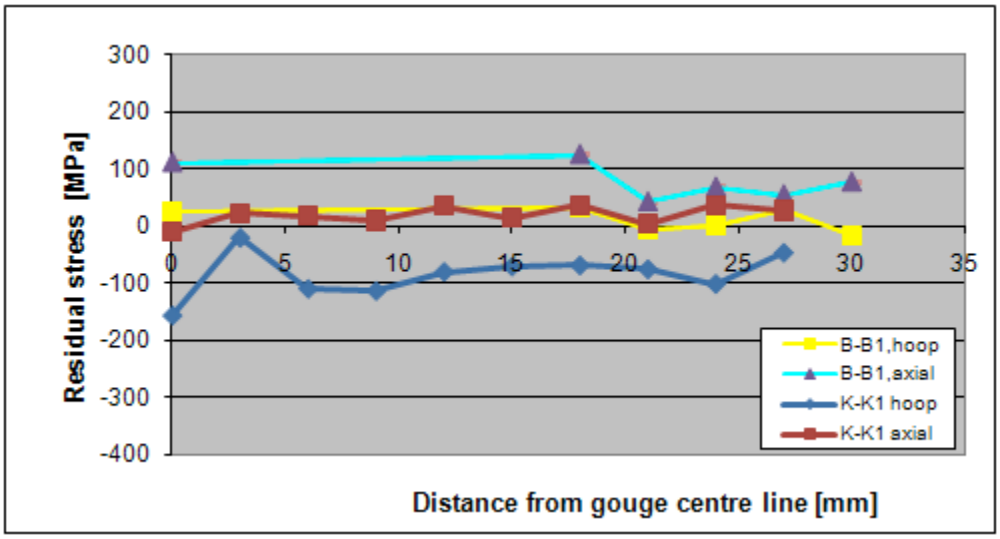

Figure 7-8: Lateral scans from the outer extreme points – beyond the ends of the gouge.

7.4.4 P22: Residual stress depth scan results for selected locations

Figures 7-9 and **7-10** show the depth scan results for the hoop and axial residual stresses, respectively. As seen in these figures, the depth scan results for the hoop and axial stress are far less consistent than the lateral scans at the outer surface. However it is interesting to note that the residual stresses are very high at some locations through the thickness. The hoop stress results suggest an "S-shaped" residual stress distribution, which is typical of a residual bending hoop stress. This is typical in sections that have been cut from pipe sections, since the release of the constraint causes the coupon to 'spring back' thus producing the hoop bending stress. These depth scans suggest a significant variation of residual stress with depth. However because the sample is a coupon, and thus has been cut out of the original pipe and had its constraints released, it is difficult to draw any definitive conclusions.

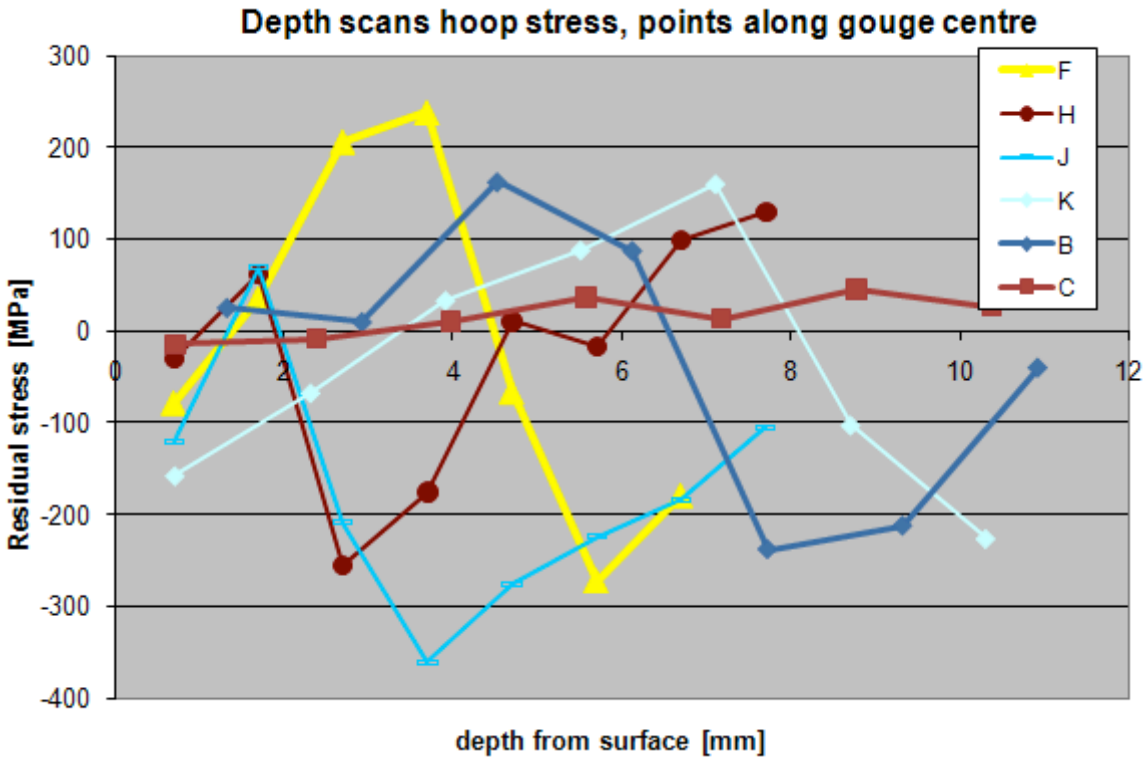

Figure 7-9: Depth scans of hoop stress at the specific points listed – along the gouge center.

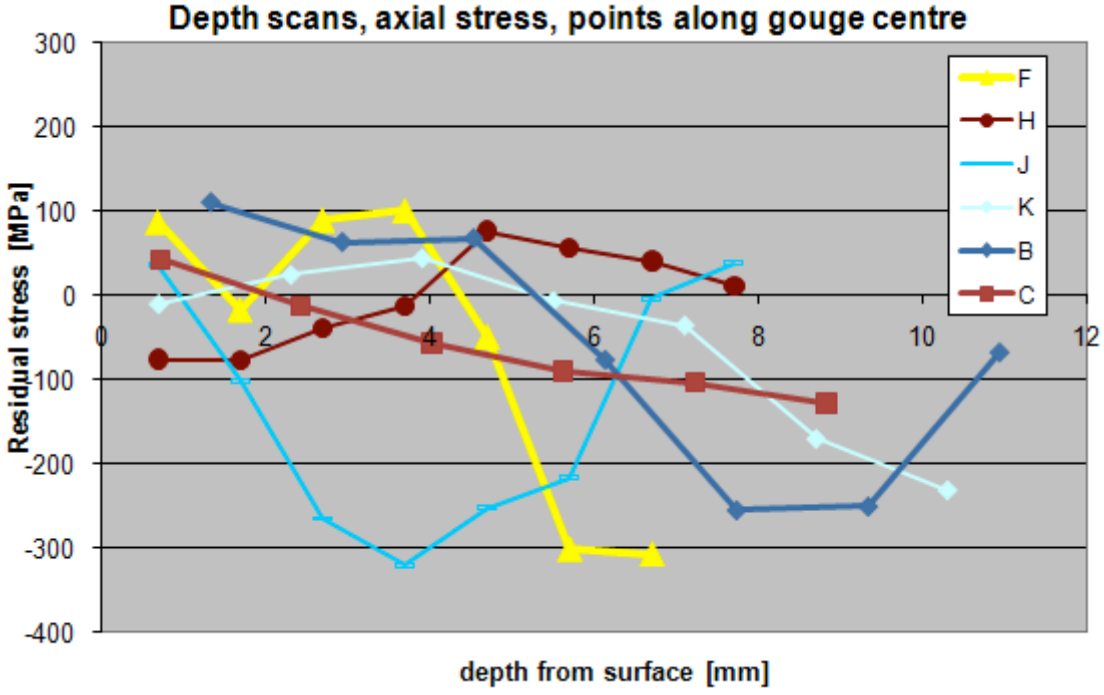

Figure 7-10: Depth scans of axial stress at the specific points listed – along the gouge center.

7.4.5 P22: Conclusions

As mentioned above, the fact that P22 is contained in a coupon sample gives its residual stress results limited credibility; however a number of valuable observations can be made:

- The stresses at the top surface, along the gouge center, are surprisingly small; however there are very significant stresses through the thickness. This indicates that there is considerable value in depth profiling (in preference to surface scanning, for example). Thus in the subsequent scans of BEA161 and BEA178 the focus was on depth scanning.
- The P22 gouge has very little denting apparent. The neutron diffraction results shown in **Figures 7-6** and **7-7** suggest that in this type of gouge the lateral extent of the residual stress field is very small with the stress field back to background levels within about 10 mm of the edges of the gouge.

Therefore, P22 provided some useful information regarding the extent of the strain fields at the outer surface. It also was useful in guiding location selection in the subsequent experiments with BEA161 and BEA178.

7.5 Results: Residual stresses in pipe ring sample BEA161

BEA161 is shown in **Figure 7-11** (and earlier is **Figure 7-2**), was created in an end-capped, pressurized pipeline section of X52 pipe of diameter 24 in. The gouge is approximately 14 cm long, and 20 mm at its widest point. The entry point of the PAR tool is at the right hand (narrow) end of the gouge, and the exit point is at the wider region at the left. The gouge is slightly asymmetric about its midplane. At the inner pipe wall the gouge displays a dent, but that dent is associated only with the last approximately 4cm of the gouge (**Figure 7-12**).

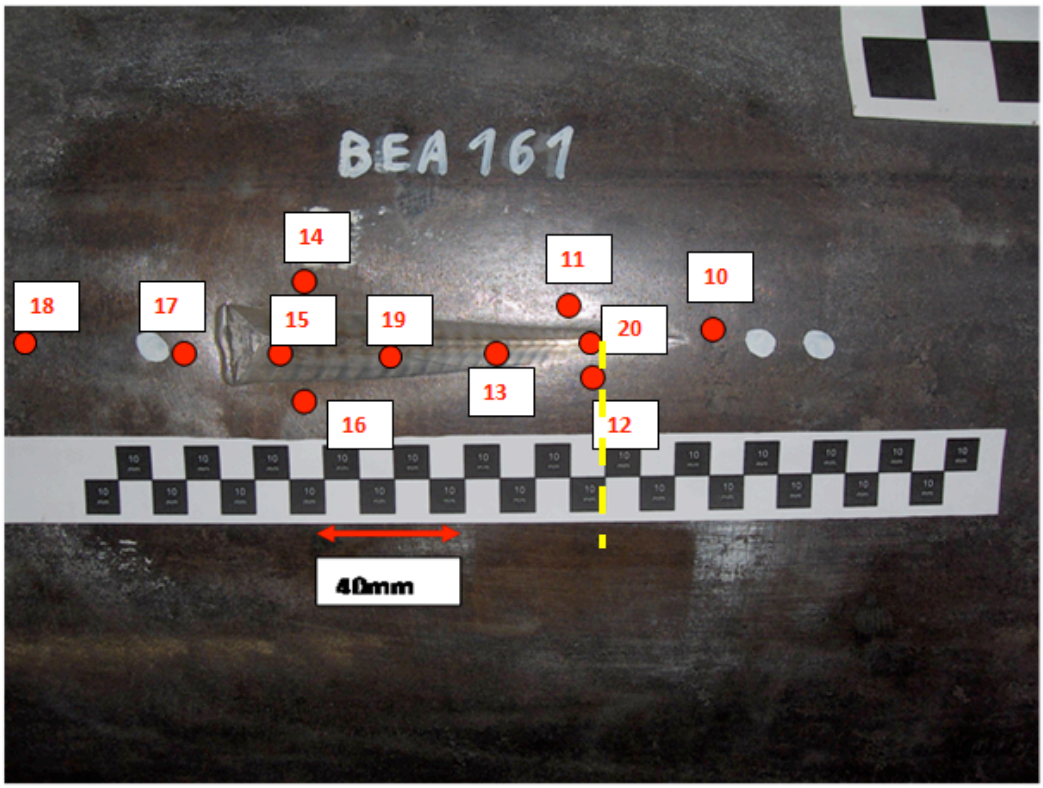

Figure 7-11: Photograph of the gouge BEA161 produced using the PAR facility at GdF Suez in St. Denis, France. The scale at the bottom indicates 10 mm for each square. The red points are locations at which depth profile information was obtained.

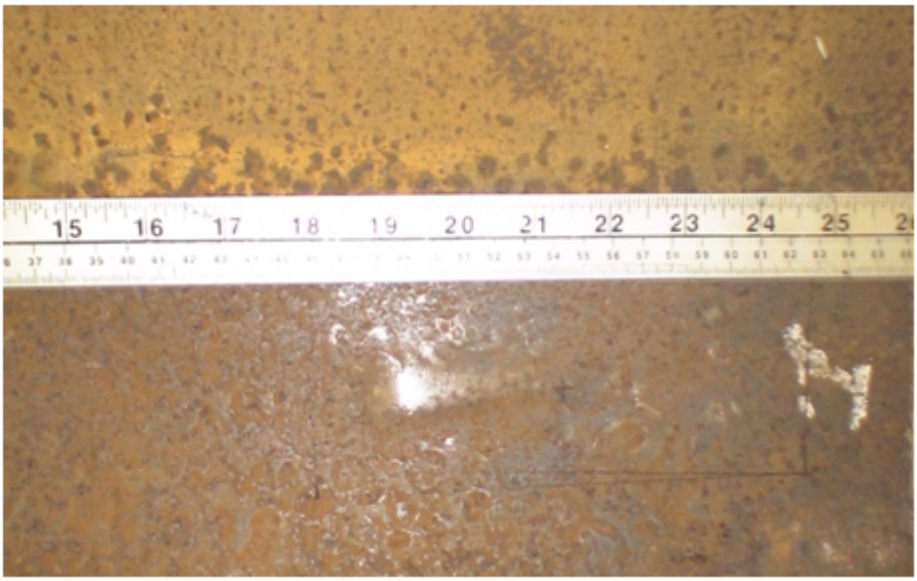

Figure 7-12: Photograph of the gouge BEA161 taken at the inside surface of the pipe. The exit end of the gouge was associated with a very obvious dent on the inside surface – this denting became less severe toward the entry end of the gouge. Overall the observable dent on the inner wall was approximately 5 cm long – while the gouge damage on the upper surface was approximately 14 cm.

After gouge creation, a pipe ring of length 60 cm containing the gouge was cut out of the pipe section. In order to facilitate the neutron diffraction measurements the section was cut such that the gouge was close to one end, as shown in **Figure 7-13** (although this later proved to be problematic for MFL measurements). This pipe ring was shipped to NIST for residual stress analysis using neutron diffraction, and then after that to Queen's labs for MFL analysis. **Figures 7-13** and **7-14** respectively show photographs of the pipe ring section containing the BEA161 gouge and the MFL measurement setup at Queen's with the MFL magnet mounted inside the pipe.

Figure 7-13: Pipe section containing showing gouge BEA161 location

At each of the locations shown in **Figure 7-11** a depth profile was obtained. The neutron diffraction measurements on this gouge took a total of six weeks of dedicated (24 hour) beam time at NIST. All measurement locations were selected in advance, and unfortunately it was not possible to review the data and alter the measurement locations as the experiment proceeded. As a result, retrospectively there are some locations that would have been of interest that were not measured. Despite this, a considerable amount of interesting data was obtained.

As seen in **Figure 7-11,** the locations for neutron diffraction measurements were of two types; 1) locations that lay along the axis of the gouge (points 18, 17, 15, 19, 13, 20 ,10) and also 2) two sets of lateral locations - one near the tool entry end (points 11, 20, 12) and the other near the tool exit end (points 14, 15, 16). The axial locations and the lateral locations will be considered separately in the discussion that follows.

Figure 7-14: Pipe section BEA161 with MFL magnetic inside

7.5.1 BEA161: Residual Stress through-wall hoop and axial stress variations at locations along the centerline of the gouge

Figure 7-15 is a summary plot of all data obtained for locations along the gouge centerline. For easy reference, the gouge including the measurement locations is shown at the top of the figure. Each graph in each row indicates the residual stress depth profile for that particular location, with the upper row being the hoop residual stress results and the lower row the axial residual stress. Also shown at the bottom of **Figure 7-15** is the result for reference Point #18. This location was sufficiently far from the end of the gouge that it was expected to be out of the 'influence zone' of the gouge.

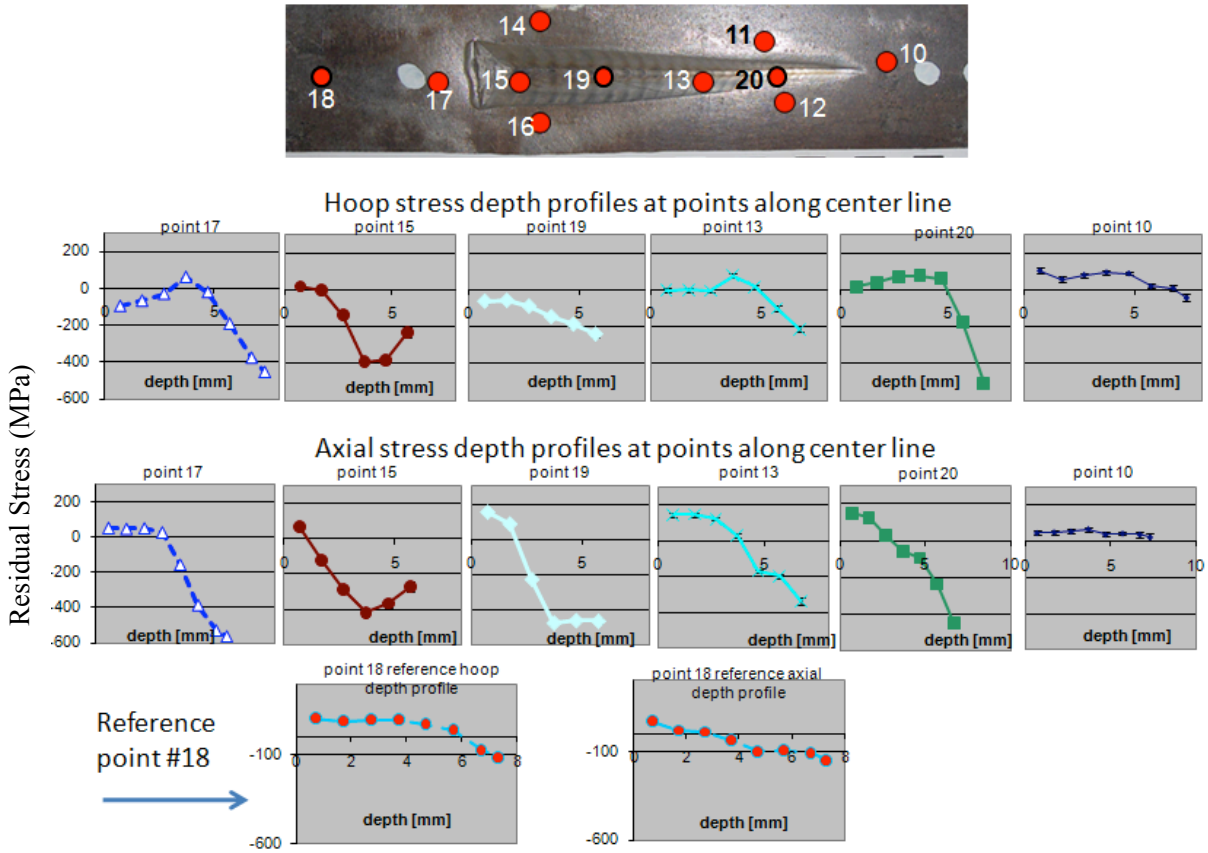

Figure 7-15: Raw data depth residual stress profiles for points along center line. All stresses are in MPa.

As with sample P22, the volume of sample measured at each data point was defined by 1 mm wide slits at the incident beam and 2 mm slits for the diffracted beam. The height of the beam was 2 mm, thus the measurement volume (gauge volume) was 4 mm^3. The measurement location closest to the surface was centered 0.7 mm below the outside surface. The through wall points were centered at depths of 0.7, 1.7, 2.7, 3.7, 4.7, 5.7, 6.7 and 7.3 mm. The last point was just inside the inside wall surface. In some cases at the base of the gouge the wall was thinned (at locations 15 and 19, in particular); for this reason the points closest to the outer wall are "missing" in the plots of **Figure 7-15**. These points are not truly missing, of course, but during the neutron diffraction measurements, the first point at the base of the gouge was considered to be 0.7 mm, and since the wall is thinner here there are no points beyond about 6 mm. In **Figure 7-15** and **Figure 7-17**, the raw data is presented, however for the "in plane" plots presented later (**Figures 7-16** and **7-18**), this data is corrected such that the 'deepest' point is that at the inner wall (and thus the "missing" points correspond to the outer wall, where the gouging has removed material).

Figure 7-15: results from locations reflecting background residual stress - points 18 and 10: At the bottom of the **Figure 7-15** are shown the results for location #18. This is considered far enough away from the gouge that it is relatively unaffected by the locally induced damage. Location #10, just to the right of the entry end of the gouge, displays a similar residual stress pattern. At both locations #18 and #10, the background residual depth profile is similar – at the

outer pipe wall surface the pipe wall is in a state of moderate tensile stress – around +100MPa. Further into the pipe wall the residual stress disappears to essentially zero or becomes slightly compressive. This is the case both for the hoop and the axial residual stress components.

Figures 7-15 and **7-16**: Results from locations affected by the gouging (points 17, 15, 19, 12, 20). In **Figure 7-15** the first row of graphs show the through-wall *hoop* residual stress data taken at each measurement location along the gouge. The second row of graphs show the through wall *axial* residual stress data taken at each location.

Figure 7-16 presents the data of the previous figure in a different way. In **Figure 7-16** the stresses are plotted at specific planes through the thickness. These plots indicate that just underneath the gouge (at depths of 0.7 mm and also at 2.7 mm), the material is predominately in a state of slight residual tension, both in the hoop and axial directions. But continuing through the thickness the region under the gouge becomes more compressive. Past the mid-thickness point compressive stress progressively increases until it is very high – near compressive yield – at the inner surface.

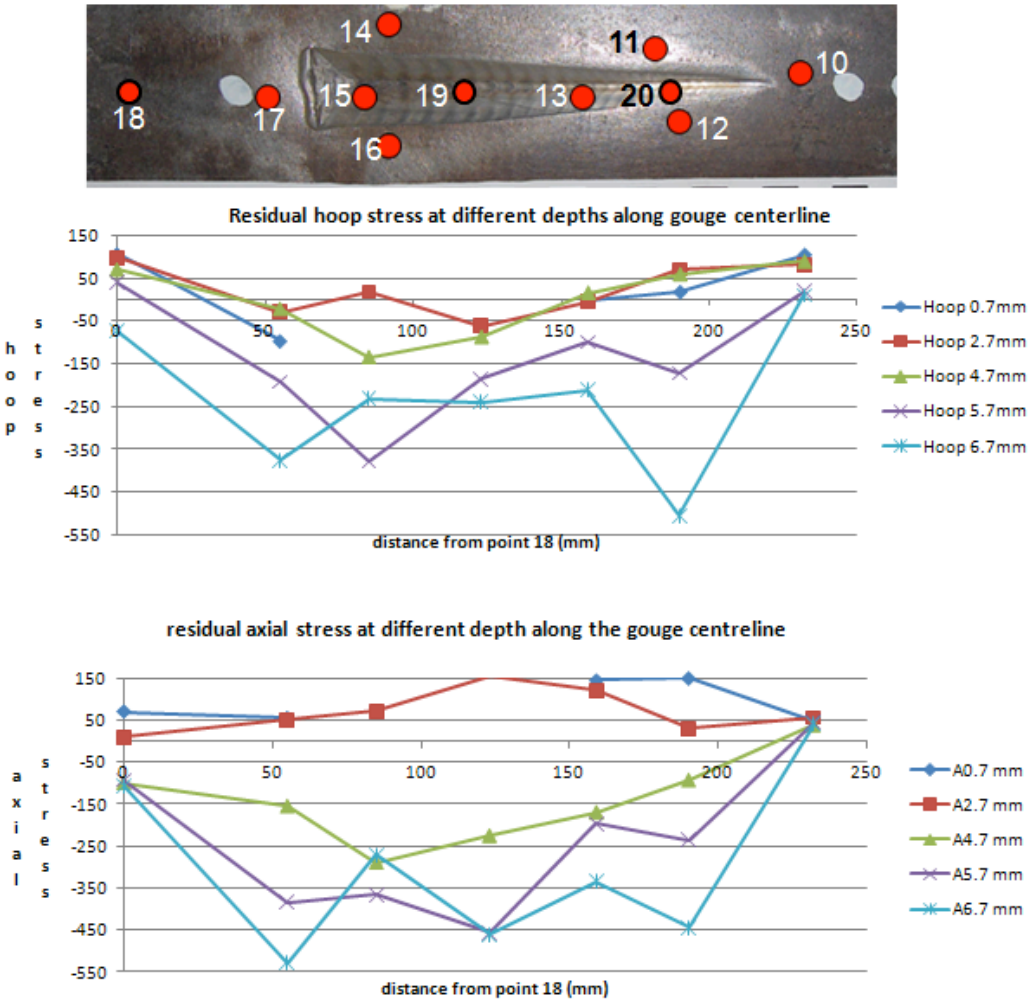

Figure 7-16: Plots of hoop (top) and axial (bottom) residual stresses along planes through the wall thickness (note that the 'lateral' points 14, 16, 11, and 20 are not included in these results but follow in the next section).

A summary of the results observed along the centerline of the gouge follows:

- Point 18 is far enough away from the gouge to be in the background. The pipe background residual stress condition is slightly tensile at the top surface, tending to zero residual stress near the center.
- Similarly, there appear to be no gouge-induced residual stresses at point 10, approximately 1cm from the tool entry point.
- There are significant gouge-induced residual stresses at point 17 – approximately 1cm from the exit end of the gouge. However, it should be noted that point 17 is likely within the associated dent region.
- Directly under the gouge, and extending approximately to the midplane of the wall, the residual stress is tensile and relatively low.
- Beyond the pipe wall midplane there is a relatively steep compressive stress gradient towards the inner wall (**Figure 7-15**).
- The highest compressive stresses along the length of the gouge appear to be just under the entry end of the gouge (point 20) and also in the "ungouged" material at the exit end (**Figure 7-16**).
- The compressive stresses at the inner wall are less in the midregion of the gouge – points 15, 19 and 13 (**Figure 7-16**)
- Point 15 displays an anomalous decrease in compressive stress at the inner wall surface (**Figure 7-15**). However, this point is associated with two other gouge features which likely complicate the scenario – first the wall is thinner at this point by about 25%. Second, this point sits right on top of the bump (dent) associated with this gouge.

7.5.2 BEA161: Residual Stress through-wall hoop and axial stress variations at LATERAL locations across the cross section of the gouge

Figure 7-17 is a summary plot of all data obtained along the lateral directions that cross the gouge – points 14, 15, 16 at the gouge exit end (results shown on the left hand side), and points 11, 20, 12 at the gouge entry end (results shown on the right hand side). In this figure, the hoop and axial residual stress results are shown side by side. The gauge volume and measurement locations through the thickness are the same as used for the points considered in the previous section.

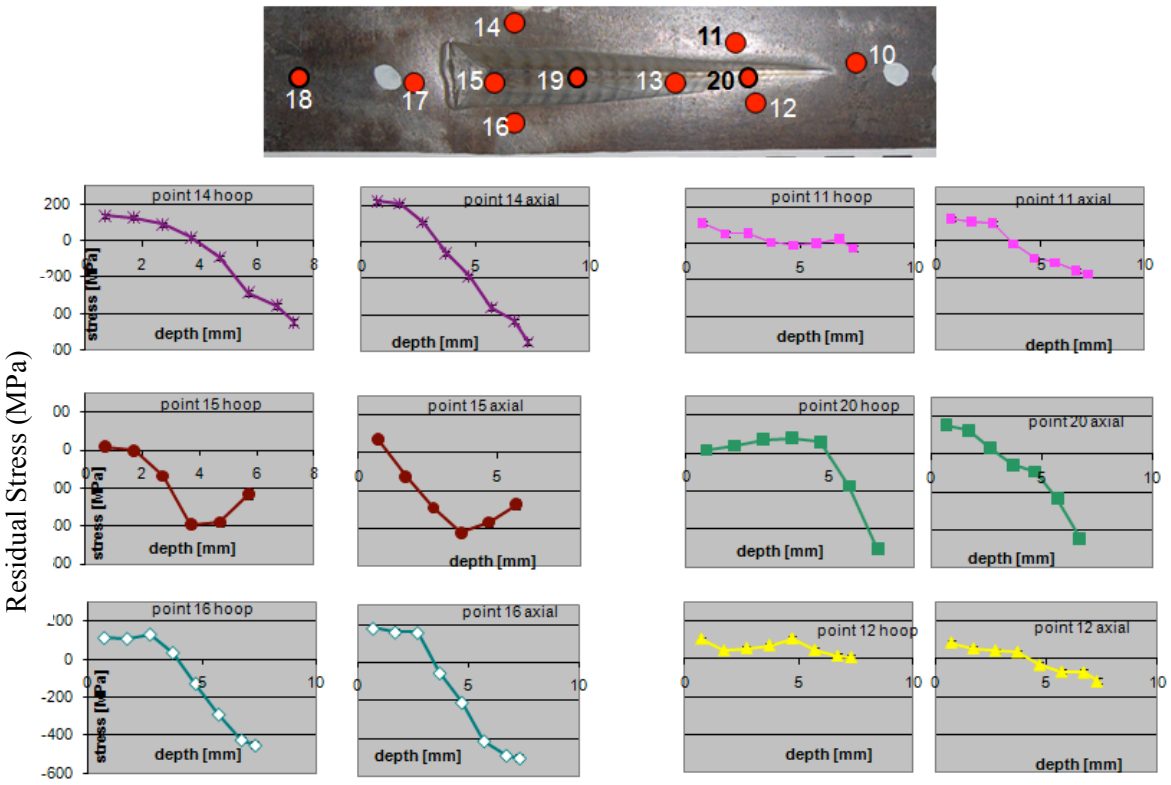

Figure 7-17: Raw data depth residual stress profiles for lateral points 14,15,16 and 11, 20,12. All stresses are in MPa

Figure 7-18 is similar to the summary diagram shown earlier in **Figure 7-16**; the data is shown along planes at particular depths through the wall thickness. The bottom two graphs show the lateral "cross section" results near the gouge entry location (see schematic). The upper two graphs show the lateral results near the gouge exit location. The results at these two locations are very different, and are summarized below:

- Near the gouge *entry* location the compressive stresses are very high at the inner pipe wall *directly beneath the gouge*. However these stresses are highly localized, since immediately to the sides of the gouge the stress is back to near-background levels.
- Near the gouge *exit* location the opposite is true. The un-gouged material at the side of the gouge near the exit displays very significant local residual stresses; both axial and hoop residual stresses are slightly tensile at the outside surface, changing to highly compressive at the inner wall. In fact, the compressive residual stress at the outer wall gouge exit location is higher *beside* the gouge than it is directly *below* the gouge (although directly below the gouge the pipe wall is thinner which may contribute to the lower value).

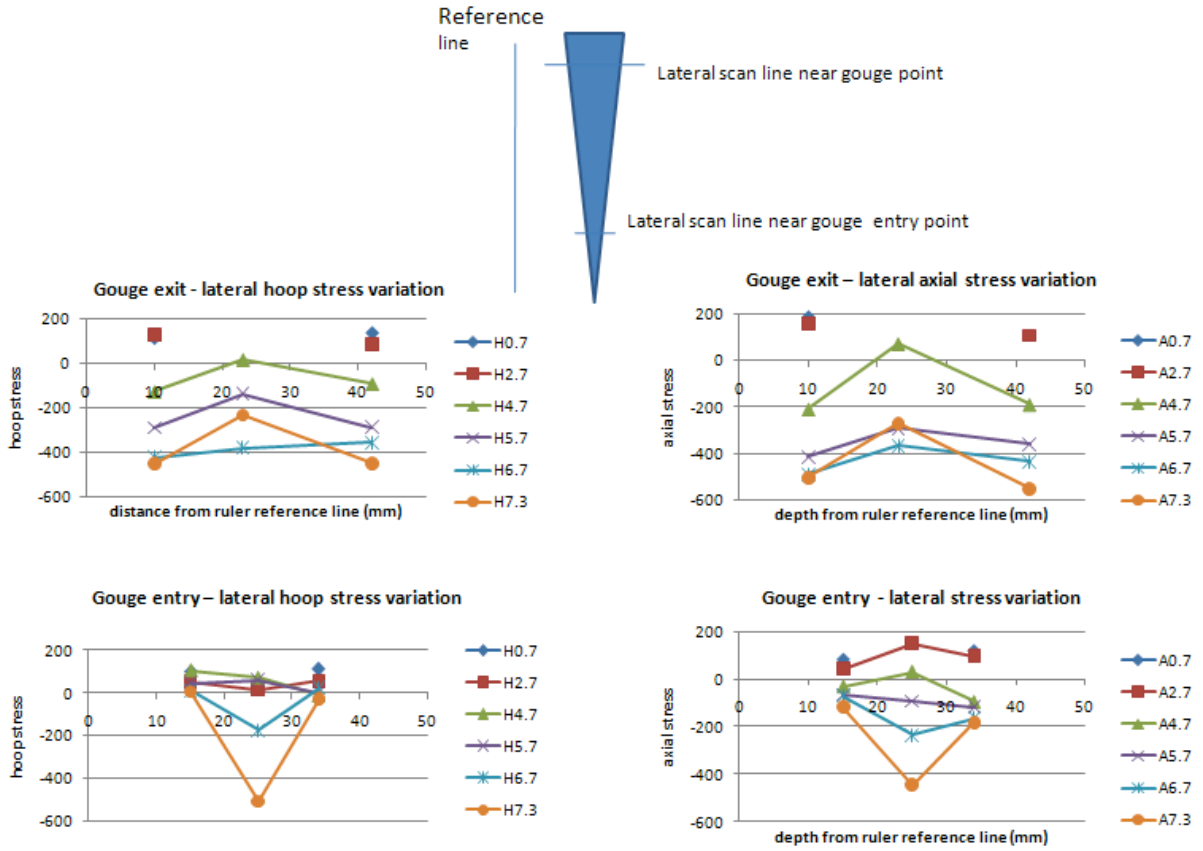

Figure 7-18: Stress data for the lateral lines that cross the gouge near the entry and exit locations.

To summarize the lateral scan results: at the gouge entry location the residual stress is highly localized to the immediate gouge region. However, at the gouge exit location there is a significant lateral strain field directly adjacent to the gouge.. This location also corresponds to the dent location. Unfortunately the lateral extent of this strain field was not investigated due to time constraints.

7.5.3 BEA161: Conclusions

The following are general conclusions drawn from the results of the residual stress determination for the BEA161 sample (gouge, small dent):

- The residual stress depth profiles are generally consistent from location to location within the gouge region – i.e. all exhibit a stress gradient with a small tensile stress at the outer surface and a more significant compressive stress at the inner wall.
- Axial and hoop residual stress results look similar:
    - Outer wall residual stresses are moderately tensile (50-100MPa).
    - Inner wall residual stresses are near yield and compressive

  The lateral extent of the residual stress field varies along the gouge. At the entry end the residual strain field only exists in the immediate region of the gouge itself. However, at

the exit end (where the dent is located) there is more extensive laterial spreading of the lateral strain field.

7.6 Results: Residual stresses in pipe ring sample BEA178

BEA178 is a gouged+dented pipeline section produced using the PAR at the GdF Suez laboratories in St. Denis, France. The damaged region, shown in the photographs of **Figures 7-19** and **7-20** was created at the center of a length of pressurized X52 pipeline section of diameter 60 cm (see **Figure 7.1**). The gouge itself is approximately 37 cm long, and 20 mm at its widest point. As shown on the left hand photograph in **Figure 7-19**, the entry point of the PAR tool is at the left hand end of the gouge, and the exit point is the at the right end. This is not a simple gouge, however, it is surrounded by a very large, symmetrical dent. The extent of this dent can be appreciated by examining the photos of **Figure 7-19** and **7-20**. The overall dent extends to approximately 7 cm to each side of the gouge centerline, for a total dent width of 14 cm.

At the inside surface this dent+gouge also displays a very large deformed area. **Figure 7-20** includes two photographs which capture the extent of the inner pipe wall perturbation. The chalk marks on the photo at the left correspond to the perimeter of the dent.

After gouge was created at GdF Suez, a 500 mm long pipe ring containing the gouge and dent was cut from the pipe section, as seen in **Figure 7-19**. This pipe ring was shipped to NIST for residual stress analysis using neutron diffraction, and after that to Queen's University labs for MFL analysis.

Figure 7-19: Photographs of gouge+dent BEA178 in pipeline section sent to NIST for residual strain measurements.

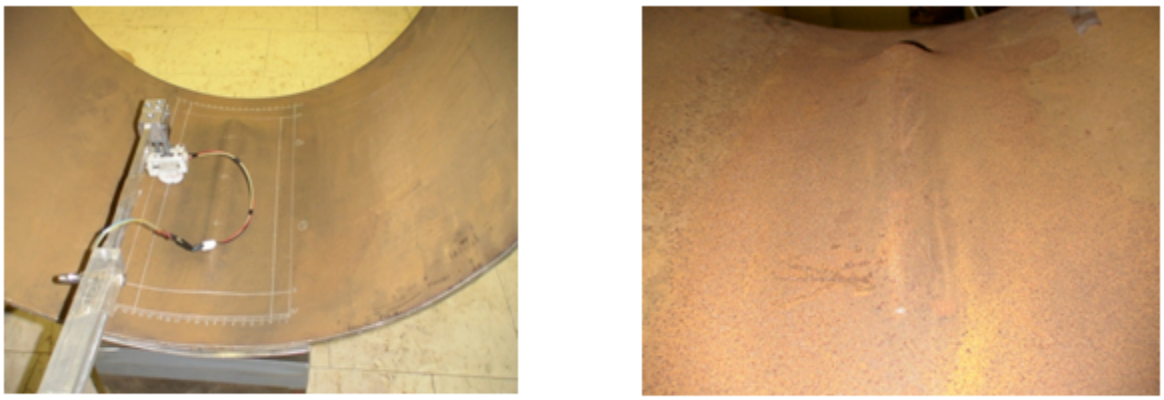

Figure 7-20: Photographs of the gouge BEA178 taken at the inside surface of the pipe. On the left is shown axial extent of the gouge (note the MFL tool arm is also in view). Only the geometry of the immediate gouge-dent is obvious in the photograph; however the chalk lines outline the perimeter of the dent geometry. The photograph on the right is a close-up of the inner wall gouge-dent taken from one end.

For neutron diffraction experiments, measurement locations were (as with BEA161) selected in advance (shown in **Figure 7-21**). Because of the nature of the work it was not possible to review the data and alter the measurement locations as the experiment progressed. At each of the measurement locations shown in **Figure 7-21** a depth profile of residual stress was obtained (for a total of 276 measurements). The neutron diffraction measurements on this gouge took a total of six weeks of dedicated (24 hour) beam time.

As seen in **Figure 7-21**, the neutron diffraction measurement locations were of two types: 1) locations along the gouge axis (points 11, 10, 7, 6, 3, 2 and 1), and also 2) lateral measurements at two locations; one near the tool entry end (points 7,8,9) and the other near the tool exit end (points 3,4,5). The two sets of results will be treated separately in the discussion that follows. In addition there was also a "background" residual stress depth profile obtained at point 12, which was chosen to be outside the perimeter of the deformed region.

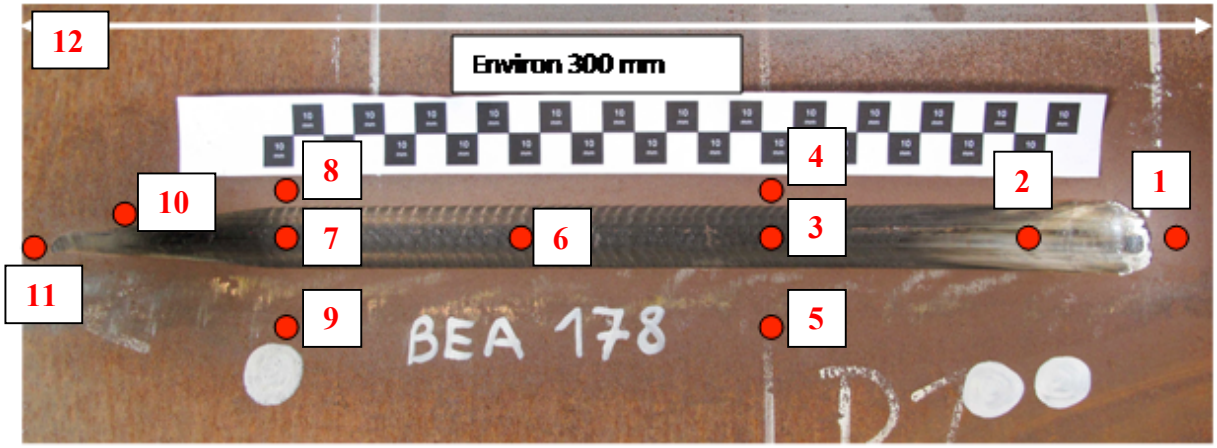

Figure 7-21: Dent+gouge region showing neutron diffraction measurement locations. At each of the numbered locations a depth profile of residual stress was made, involving separate measurements of the axial, hoop and radial strain.

7.6.1 BEA178: Residual Stress through-wall hoop and axial stress variations at locations along the centerline of the gouge

Figure 7-22 is a summary plot of all data obtained for locations along the gouge centerline. For reference, the gouge including the measurement locations is shown at the top of the figure. Each graph in the row indicates the depth profile for that particular location, with the upper row being the hoop residual stress results and the lower row the axial residual stress.

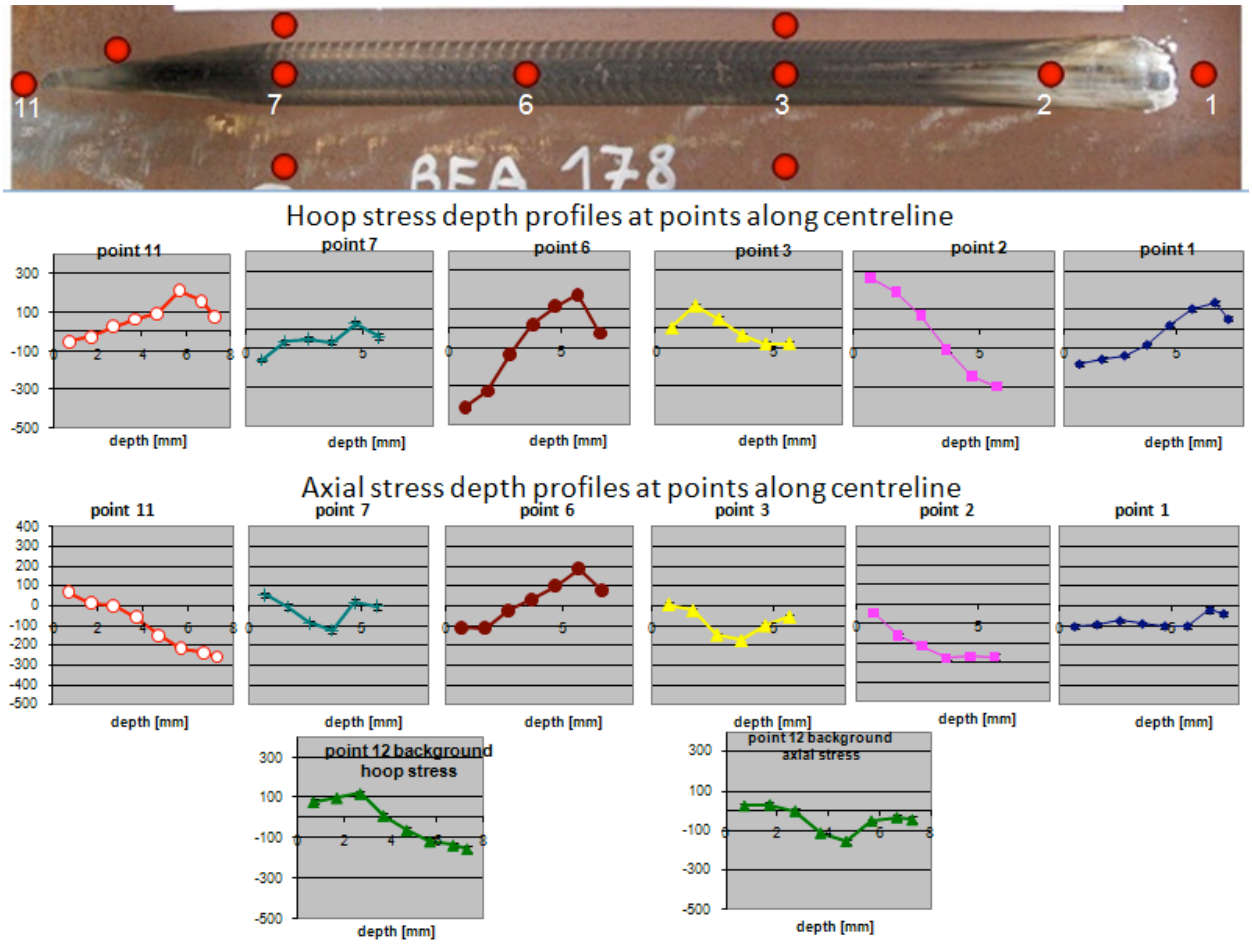

Figure 7-22: Summary plot of all data obtained along the center line of the gouge. Note points 8, 9, 4 and 5 are not included in these plots – see Figure 7.24.

As with the previous gouge sample BEA161, the volume of sample measured at each data point was defined by 1 mm wide slits at the incident beam and 2 mm slits for the diffracted beam. The height of the beam was 2 mm, thus the measurement volume (gauge volume) was 4 mm^3. The measuring location closest to the surface was centered 0.7mm below the outside surface. The through wall points were centered at depths of 0.7, 1.7, 2.7, 3.7, 4.7, 5.7, 6.7 and 7.3 mm. The last point was just inside the inside wall surface. In some cases at the base of the gouge the wall was thinned (at locations 7, 3 and 2); for this reason the points closest to the outer wall are "missing". These points are not truly missing of course, but during the neutron diffraction measurements the first point at the base of the gouge was considered to be 0.7 mm, and since the wall is thinner here there are no points beyond about 6 mm. In **Figure 7-22** and **7-24** the raw data is presented, however for the "in plane" plots presented later (**Figure 7-23**); this data is corrected such that the 'deepest' point is that at the inner wall (and thus the "missing" points correspond to the outer wall, where the gouging has removed material).

Figure 7-22: Results from location reflecting background residual stress - points 12: At the bottom of **Figure 7-22** are shown the depth profile results for location 12. This point is far from the gouge and just outside the dent perimeter. It is expected to reflect the 'background'

residual stress through-wall variation in the pipe wall. As seen in the figures showing the residual hoop and axial stress for this point, there are variations but in general the stress remains within the ±100MPa range. This is consistent with that found in BEA161, the other gouge measured using neutron diffraction. It should be noted, however, that the dent is very large in BEA178 and thus there may still be some stress influence, even at distances as far away as point #12.

Figures 7-22 and **7-23**: Points along the gouge centerline 11, 7, 6, 3, 2, 1 In **Figure 7-22,** the first row of graphs show the through-wall *hoop* residual stress data taken at each measurement location along the gouge. The second row of graphs show the through wall *axial* residual stress data taken at each location. These results are essentially the raw data provided by the residual stress determination.

Figure 7-23 presents the raw data of the previous figure in a different way. In **Figure 7-23** the stresses are plotted at three different planes through the thickness: 2.7mm, 4.7mm, and 6.7mm (note they are not plotted on single graphs like they were for sample BEA161).

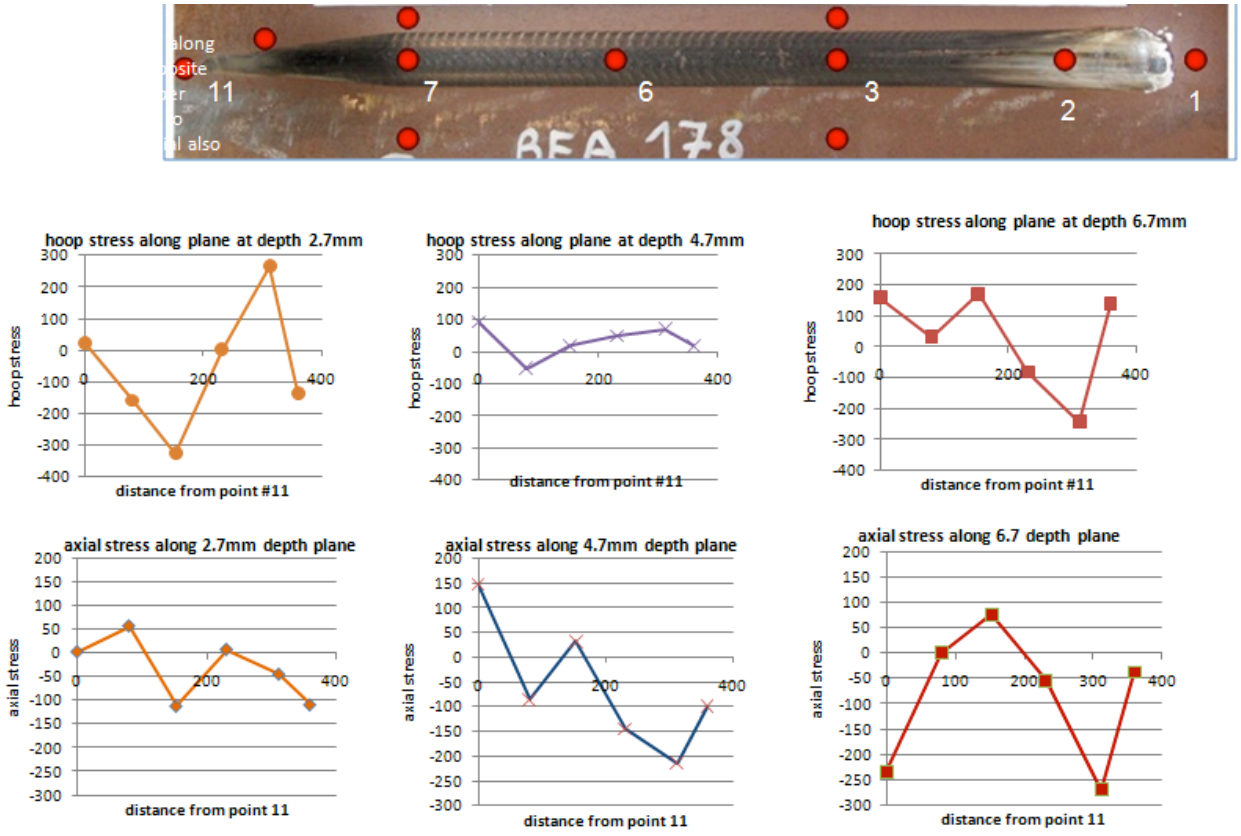

Figure 7-23: Hoop distributions along planes – show opposite behavior from upper surface compared to lower surface – axial also shows different behavior but more complex.

The most striking observation about gouge+dent BEA178, as observed in **Figures 7-22** and **7-23**, is the lack of consistency from point to point along the length of the gouge. **Figure 7-22** shows that residual stress results through the thickness vary significantly; compare, for example, the residual hoop stresses at point 6 with those of point 2. Both show stresses varying markedly from the inner to the outer wall surface, but the stress gradient is almost exactly opposite in the two cases. The same lack of consistency is seen in the axial residual stresses. **Figure 7-23** shows the same general lack of consistency in stress values along any chosen plane.

The lack of consistency is likely to be due to the fact that this gouge is included in a very large dent. Earlier work on dent structural simulations [5] indicated that "plain denting" involves a fairly complex bending behavior. In the present case, where denting occurs during gouging, the dent introduction process is much more complex than it is in the case of plain denting. Thus, a complex through-wall residual stress pattern is not unexpected when such a large gouge+dent is present.

7.6.2 BEA178: Residual Stress through-wall hoop and axial stress variations at LATERAL locations across the cross section of the gouge

Figure 7-24 shows the residual stress depth profiles for lateral scan points at two locations along the gouge – points 7, 8 and 9 and also points 4, 3, and 5. The depth profile data are plotted on the same graphs in **Figure 7-25** in order to facilitate comparison. **Figure 7-25** shows that the general trend in through-wall residual stress is similar on either side of the gouge (compare the profile for 8 and 9, and 4 and 5). The depth profile at the gouge center is not always consistent with this; however this may be due to wall thinning in this region. Ideally, more lateral data locations would have been selected further away from the gouge, however at the time when the measurement locations were being selected the Queen's team was not aware of the large extent of the dent associated with the gouging.

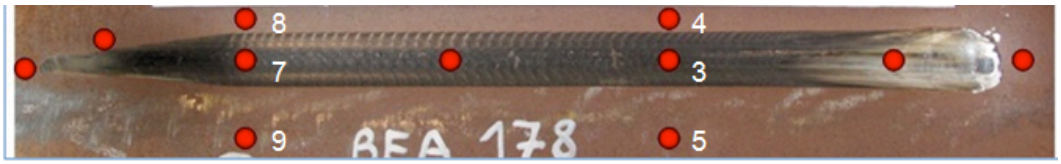

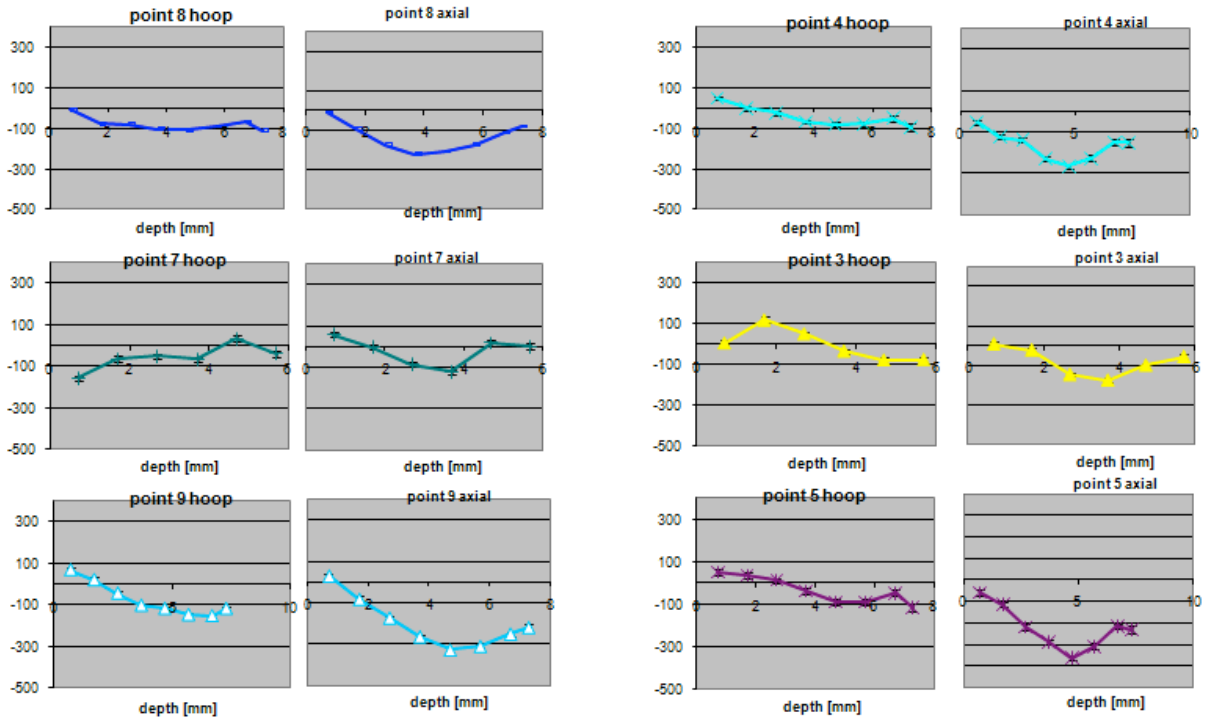

Figure 7-24: Shows the depth profile for lines in the lateral direction at point 7 and point 3. See next plot for combined plots (more instructive).

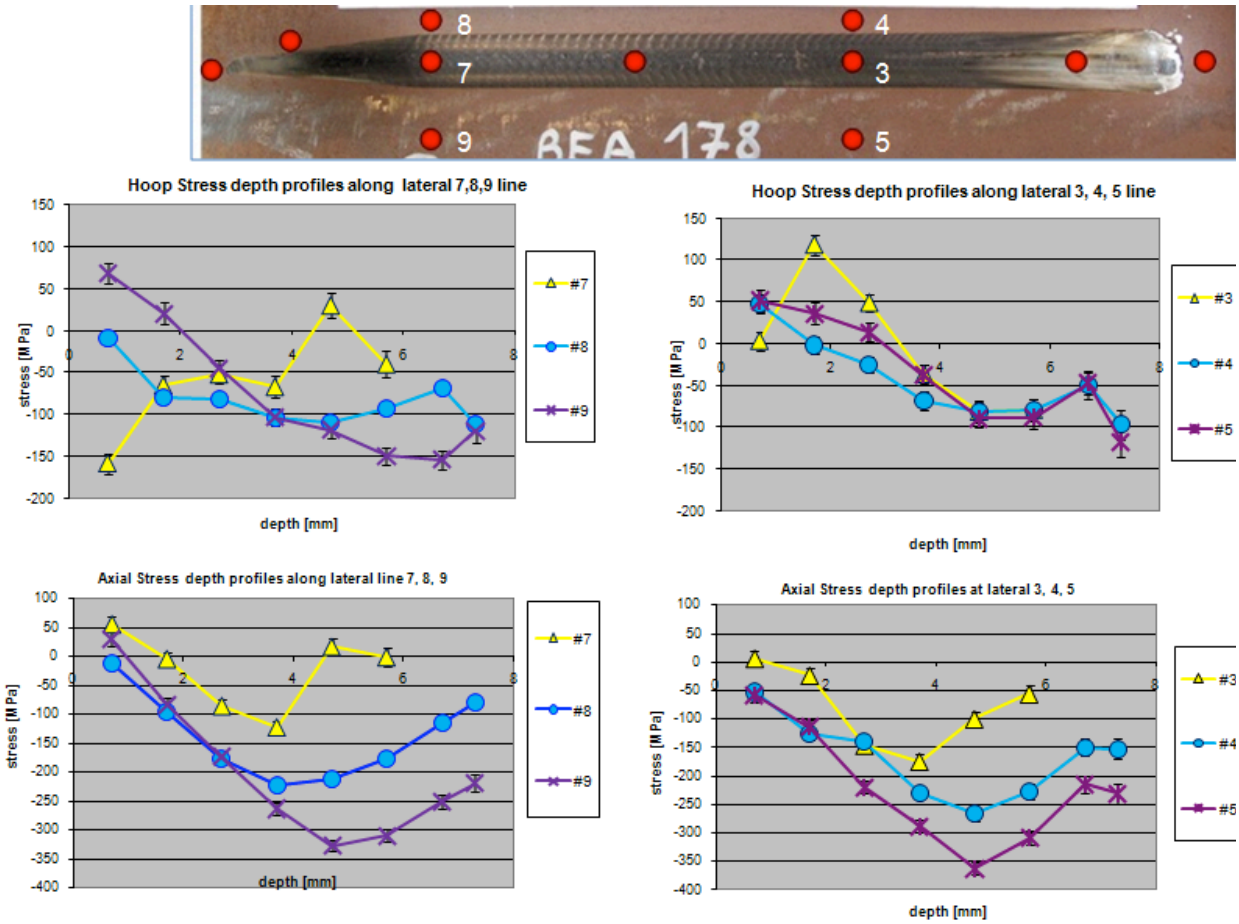

Figure 7-25: Combined versions of the plots on the previous page – note the difference in stress values from hoop to axial.

7.6.3: BEA178: Conclusions

The residual stress results from this gouge+dent were inconsistent from point to point, and suggested a complex bending stress resulting from the gouging process. The symmetrical nature of the results (on either side of the dent) suggested that future neutron diffraction scans could focus on only one side of the gouge, thus reducing the number of points needed.

7.7 Comparison of residual stress distribution results for all 3 samples – P22, BEA161 and BEA178

In comparing the three gouges studied, it should be noted that the first two – P22 and BEA161 – were gouges having very little denting apparent. The third sample – BEA178 – was actually more of a severe dent than it was a gouge, so if anything the damage associated with denting overwhelmed those of gouging.

The results of P22 and BEA161 were somewhat similar (although the results of P22 need to be considered with care since a coupon sample was involved). In both cases the axial and hoop stress variations were quite similar. In addition, the local residual strain field was observed to be highly localized, existing only in the immediate gouge vicinity. Also for both gouges, the residual stresses near the outer wall were moderate at the center of the gouge. The P22 results suggested that the outer wall residual stresses vary considerably laterally across the gouge itself, going from near neutral (at the centerline) to compressive and then tensile as one approaches the gouge side edge. The detailed residual stress variations laterally across the gouge itself were not studied in the BEA161 sample. .

The depth profiling done on gouge BEA161 indicates that the residual stress pattern was fairly consistent from location to location:

- Axial and hoop residual stress look similar
- Outer wall residual stresses are moderately tensile (50-100 MPa)
- Inner wall residual stresses are highly compressive.

Furthermore, except in the region associated with denting, the local residual strain field was found to be very localized.

The result of BEA178 was very different than either P22 or BEA161, and this has been attributed to the presence of a large associated dent. The complex denting process associated with this kind of gouge+dent dominates the residual stresses, making the residual stress distribution very complex. In addition, rather than having a residual stress field that is localized in the immediate gouge vicinity, the varying stress distribution extends to the edge of the dented region. Further studies are needed to quantify the behavior in these large, complex damage situations.

8.0 MFL Signals—Measured and Modeled MFL Results from Gouge Sample BEA161

8.1 Introduction

As mentioned in Chapter 6, neutron diffraction measurements were not completed on the SES gouge samples, thus the modeling work for those gouges included only the geometry component, without the associated residual stress component. However, neutron diffraction measurements were conducted on BEA161 (moderate gouge, small dent) and BEA178 (mild gouge, severe dent). The results for BEA178 were very complex and will require more information before accurate modeling can be completed. However the residual stresses around BEA161 were fairly localized and consistent, therefore it was possible to incorporate them into the magnetic models. This section describes the experimental MFL signals obtained for BEA161, outlines the magnetic modeling, and compares the modeled and experimental MFL signals for this defect.

8.2 Experimental MFL measurements on BEA161

Figure 8-1 shows two photographs of the gouge BEA161. The one on the left shows the defect 'close up', while the right photograph shows the pipe ring containing BEA161. In the latter, it is clear that the gouge is located close to the cut end of the pipe; this was done to facilitate neutron diffraction measurements at NIST.

It should also be noted that, although the outside surface was "clean" as seen in the photos of **Figure 8-1**, the inner wall was pitted and covered in a layer of corrosion product. The inner wall surface can be seen in the previously presented **Figure 7-12**.

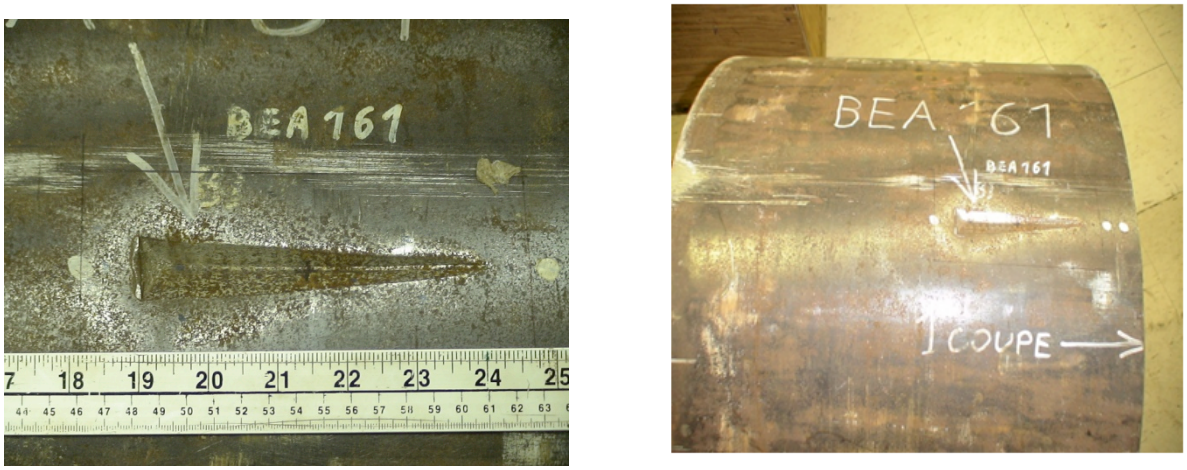

Figure 8- 1: Photographs of BEA161 – on the left is a closeup of the gouge, with a ruler indicating the size. On the right is shown the pipe ring that was sent to NIST and Queen's which contained the gouge. Note the close proximity of the gouge to the end of the pipe ring - this was done deliberately to facilitate neutron diffraction measurements at NIST.

Although having the gouge in close proximity to the end of the pipe section was ideal for neutron diffraction measurements, this asymmetry proved to be problematic for MFL measurements. One of the magnet pole pieces was placed near the center of the pipe, however, the other one was very close to the end of the pipe section (actually it was hanging off slightly). This caused significant anomalies in the magnetic flux pattern in the pipe, resulting in a very unusual background MFL pattern. As a result, background subtraction had to be done manually, with some subjectivity introduced when interpreting the pattern. Furthermore, the manual background subtraction method proved less successful for the inner wall MFL (radial) signal. **Figure 8-2** shows the MFL (axial) and MFL (radial) signals measured at the outside (top) and the inside (bottom) of the pipe wall. Note that the problematic background signal is responsible for the peak at the extreme right hand side of all of the MFL signal plots in this figure. In addition the inside wall MFL (radial) signal is unusual because the aspects of the background signal could not be successfully extracted from the raw data.

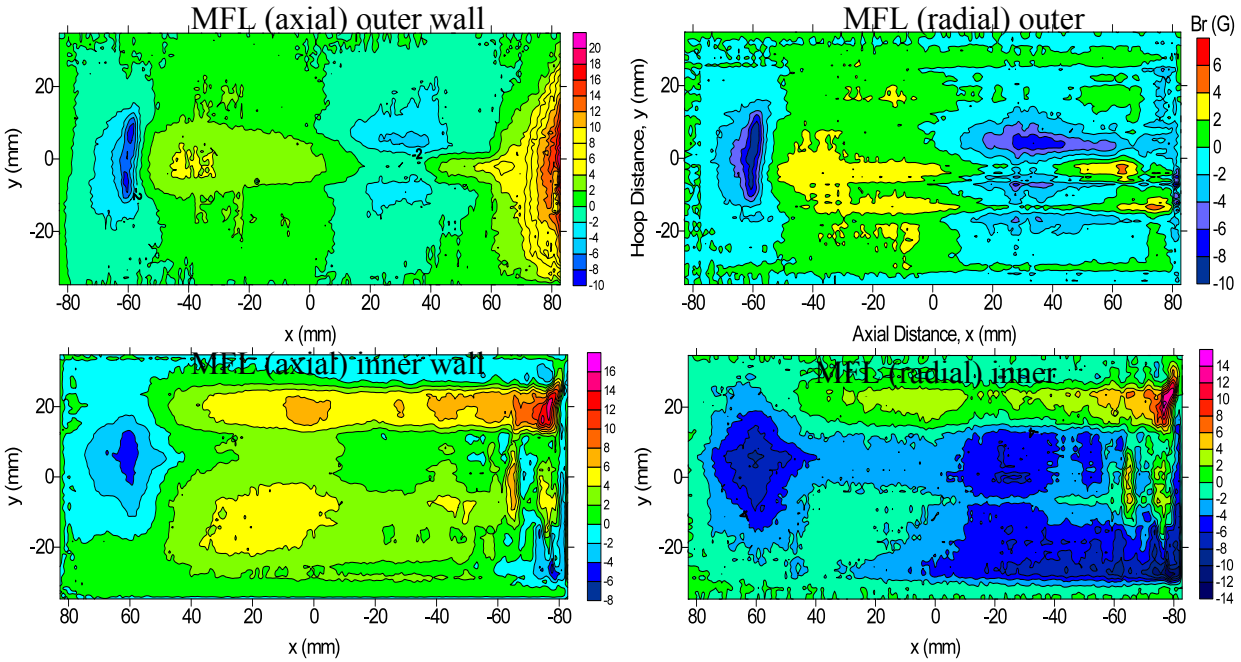

Figure 8- 2: Experimental MFL signals of BEA161 taken at the outside surface (top) and the inside surface (bottom). MFL (axial) on left and MFL (radial) are on the right. The inside wall MFL (radial) signal is unusual because the aspects of the background signal could not be successfully extracted from the raw data.

8.2 Magnetic models of gouge BEA161

Geometry modeling: The geometrical magnetic modeling of this defect was complex because of its "triangular" nature and the fact that an inner wall perturbation and also wall thinning developed as the tool progressed along the pipe wall. **Figure 8-3** shows the magnetic model of BEA161.

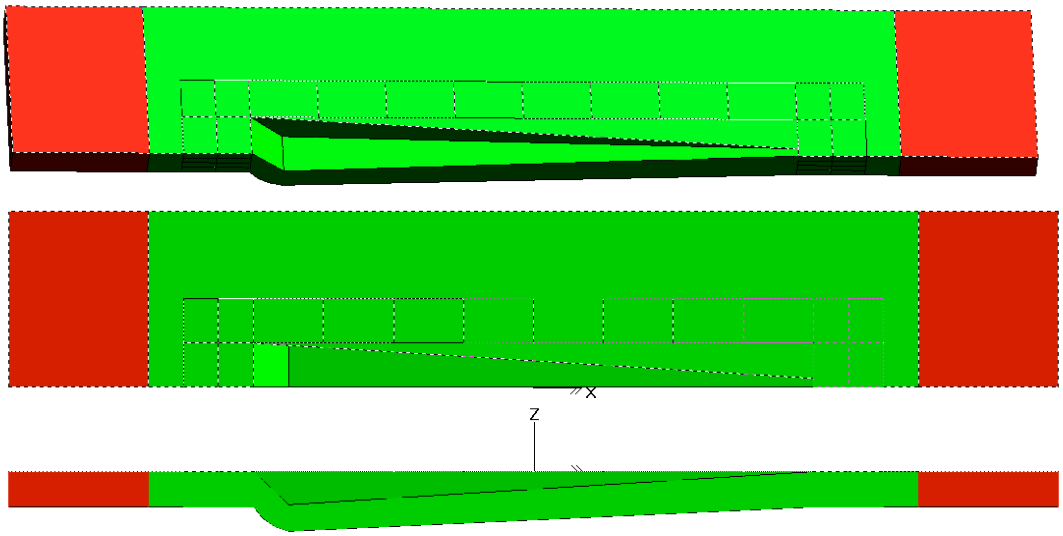

Figure 8- 3: Magnetic model of BEA161 geometry. The upper diagram shows an oblique view, the middle a plan view, and the lower a side view of the modeled defect. In addition to the triangular geometry, note the wall thinning and inner wall perturbation near the tool exit end. This is consistent with the geometry of the actual BEA161 gouge.

Residual stress modeling: Residual stresses were accounted for in a similar manner to previous work[5], by modification of the relative magnetic permeability function in each of the three component directions (hoop, radial, axial). The magnetic model was segmented into 'blocks' into which different "residual stress effects" could be introduced. These blocks, shown in **Figure 8-4**, are 2 mm thick and have varying sizes from 8 mm x 2 mm (length x width) to 16mm x 10 mm. There were four blocks used to represent the 8 mm thick pipe. The residual stress results obtained from neutron diffraction (Section 7.5) were used to develop the magnitude and direction of the magnetic permeability variation in the model shown in **Figure 8-4** (although the measured result is more detailed than what can be accommodated in the magnetic model).

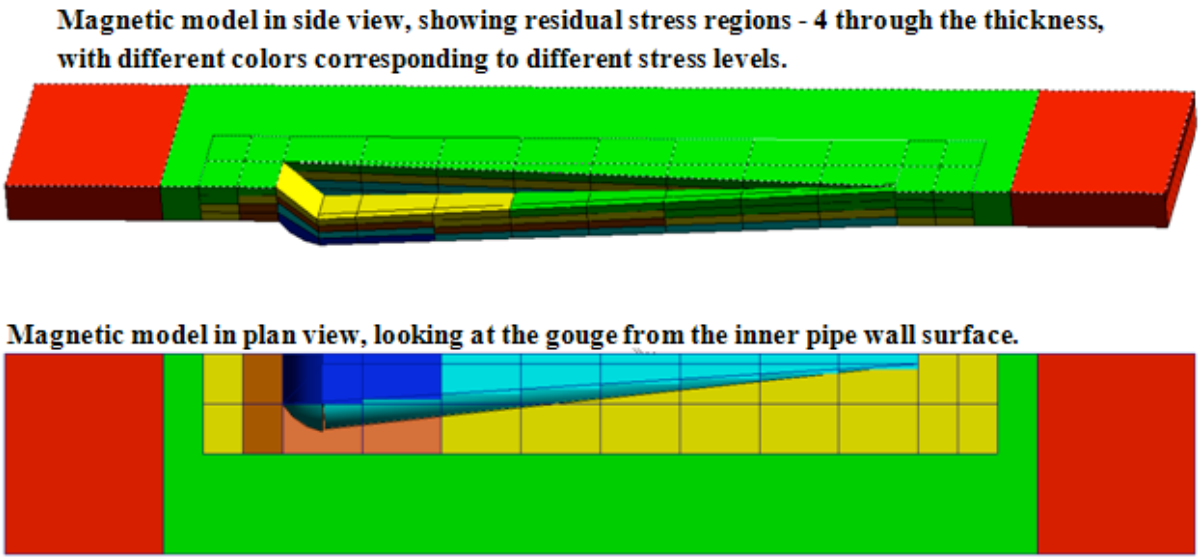

Figure 8- 4: Magnetic model for BEA161, showing block regions into which differing residual stress effects are introduced. The top diagram is the side view, and the lower diagram is a plan view.

8.3 MFL results of magnetic modeling of gouge BEA161

The results of the magnetic modeling for gouge BEA161 in comparison with the experimental results are shown in the following figures:

- **Figures 8-5** MFL (axial) outer wall
- **Figure 8-6** MFL (axial) inner wall
- **Figure 8-7** MFL (radial) outer wall
- **Figure 8-8** MFL (radial) inner wall

Note that in all of the modeled results the dashed lines indicate the modeled gouge dimensions, which were measured from BEA161.

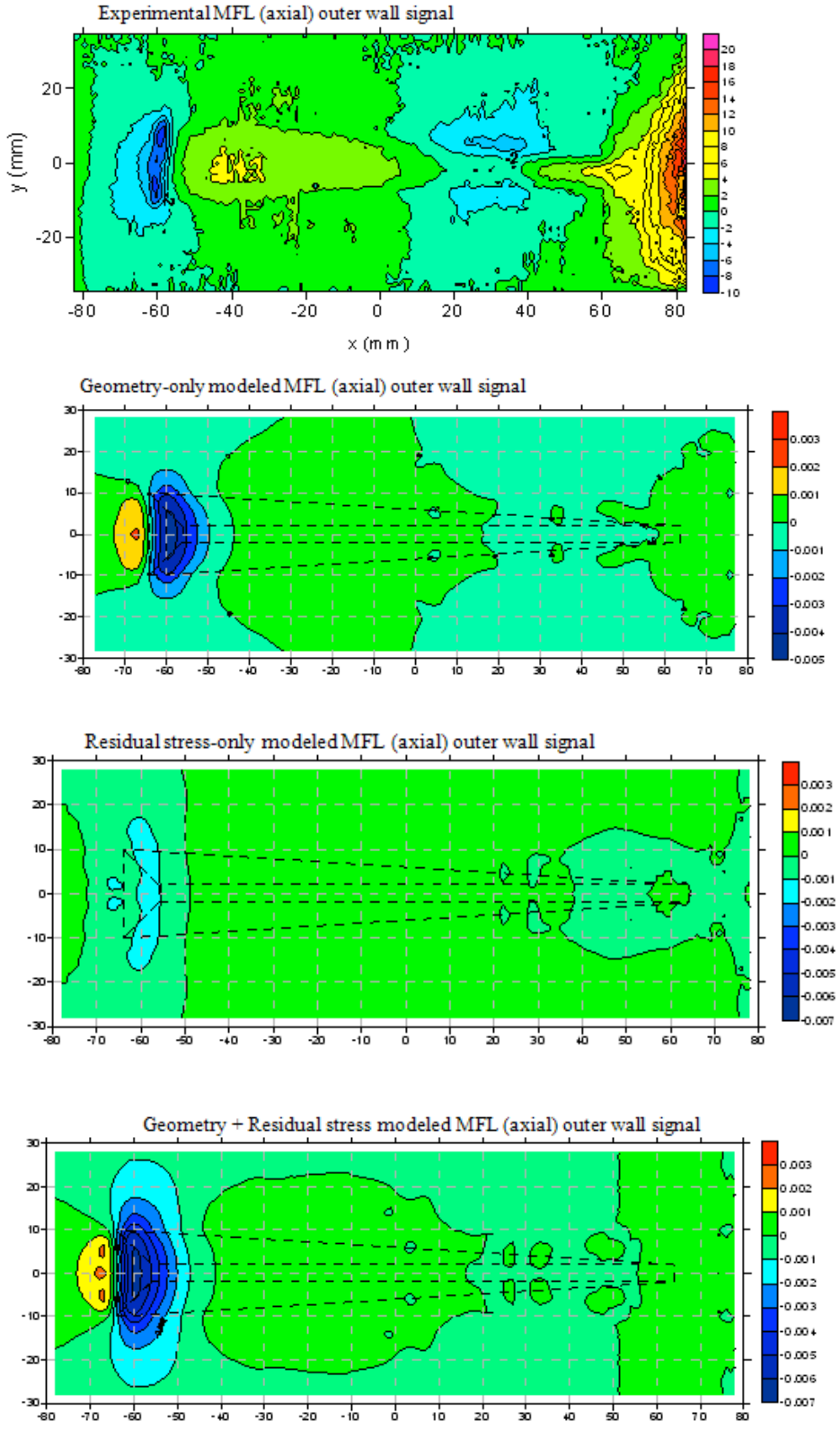

Figure 8- 5: MFL (axial) signals, outer wall

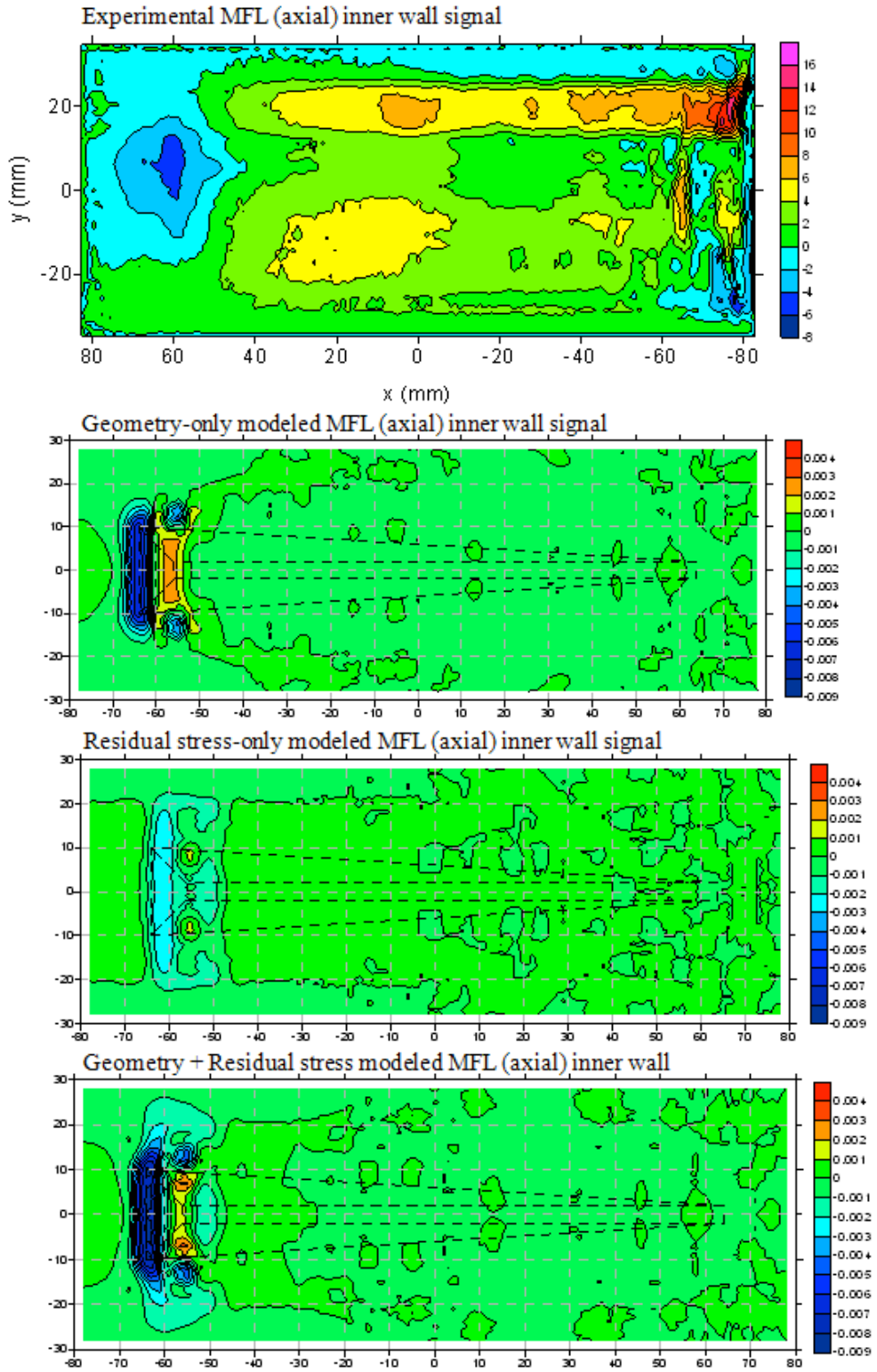

Figure 8- 6:MFL (axial) signals, inner wall

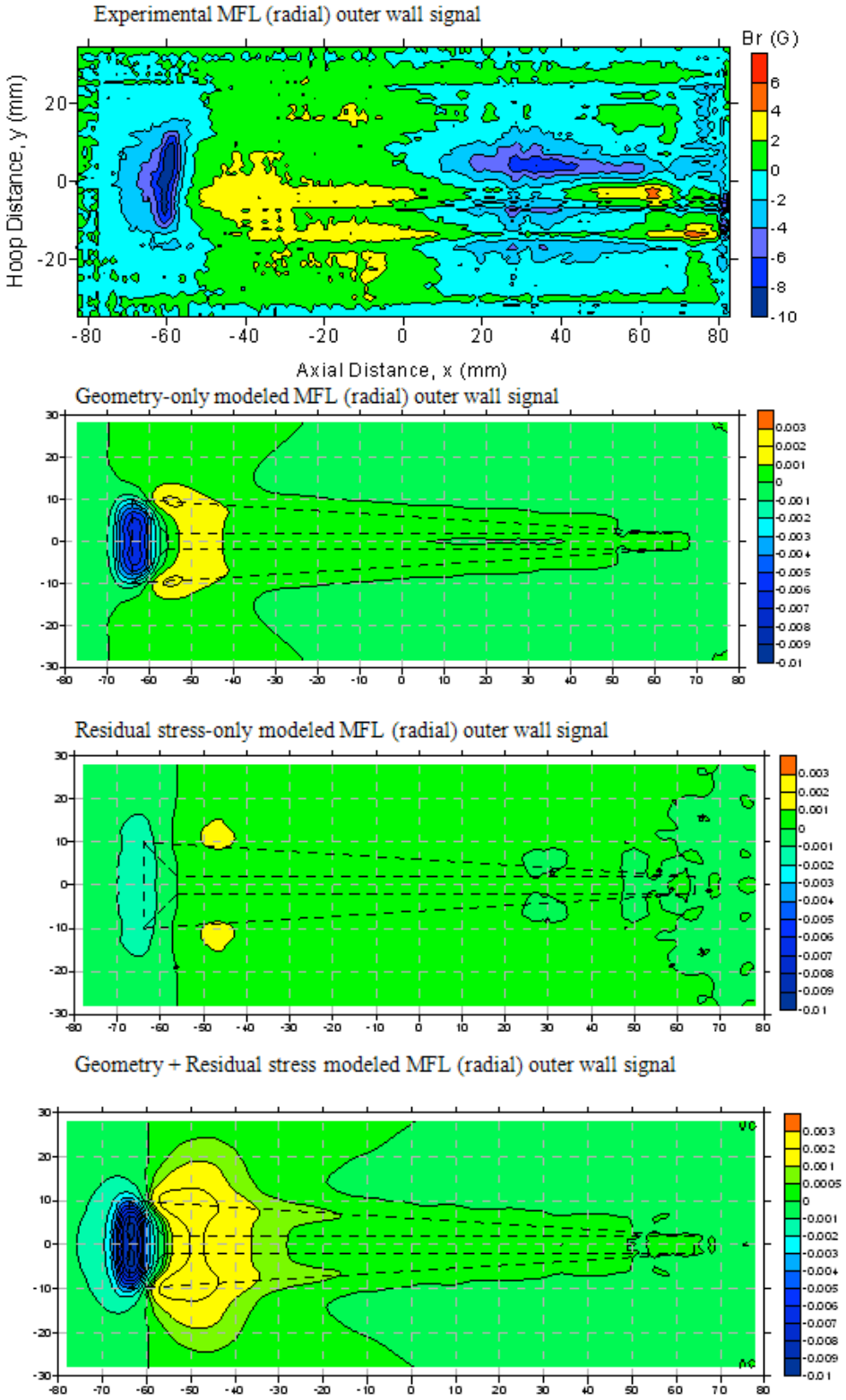

Figure 8- 7: MFL (radial) signals, outer wall

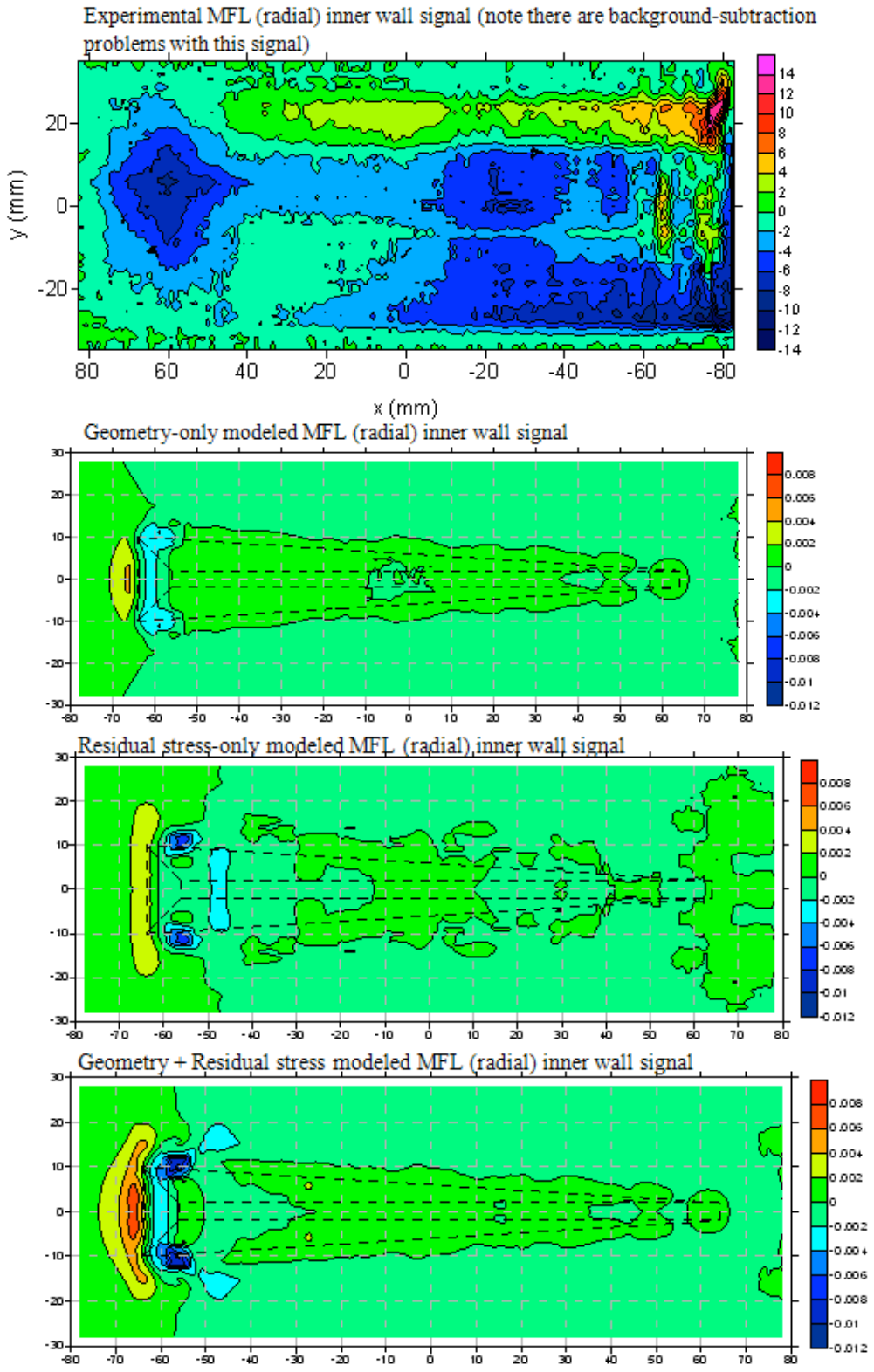

Figure 8- 8: MFL (radial) signals, inner wall.

The geometry-only results indicate that there are small elongated MFL peaks extending axially along the length of the gouge, however the dominant feature in all plots is a large MFL signal at the tool exit end (left on the figures). This is consistent with the experimental results. At this tool exit end there is a small amount of exfoliation, but primarily there is metal loss as well as a significant edge discontinuity.

The residual stress MFL signals are, in general, smaller than the geometry features at the outer wall, but tend to be approximately the same magnitude at the inner wall (where very large compressive axial and hoop stresses are present). The dominant residual stress peaks are, as with the geometry peaks, at the tool exit end, and in most cases will enhance this signal.

Most of the significant model-predicted MFL peaks are observed in the experimental signals. In some cases the modelling predicts a smaller, positive "companion" peak at the tool exit end, which is generally not seen experimentally. This is likely occurs because the geometric features at the tool exit end (exfoliation at the outer wall, and the 'dent bump' at the inner wall) will prevent the detector from measuring the "companion" peak. Or in other words, the "companion" peak may get 'lost' in the larger negative peak result.

Finally, there are a number of peaks present in the experimental signals which are not predicted by the modelling.

- In the MFL outer wall signals these peaks lie along the centerline of the gouge (**Figures 8-5 and 8-7)**. The researchers believe that these are associated with the severe deformation at the gouge base, since the experimental studies (Section 5) indicated that the outer wall MFL measurement will be sensitive to this deformation. A severe deformation layer was not included in the modelling; in part because it is difficult to model, but primarily because the results of Section 5 indicated that this layer does not influence the MFL inner wall signal, which is the only relevant signal for field measurements.
- In the MFL inner wall signals there are peaks that lie outside the gouge region that are not accounted for in the model. The team did not obtain neutron diffraction measurements from these points, and therefore they may not be aware of some significant residual stresses. But more likely these additional features arise due to the fact that the inner wall pipe surface was corroded and pitted, and these features may have been associated with these surface effects.

The primary and defining characteristic of these MFL signals, axial and radial, modeled and experimental, is a dominant peak feature at the tool exit end of the gouge. There are both geometrical and residual stress contributions to this dominant peak. It is also very important to note that, as discussed above, there are other MFL features present which do not appear to be associated with either the gouge geometry or the gouge residual stresses. Such features are real, and reproducible, and may have little to do with the presence of a gouge. Rather they reflect the reality of attempting to make, and interpret, sensitive measurements on "real" materials where those materials have an unknown processing history.

9.0 Comparison of MFL gouge signals from the present study with those from previous studies

At the conclusion of the Phase III project it is worthwhile to revisit and compare the MFL signal results of earlier studies with those observed in the present work. In Chapter 5 MFL signals of gouges from other studies were shown; these are reproduced below in **Figure 9-1** for convenience.

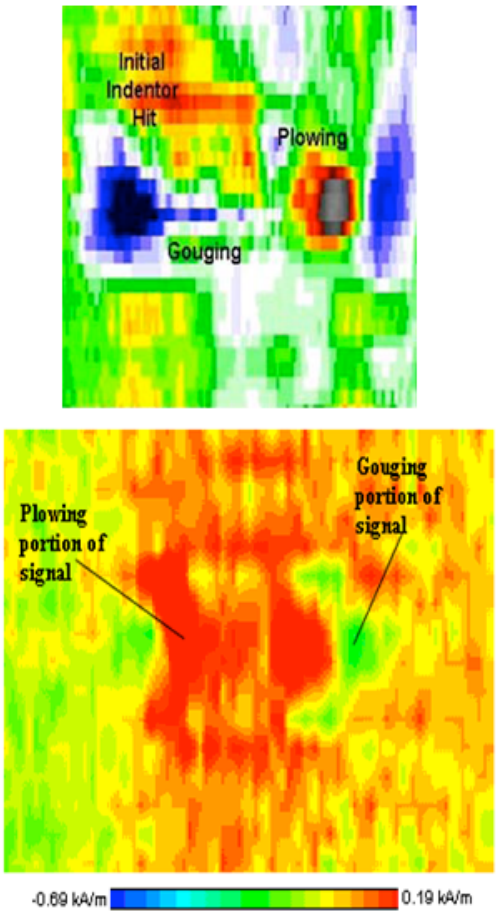

Figure 9- 1 MFL (axial) signals, inner wall. These two plots (reproduced from Figure 5-1) are results from earlier studies of MFL signals from gouges.

As discussed earlier, in a few previous studies of isolated gouges, a characteristic feature of of the inner wall MFL (axial) gouge signal has been interpreted as a "dipole" (i.e. a positive and negative peak, believed to be associated with either end of the gouge). This is unusual in an MFL (axial) signal since a dipole signal is more commonly associated with the MFL (radial) component. In the two MFL (axial) plots shown in **Figure 9-1**, certainly the top diagram suggests a dipole, although there are also other peaks present. In the lower diagram, however, the interpretation of a 'dipole' is somewhat questionable.

Figure 9-2 shows a collection of MFL (axial) inner wall signals obtained in the present study. The group of figures at the top are from the SES pipe gouges and gouges+dents; while the plot at the bottom is the MFL (axial) inner wall measurement from BEA161 (note that BEA178 was too large, and the dents too close to the pipe ends, to obtain reasonable MFL signals).

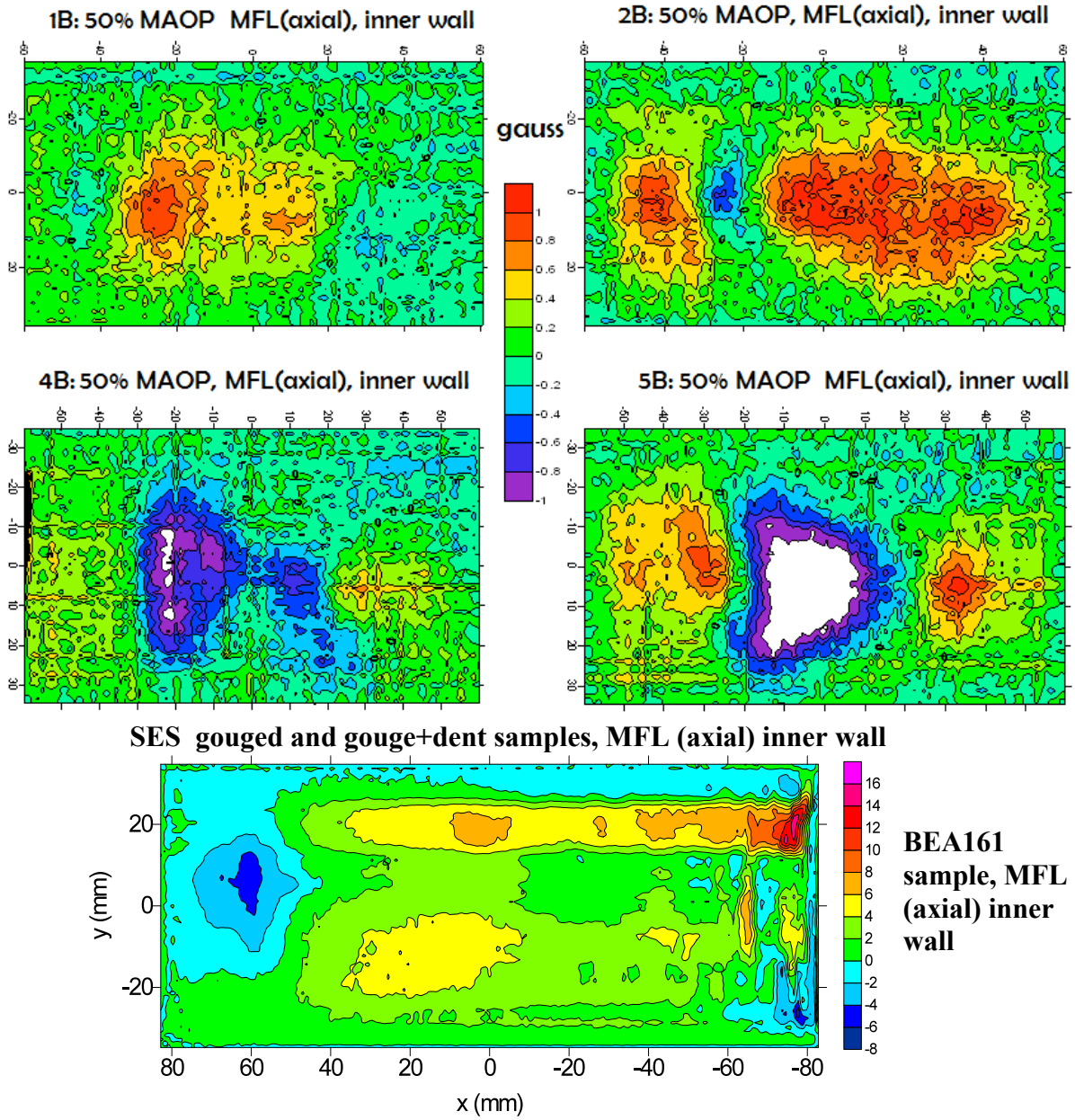

Figure 9- 2: MFL (axial) signals, inner wall. Top group are from the SES sample study. Bottom plot is from the BEA161 sample.

In all of the results shown in **Figure 9-2:**

- At the tool exit point there is always the distinctive MFL (axial) peak discussed earlier in Section 8. This is true even in the SES sample 1B, where no gouge is present – only residual stresses.
- At the tool entry point the MFL signals are inconsistent:
    - In some cases, such as BEA161, there is no peak near the tool entry end (recall that the peaks at the extreme right of BEA161 should be ignored – they are due to an anomalous background signal).
    - In the SES pipe gouges, there are peaks closer to the tool entry end in some cases, but often there are other peaks present as well, typically associated with the associated denting.

Thus we conclude that the only defining feature of a gouge MFL (axial) inner wall signal is a fairly localized peak associated with the tool exit point. This appears to be present regardless of the geometry at the tool exit end, since it is even observed when there is no geometrical feature present. However, while a MFL (axial) inner wall "dipole" signal may be present in some cases, it is not a defining characteristic a gouge signal.

Finally, it is also worthwhile to note while the field results of **Figure 9-1** clearly show the localized peak feature associated with tool exit, there are many 'anomalous' features present in the overall signal which may not be directly associated with the gouging. As commented at the end of Section 8, these are likely associated with surface anomalies (corrosion pitting, etc) or the pipe processing history.

10.0 The MFL Signal Template Database for MD 1-3

The number of MFL signals made during the course of a project such as this is very high, and as such many relevant signal plots are relegated to appendices. Many of these signal plots may be of interest to a reader that is looking for a specific behavior. As such, it is worthwhile to have all of the signals available on-line in a searchable form. To this end, a web-based database has been created of all of the MFL signals obtained since the beginning of the MD 1-3 project. The latest results for Phase III (also seen in the Appendices of this final report) are being been added to the database. The database is currently housed on Dr. Clapham's website but it will be moved to the PRCI website.

11.0 Summary and Conclusions

MFL signals from gouges and gouge+dents are complex because three aspects may contribute to the signal:

4) Severe plastic deformation region may be created when a deformation tool contacts the pipe wall which may contribute additional MFL signal features.

5) Geometry effects will change the applied MFL field and includes any pipe wall perturbation associated with damage (i.e., metal loss, exfoliation, pipe wall bending, and gouge orientation with respect to the applied MFL field)
6) Residual stresses are elastic stresses that often surround mechanical damage which alter the magnetic permeability of the pipe wall and, thus, the MFL signal

In Phase III the Queen's project team examined all three of these factors, both experimentally and, where feasible, through modeling. Of the three contributing factors, the one that is unlikely to strongly affect MFL signals during field testing is the severe plastic deformation at the base of the gouge. Our studies found that, although MFL is quite sensitive to this when the detector located on the same side as the damage, the MFL signal from this region did not extend through to the other side of the wall. Thus a thin, severe deformation layer on the outer surface of a pipe is not likely to produce a noticeable signal when measured by a passing MFL detector on the inside of a pipe.

The other two factors, geometry and residual stress, have a significant influence on the MFL signals. The researchers from Queens drew the following conclusions from the SES gouge samples:

The team found that the MFL measurements made while the pipe is under pressure do not differ significantly from those made of the same defect under zero pressure. A difference may have been expected, since internal pressure is expected to "level out" the residual stress variation in the pipe wall and thus reduce the MFL signal. However any differences between pressurized and unpressurized cases were very slight or inconsistent.

A second conclusion from the team is that damage introduced at higher internal pressures exhibits slightly smaller and less extensive signals than that created at lower pressures. This is consistent with the fact that the pipe wall is more highly constrained at high pressures and thus is more resistant to deformation.

The study involving gouges of increasing severity produced mechanical damage ranging from "residual stress-only" to severe "gouge+dent" areas. The MFL signals progressively changed as follows:

- Inner wall MFL signals: in the least severe case only residual stresses were present yet these created a significant MFL signal, with the largest signal associated with the tool exit location. As the gouge geometry developed, a large peak at the tool exit end was associated both with these residual stresses and also the exfoliation. The tapered sidewalls of the gouge contributed smaller 'side peaks' to the MFL signal. Finally, the most severe gouges also exhibited large dents, and thus typical MFL "dent peaks" were superimposed on the gouge signals.
- Outer wall MFL signals: The outer wall MFL signals follow a similar progression to the inner wall signals, with the exfoliation peak dominating. However at the outer wall there is also a MFL signal contribution from the thin layer of severe plastic deformation (created by direct tool contact) at the gouge base. The MFL signal from this severe deformation layer is not seen in the inner wall signal.

A pressure cycling verses MFL study was also conducted as part of the series of tests on the SES samples, where MFL measurements were made on gouged pipes cycled to 50% MAOP for up to 10,000 cycles. The Queen's team did not observe any variation in the MFL measurements with pressure cycling. This is contrary to anecdotal reports on isolated samples that pressure cycling produces an "MFL halo" around mechanical damage.

Conclusions of neutron diffraction residual stress measurements

Determination of the residual stress contribution to the gouge MFL signal is problematic because the residual stresses around gouges are complex and, to date, have not been accurately modeled using stress modeling software. Therefore, the team believed that measurement of these stress distributions was necessary, and neutron was is the only experimental method available to do this. NIST performed the neutron diffraction measurements on two MD4-1 samples: BEA161 (primarily a gouge with little denting), and BEA178 (mild gouging, very large dent). Measurements were also conducted on a coupon sample – P22 containing a gouge that was part of an earlier study. Results are summarized as follows:

Samples BEA161 and P22 – primarily gouges with little denting:

- The local residual strain field is localized around the immediate gouge vicinity, except where there was some denting present.
- The axial and hoop stress variations thought the wall, and laterally were similar to one another.
- Through-wall residual stresses underneath and in the immediate gouge region the hoop and axial stresses were neutral or moderately tensile (50-100 MPa) at the outer wall, gradually becoming highly compressive (-600 MPa in some locations) at the inner wall surface.

Sample BEA178 – mild gouge with significant denting:

- This exhibits a very different residual stress pattern than P22 or BEA161 which the team attributes to the presence of the large associated dent. The complex denting process associated with this kind of gouge+dent dominates the residual stresses, making the residual stress distribution very complex. In addition, rather than having a residual stress field that is localized in the immediate gouge vicinity, the varying stress distribution extends to the edge of the dented region. Further studies are planned to quantify the behavior in these large, complex damage situations.

Finally, the researchers applied a full model, including geometry and residual stress to sample BEA161 and compared to experimental MFL results for this gouge. The MFL modeling was able to account for many of the experimental features with the predominant geometry and residual stress peaks being associated with the tool exit end. The MFL (axial) "dipole" signal which is anecdotally associated with gouges was not apparent in either the modeling results, nor in the experimental measurements for BEA161. Some of the SES sample results indicated a dipole-type MFL result as a result of a combination of denting +gouging effects, but this was by no means "typical.

The primary and defining characteristic of these MFL signals is a dominant, localized peak feature at the tool exit end of the gouge. There are both geometrical and residual stress contributions to this dominant peak. It is also very important to note that, as discussed above, there are other MFL features present which do not appear to be associated with either the gouge geometry or the gouge residual stresses. Such features reflect the reality of attempting to make, and interpret, sensitive measurements on "real" materials which may have an unknown processing history.

12. Future work

The study on MFL signals from dents and gouges will continue. The neutron diffraction study indicated that the residual stress patterns may be very different from one gouge to another. Further neutron diffraction measurements need to be done to clarify the residual stress patterns associated with gouges, and this work (MD1-9, funded by PRCI in a 2-year study) will begin in June, 2011. Queen's will also conduct MFL measurements and continue modeling work on gouged samples that are part of the MD4-1 projects.

13.0 References

[1] D.L. Atherton. (Oct. 1986) "Effect of line pressure on the performance of magnetic inspection tools for pipelines", Oil and Gas J., V84, No.43, 86-89.

[2] Gas Research Institute contract #5093-260-2605 "3D details of Defect-Induced MFL and Stress in Pipelines", Annual Reports 1998-2002.

[3] Gas Technology Institute contract # PR-GRI-8682 "3D Details of Defect-Induced MFL and Stress in Pipelines (Detection of Mechanical Damage using Magnetic Flux Leakage)", Annual Report 2004

[4] US DOT PHMSA contract #DTPH56-05-T-0001, L. Clapham, V.J. Babbar, A. Rubinshteyn, R. Hutanu and P. Weyman, Phase I Final Report: Understanding MFL signals from Mechanical Damage in Pipelines June 2007.

[5] US DOT PHMSA contract #DTPH56-05-T-0001, L. Clapham, V.J. Babbar, K. Marble and P. Weyman, Phase II Final Report: Understanding MFL signals from Mechanical Damage in Pipelines June 2008.

[6] L. Clapham, V. Babbar and J. Byrne "Detection of Mechanical Damage using the Magnetic Flux leakage Technique", 2004 International Pipeline Conference, Oct 2004, Calgary, Alberta.

[7] Vijay Babbar, James Byrne and Lynann Clapham, "Mechanical Damage Detection using Magnetic Flux Leakage tools: Modeling the Effect of Dent Geometry and Stresses", Non-destructive Testing and Evaluation (NDT&E) International, 2005, V38, 471-477.

[8] L. Clapham, A. Rubinshteyn and V. Babbar, "Understanding Magnetic Flux Leakage Signals from Pipeline Dents" 2006 International Pipeline Conference Sept 2006, Calgary, Alberta.

[9] L. Clapham, V. Babbar and J. Bryne, "Mechanical Damage and Magnetic Flux Leakage", 16th annual World Conference on Non-destructive Testing, Montreal, August 2004.

[10] A. Rubinshteyn, Steffen Paeper, and Bruce Nestleroth, "Testing of a dual field magnetic flux leakage (MFL) inspection tool for detecting and characterizing mechanical damage features" 2008 International Pipeline Conference Sept 2008, Calgary, Alberta.

[11] Massopust P., Torres C., Dean A., "Improving In-Line Inspection for Mechanical Damage in Natural Gas Pipelines", GRI Contract No. 5096-270-3698, Prepared for the Corrosion and Inspection Technical Committee of Pipeline Research Council International, Inc.

[12] M. Zarea, R. Batisse and ? "Full Scale Experimental Database for Mechanical Damage – Dent +Gouge Work in Progress and Results", presented at the PRCI Pipeline Program Research Meeting, Atlanta, GA, USA February 2011.

[13] Hutchings M. and Krawitz A., eds. Measurement of Residual and Applied Stress using Neutron Diffraction. Kluwer Academic Publishers, Dordrecht, Netherlands, 1992.

[14] Withers P. and Holden T. Materials Research Society Bulletin, 1999; 24: 17-22.